SEISMIC RISK ASSESSMENT OF CODE-CONFORMING SPECIAL CONCENTRICALLY BRACED FRAME BUILDINGS IN TURKEY

by

Hava Nur Yavaş

B.S., Civil Engineering, Istanbul Technical University, 2019

Submitted to the Institute for Graduate Studies in
Science and Engineering in partial fulfillment of
the requirements for the degree of
Master of Science

Graduate Program in Civil Engineering

Boğaziçi University

2023

To Y.Hn

ACKNOWLEDGEMENTS

Before anyone else, my family deserves the greatest thanks for their constant support and all the sacrifices they have made for me throughout my life.

Besides, I would like to thank my thesis supervisor Associate Professor Serdar Selamet for his guidance and assistance throughout my dissertation.

Also, I would like to thank Professor Serdar Soyöz and Professor Bülent Akbaş for accepting to be on my jury and for their valuable feedback.

In addition, I would like to thank Associate Professor Cüneyt Vatansever, who inspired me to become a structural engineer and built my foundational engineering knowledge. During my academic and engineering life, the kindness and generosity he has shown me at any time I need it really means a lot to me.

Furthermore, I would like to express my sincere thanks to Raşit Çömlek for not only teaching me how to be a qualified engineer but also for showing interest in my graduate studies and providing me with guidance throughout my master's degree. Also, I am grateful to Özcan Keçelioğlu for his support and invaluable contributions to my engineering career. In addition, I would like to thank the entire Balkar team for their contributions.

Moreover, I would like to express my deepest gratitude to Dr. Şamil Şeref Polat for his continuous guidance during this study and my engineering life. He has been a help call many times.

Last but not least, from the bottom of my heart, I would like to thank my dearest friends Betül Bozkurt and Cem Burak Baydar for their persistent support during my master's program.

ABSTRACT

SEISMIC RISK ASSESSMENT OF CODE-CONFORMING SPECIAL CONCENTRICALLY BRACED FRAME BUILDINGS IN TURKEY

In the Turkish Seismic Code, Seismic Hazard Maps are used for the design of new buildings, which assumes uniform hazard over the country; design acceleration values for all locations have the same probability of exceedance in a defined period. However, even if buildings with similar structural systems located in different regions are designed to comply with the code requirements, they might have a different probability of collapse since the collapse capacity and the hazard curve shape are unknown. In this study, three buildings with different fundamental periods are investigated to confirm that the seismic risks are within acceptable limits. Special Concentrically Braced Frames (SCBFs) are preferred since they are widely used in seismic regions and have relatively low ductility capacity. Nonlinear time history analysis is performed for each building with 22 earthquake record pairs taken from the PEER. The corresponding fragility curves are developed for the risk assessment using Incremental Dynamic Analysis and the FEMA-P695 procedure. The risk integrals are utilized to determine the collapse probability of the structure. Sensitivity analysis of different parameters in the construction of the fragility curve is performed. This study shows that while all the buildings are designed according to the same hazard level, each building has a clearly distinct collapse risk. Collapse risks of the buildings in 50 years are calculated as 0.61%, 1.9%, and 0.62% for Building-1, Building-2, and Building-3, respectively. While the collapse risk of Building-1 and Building-3 stays within acceptable limits, Building-2 fails to satisfy the required structural performance. Deaggregation of the mean annual frequency of collapse emphasizes that small to medium acceleration intensities make the biggest contribution to collapse risk. Under high levels of intensity, SCBFs might undergo critically strength deterioration and some additional restrictions in the Code may be necessary to reduce risk.

ÖZET

TÜRKİYE DEPREM YÖNETMELİĞİNE GÖRE TASARLANMIŞ SÜNEKLİK DÜZEYİ YÜKSEK MERKEZİ ÇAPRAZLI BİNALARIN DEPREM ETKİSİNDE GÖÇME RİSKİ

Türkiye deprem yönetmeliğine göre yeni yapılacak binaların tasarımında, tüm ülke boyunca deprem tehlikesini aynı kabul eden deprem tehlikesi haritaları kullanılmaktadır. Diğer bir değişle bu haritalar, her bir noktada belirli bir tekrarlanma periyodu için aynı aşılma olasılığını vermektedir. Fakat, yapı sisteminin kendisinden kaynaklanan göçme olasılığının bilinmemesi ve deprem tehlike eğrisinin şeklindeki bilinmezlikler, benzer kapasiteye sahip ve yönetmeliğe uygun olarak tasarlanmış farklı binaların yaşam boyu karşılaşacağı göçme olasılığını farklılaştırmaktadır. Bu çalışmada, farklı periyotlara sahip üç binanın göçme riskinin kabul edilir değerler içinde olma durumu araştırılacaktır. Deprem bölgelerindeki yaygın kullanımı ve diğer sistemlere göre düşük olan sünekliği dolayısıyla süneklik düzeyi yüksek merkezi çaprazlı çelik çerçeveler ele alınmıştır. Tüm yapılarda PEER'dan alınmış 22 deprem kaydı altında doğrusal olmayan zaman tanım alanında deprem analizi yapılmıştır. Artımsal dinamik analiz ve FEMA-P695'te verilen prosedür kullanılarak kırılganlık eğrileri elde edilmiştir. Yapının göçme olasılığına ulaşmak için risk integralleri kullanılmıştır. Kırılganlık eğrisindeki parametrelerin değişkenliğinin analiz sonucuna etkisi tartışılmıştır. Çalışma sonucunda, yapılar aynı deprem tehlikesine göre analiz edilmesine karşın farklı göçme olasılıklarıyla karşılaşmaktadır. Üç yapının 50 yıl boyunca deprem etkisinde göçme olasılıkları sırasıyla %0.61, %1.9 ve %0.62 olarak bulunmuştur. Birinci ve üçüncü bina izin verilen göçme sınırının içerisinde kalırken, ikinci bina gerekli performansı gösterememiştir. Yıllık ortalama göçme sıklığının bileşenlere ayrıştırılması ile, küçük ve orta ölçeklikteki deprem ivmelerinin göçme olasılığına daha fazla katkı sağladığı görülmektedir. Çalışma sonucunda, yüksek deprem büyüklüklerinde süneklik düzeyi yüksek merkezi çaprazlı çelik çerçevelerin büyük ölçüde dayanım kaybı yaşadığı görülmektedir. Bu sistemlerin göçme risklerinin azaltılabilmesi için mevcut yönetmelikte ilave önlemlerin alınması gerekebilir.

TABLE OF CONTENTS

LIST OF FIGURES

LIST OF TABLES

LIST OF SYMBOLS

A	Cross-sectional area of section
C_{DM}	Limit value for a specified performance level
C_d	Deflection amplification factor
E	Elasticity modulus
$E_d^{(Z)}$	Earthquake load on Z direction
F_{CRE}	Expected critical buckling strength
$f_{Capacity}$	Fragility curve
$f_M(m)$	Probabilistic distribution function for magnitude
$f_R(r)$	Probabilistic distribution function for distance
F_y	Yield strength
F_{ye}	Expected yield strength
G	Gravity loads
I	Moment of inertia
L	Length of the member
n	Live load contribution factor
Q	Capacity
Q_y	Yield capacity
P	Axial force
$P_C(t)$	Probability of collapse in a predefined year, t
P_c	Compressive strength
P_T	Tensile strength
R	Structural behavior factor
R_{JB}	Joyner-Boore distance
R_y	Ratio between expected yield strength to characteristic yield strength
S_1	Spectral acceleration coefficient for 1s period
S_S	Spectral acceleration coefficient for short period
$S_a(T)$	Elastic spectral acceleration at period T
S_{CT}	Median collapse capacity

S_{D1}	Design spectral acceleration coefficient for 1s period
S_{DS}	Design spectral acceleration coefficient for short period
S_{MT}	MCE ground motion intensity
T	Natural vibration period
T_x	Fundamental period in X direction
T_y	Fundamental period in Y direction
V_{S30}	Shear wave velocity at first 30m of soil
W_p	Plastic section modulus
β_d	Standard deviation of the natural logarithm of the capacity
β_{RTR}	Record-to-record uncertainty
β_{DR}	Design requirement uncertainty
β_{TD}	Test data uncertainty
β_{MDL}	Modeling uncertainty
β_{TOT}	Total system uncertainty
Δ	Yield deformation under compressive force
Δ_c	Yield deformation under compressive force
Δ_T	Yield deformation under tensile force
γ_c	Specific weight of concrete
γ_s	Specific weight of steel
ξ	Damping ratio
Φ	Standard normal cumulative distribution function
λ_C	Mean annual frequency of collapse
λ_x	Seismic hazard curve
μ_T	Period based ductility
ν	Mean annual rate of occurrence
θ	Rotation
θ_d	Median capacity
θ_{max}	Maximum inter-story drift ratio
θ_y	Yield rotation
Ω	Overstrength factor

LIST OF ACRONYMS/ABBREVIATONS

ACMR	Adjusted Collapse Margin Ratio
ASCE	American Society of Civil Engineers
ATC	Applied Technology Council
CMR	Collapse Margin Ratio
DD1	Earthquake Level-1
DM	Damage Measure
FEMA	Federal Emergency Management Agency
IDA	Incremental Dynamic Analysis
IM	Intensity Measure
MCE	Maximum Considered Earthquake
NM	Normalization Factor
PBD	Performance-based design
PEER	Pacific Earthquake Engineering Research Center
PGA	Peak Ground Acceleration
PGV	Peak Ground Velocity
PSHA	Probabilistic seismic hazard analysis
SCBF	Special Concentrically Braced Frame
SDC	Seismic Design Category
SEAOC	Structural Engineers Association of California
SSF	Spectral Shape Factor
TEHM	Turkish Earthquake Hazard Map
TSC	Turkish Seismic Code
UBC	Uniform Building Code
USGS	US Coast and Geodetic Survey

1. INTRODUCTION

1.1. Motivation

In the Turkish Seismic Code (TSC) [1], Seismic Hazard Maps are used for the design of new buildings, which assumes uniform hazard over the country. For all locations, the design PGA value has the same probability of exceedance in a defined period of time (e.g., 2% probability of exceedance in 50 years). Yet, even if two buildings with similar structural systems located in different regions are designed to comply with the code requirements, they might have a different probability of collapse.

There are two types of uncertainty in the collapse of a building: uncertainty in the ground motion demand and uncertainty in the collapse capacity of the structure. Uncertainty in ground motion demand is covered by probabilistic seismic curves in TSC. On the other hand, uncertainty in the collapse capacity of the structure depends on the structural system and construction details of the structure, and also depends on other characteristics of the ground motion. Since this information is uncertain, so is the spectral acceleration that the structure can resist without collapsing. Uncertainty in the collapse capacity is not covered by TSC and this leads to a different probability of collapse values for each building.

In the United State, to provide the same level of seismic performance to all buildings, the new “risk-targeted” maps are developed and adopted by ASCE 7-10 [2]. In Europe and some other countries, a lot of research regarding this new approach is carried out and some countries have revised current seismic maps according to this approach. These risk-targeted maps give the same probability of collapse for all buildings in their lifetime. ASCE 7-10 limits the probability of collapse to 1% in 50 years by using generic fragility curves with a constant standard deviation value in the risk assessment (ATC-63 Project) [3].

In Turkey, there is no study for risk-targeted seismic maps, and there is doubt about whether newly designed buildings complying with the code requirements satisfy a 1% probability of collapse in 50 years.

1.2. Scope of the Research

In this study, three buildings with different fundamental periods will be investigated to confirm seismic risks are within acceptable limits. Since wide usage in seismic regions and relatively low ductility capacity, the structural system of the buildings is decided to be Special Concentrically Braced Frame (SCBF). Chevron-type bracing is used in all buildings. The linear design of the buildings is performed to satisfy all the requirements of the Turkish Seismic Code 2018, and Demand/Capacity ratios for each member are kept high as possible. Nonlinear time history analysis is performed for each building with 22 earthquake record pairs.

For the risk assessment, the fragility curve for each structure is developed by employing Incremental Dynamic Analysis and FEMA P695 [3] procedure. Acceptability of the structural behavior factor, *R,* is argued. Sensitivity analysis for different values of fragility function parameters is performed. For all buildings, four different points of the seismic hazard curve are obtained from TEHM – Turkish Earthquake Hazard Map Website [4], and a complete hazard curve is created by using these points. Risk integrals are utilized to determine the collapse probability of the structure, which consider all the collapse possibilities in the seismic hazard curve and the fragility curve. Acceptability of collapse risk is argued. Sensitivity analysis of different parameters in the construction of the fragility curves for collapse risk is performed.

1.3. Organization of the Research

The thesis is divided into five different chapters. Chapter 1 makes a brief introduction to the study and explains the motivation. Chapter 2 provides the development history of methodologies and procedures, summarizes previous research on this subject, and builds a brief technical background related to the topic. Chapter 3 focuses methodology employed in this study and gives the required details about the buildings and analysis procedures. Chapter 4 demonstrates the result of the analysis and evaluates the performance of the buildings. And last but not least, Chapter 5 summarizes the study, and outcomes of results and includes recommendations for future studies.

2. LITERATURE REVIEW AND BACKGROUND

2.1. From Performance Based Design to Incremental Dynamic Analysis

Design methodologies for buildings are mainly based on the evaluation of acting forces and required strengths of structural members and the provision of necessary ductility requirements given by the Codes and Standards. Some big earthquake events and significant damage to the structures have brought the necessity of more advanced and accurate methods in the design and evaluation of the structures. Also, to achieve higher performance levels and more predictable structural behavior, Performance-based design approach has begun to take place in seismic codes [5].

The performance-based design procedure is defined first in SEAOC Vision 2000 [6], ATC40 (1996) [7], and FEMA 273/274 (1996) [8]. In 1995, Vision 2000 document published by the Structural Engineering Association of California (SEAOC) aimed to describe the main concepts and performance objectives. Performance levels such as operational, life safety, and collapse are defined first in this document. In 1996, ATC40 document is published to outline performance-based design procedures. In this document, nonlinear static (pushover analysis) is employed, and capacity and demand spectra are generated. FEMA 273 document by The Federal Emergency Management Agency has defined various performance objectives with different design approaches ranging from linear analysis to nonlinear time history analysis [5].

The same with extending a single static analysis to incremental pushover analysis, a dynamic time history analysis can be expanded to an incremental dynamic analysis by scaling earthquake records. In 1977, this concept has been created first by Bertero [9] and adopted by guidelines of the Federal Emergency Management Agency (FEMA) as The Incremental Dynamic Analysis (IDA). Various research based on this methodology is performed.

In 2002, a basis and terminology for Incremental Dynamic Analysis (IDA) has formed by Vamvatsikos and Cornell [10]. This study has been used for many research. Incremental Dynamic Analysis aims to clarify the response pattern of a structure to a range of earthquake magnitudes. In this procedure, selected earthquake records are increased or decreased gradually to different levels of Intensity Measures (IM) with different scale factors. For each intensity measure level, the response of the structure is observed by the means of a well-defined Structural State Variable or Damage Measure (DM). IDA curve is created by recording each damage measure of the structure exposed to corresponding intensity measure. Y axis of the plot represents the intensity measure which can be characterized differently. For instance, Peak Ground Acceleration (PGA), Peak Ground Velocity (PGV), $\xi = 5\%$ damped Spectral Acceleration at the structure's first mode period ($S_a(T_1, 5\%)$) and the normalized factor $R = \lambda/\lambda_{yield}$ can be used as IM. X-axis of the plot represents the Damage Measure (DM). Likewise, the damage measure can be assigned by different characteristics. For example, maximum base shear, peak story ductilities, roof drift ratio, and maximum inter-story drift ratio can be adopted as DM. In the following, an example of IDA curve for a building subjected to a single earthquake record is given.

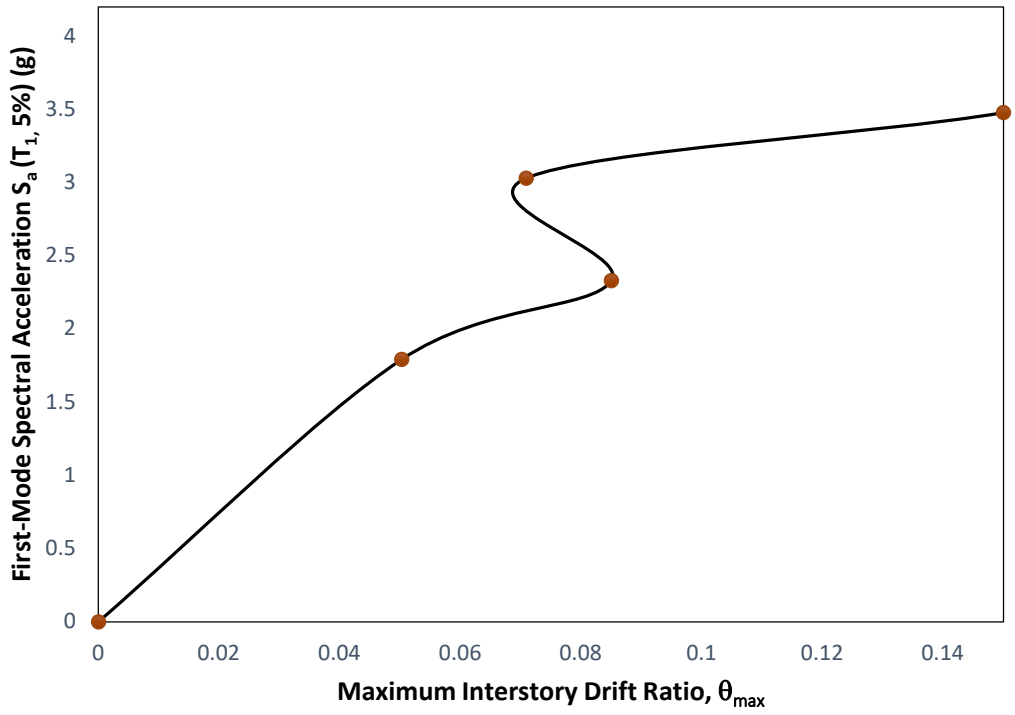

Figure 2.1. An example of an IDA curve.

According to the IM-based rule, evaluation of a structure by IDA curve can be performed by defining a C_{DM}, the limit value for a specified performance level. This value can be determined based on experiments, tests, or engineering judgment. As an example, $C_{DM} = 2\%$ maximum inter-story drift ratio is decided for Type 1 connections in steel moment resistant frames by FEMA 351 [11].

For the same structure under different earthquake records, the behavior of the structure can be observed by scaling each record to an intensity level gradually and recording the damage level of the structure one by one. To plot and evaluate all analysis results together, the same intensity measure and damage measure should be chosen. In the following figure, the IDA curve set for a 3-story steel braced frame is given. On the plot, each curve represents a different earthquake record, and each curve is composed of the response of the structure to the same earthquake record with different scaled magnitudes.

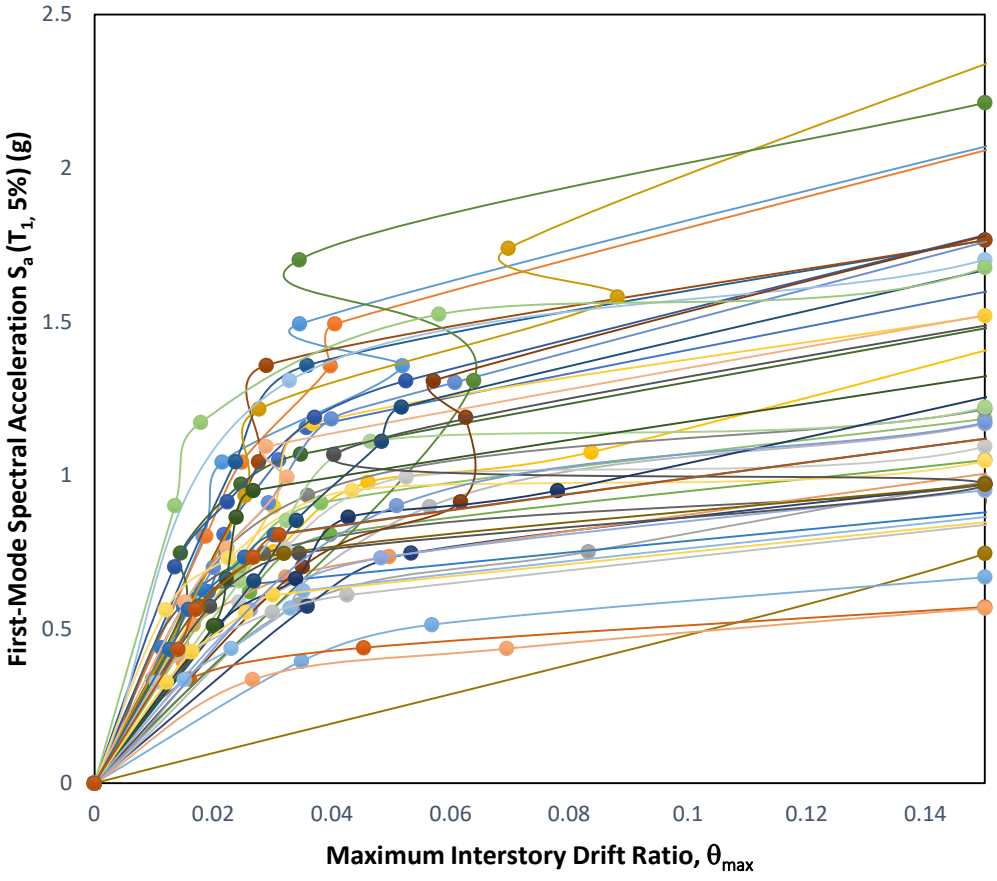

Figure 2.2. IDA curve set for a 3-story steel braced frame.

2.2. Fragility Functions

The application of fragility functions in earthquake engineering dates back to Kennedy at al. (1980). The fragility function in this study represents the involvement of probability of the failure of a component in a nuclear power plant under peak ground acceleration [12].

Different methodologies are improved over time to estimate the loss from an earthquake. In 1997, Whitman et al. [13] generated a methodology for National Earthquake Loss estimation, and this methodology is adopted by HAZUS. In this methodology, inelastic building capacity and site-specific response spectra are created to define the damages of structural and non-structural components. For building capacity, a probabilistic approach is adopted by using fragility curves. Damages are expressed in terms of probability. In this way, fragility curves have begun to be used in earthquake engineering for various types of purposes.

In the risk assessment of buildings, the fragility function can be defined as the capacity of a structure or a component to withstand a defined damage level. Another definition of a fragility curve is that it shows the likelihood of an unwanted situation occurring under a predefined intensity measure. For instance, a fragility function gives the probability of the collapse of a structure at each level of peak ground acceleration or another damage measure.

The most common form of fragility curve is a lognormal cumulative distribution function having a median, θ_d and standard deviation, β_d value. Studies show that the lognormal cumulative distribution well fits nonlinear response of structures, and it is practical to use in the collapse assessment of structures. Thus, knowing these two parameters allows us to determine a structure's fragility (capacity) curve. [14].

The X-axis of the fragility curve represents an intensity measure, the same as the Y-axis of the incremental dynamic analysis curve. It can be any measure suitable for the purpose of analysis. On the other hand, the Y axis of the fragility curve gives the probability of collapse of the structure under the defined intensity measure.

The fragility curve can be defined as

$$f_{Capacity}(x) = P[D \geq d \; I \; X = x] \qquad d \in \{1,2, \dots N_D\}$$

$$= \Phi\left(\frac{In\left(\frac{x}{\theta_d}\right)}{\beta_d}\right), \tag{2.1}$$

where D denotes the uncertain damage state of a component, d denotes a certain damage level; X denotes an uncertain intensity measure, and x denotes a certain intensity measure.

The development of the fragility function can be performed in three different ways. In the first approach, test and observation data are used and an empirical fragility function is formed. In the second method, a mathematical model of the structure or a component is created and a significant number of analyses are conducted to create an analytical fragility function. As in the third way, past experiences and engineering judgment are used to build a fragility function [12].

A typical fragility curve with θ_d= 5.16 and β_d = 0.5 is given below to show an example.

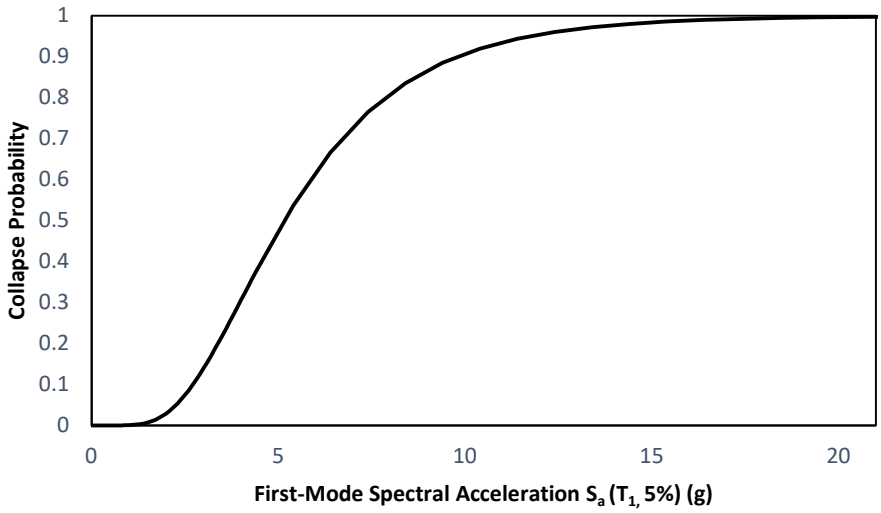

Figure 2.3. A typical fragility curve.

2.3. Uniform Hazard Maps to Risk Targeted Maps

In the United States, seismic design provisions were incorporated for the first time into the Uniform Building Code (UBC) [15] in 1927. At this time, there was no seismic hazard map, and the seismic load was considered to be equal to 7.5% of the building's weight. In the 1935 edition of UBC, a seismic zonation map was included based on the studies of Heck [16]. Earthquake force was calculated as a different percentage of building weight depending on the seismic zonation of the structure. ASCE came up with the first dynamic approach to seismic design in 1952 in the Lateral Forces of Earthquake and Wind [17]. The seismic load was started to be calculated based on the period and weight of the structure [18]. The first contiguous hazard map of the US was generated by the US Coast and Geodetic Survey (USCGS) in 1948 and a revised edition of this map was adopted by UBC in 1952. Over the years, earthquakes and improvements have led to seismic maps being updated. In 1976, seismic hazard maps based on a probabilistic approach were prepared for the first time by Perkins and Algermissen [19].

A probabilistic seismic hazard map gives design acceleration values based on past earthquake data and active faults in the area for a particular earthquake level (e.g., 2% probability of exceedance in 50 years). For a site, probabilistic hazard curves consider all possible magnitudes that can be produced by each source, all possible distances that change according to the exact event location on the faults, uncertainties in ground motion prediction equations, and the magnitude-occurrence relationship of each source. The annual rate of exceeding any acceleration value is calculated by combining all those uncertainties. All the ingredients of seismic hazard curves can be written as

$$\lambda_x = \nu \iint P[X > x \,\mathrm{I}\, m, r]\, f_M(m)\, f_R(r) dm dr, \tag{2.2}$$

where ν represents mean annual rate of occurrence for each fault, $P[X > x \,\mathrm{I}\, m, r]$ represents uncertainties in ground motion prediction equations, $f_M(m)$ and $f_R(r)$ shows probabilistic distribution functions for magnitude and distance, respectively [20].

Probabilistic seismic hazard analysis used in building codes defines a uniform hazard across the country such that the probability of exceeding a design value (e.g., PGA) is the same throughout. Since the collapse of a structure does not rely on only the earthquake probability but also the capacity of the structure, these design maps yield a distinct probability of collapse value for all code-conforming buildings. Besides, the difference in the characteristics of hazard curves for buildings located in different regions causes different collapse probabilities, accordingly [21].

Luca et al. (2007) [21] proposed a different design map approach to obtain design acceleration values by considering structural capacity too, which is known as a risk-targeted map. In those maps, the collapse probability of a structure depends on both seismicity and the building collapse capacity. Those maps aim to equalize the risk of collapse across the country. This approach has started to be widely accepted in the world. Design values of maximum considered earthquake (MCE) in ASCE 2016 are updated according to this approach. The procedure proposed by Luca et al. (2007) has been followed by France, Romania, Indonesia, Spain, Italy, etc. with slight changes in parameters.

The risk-targeting approach requires a hazard curve on the location and a fragility curve of the structure. In the seismic codes, to conduct risk-targeted maps all over the country, fragility curves are created with some estimations. Rather than the mean value, the 10^{th} percentile value and an estimated standard deviation value are used to parameterize the curve. 10^{th} percentile collapse capacity value is decided as the acceleration value corresponding to Maximum Considered Earthquake, MCE at the fundamental period. To obtain the risk, risk integrals are used to combine the seismic hazard curve with the fragility curve. The mean annual frequency of collapse can be expressed as

$$\lambda_C = \int_0^\infty \lambda_x \, f_{Capacity}(x), \tag{2.3}$$

where λ_x and $f_{Capacity}(x)$ denote the seismic hazard curve and the fragility curve of the structure, respectively.

Considering the Poisson Model which proposes time independency in the occurrences of events, the probability of collapse in a predefined year can be conducted by

$$P_C(t) = 1 - e^{-\lambda_C t}, \tag{2.4}$$

where λ_C and t shows the mean annual frequency and the time, respectively.

In most design codes, 1% in 50 years is considered to be an acceptable risk value. To achieve a design acceleration value that causes 1% of collapse risk in 50 years, an iterative procedure is followed. In the first iteration, collapse risk is calculated and if the risk is not equal to 1%, the 10th percentile collapse capacity is increased or decreased. The same procedure is repeated until the risk equals 1% in 50 years [22]. The final scaled 10th percentile collapse capacity is accepted to be the design acceleration value which gives a 1% of collapse probability in 50 years. A flowchart explaining this procedure is given below.

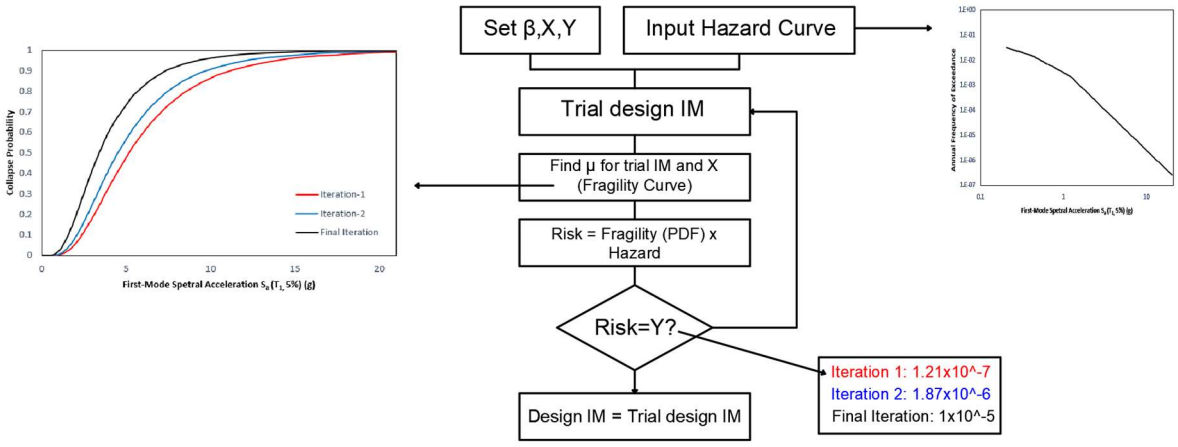

Figure 2.4. Flowchart to find risk-targeted design parameters.

2.4. FEMA P-695 Procedure

To develop a fragility curve and evaluate system behavior factor *R*, the procedure given by FEMA P-695 is followed in this study. Thus, the procedure is summarized in this chapter.

FEMA P-695 [3] procedure provides recommendations in the evaluation of some building behavior properties such as response modification coefficient, *R*, overstrength factor, Ω, and deflection amplification factor, C_d. This procedure utilizes nonlinear dynamic analysis to conduct Median Collapse Capacity, S_{CT}, and collapse margin ratio, *CMR* of the structure.

2.4.1. Median Collapse Capacity and Collapse Margin Ratio

The collapse capacity of the structure is obtained by using an incremental dynamic analysis strategy. After conducting IDA curves under each earthquake record, the median collapse capacity is determined. A median collapse capacity, or S_{CT}, is defined as an acceleration value that divides earthquake records based on that acceleration value into two equal parts: the records that the structure can resist collapse without collapsing, and the records that structure collapses.

The collapse margin ratio is a measure of safety against collapsing. It is the ratio between median collapse capacity and maximum considered earthquake (MCE) ground motion intensity, S_{MT}. Maximum considered earthquake, MCE is defined by codes with coefficients and map acceleration parameters according to the fundamental period of the structure. In the Turkish Seismic Code, MCE is equivalent to the acceleration value given for the DD1 ground motion level.

To illustrate an example, the following figure shows IDA curves of Building-1. Collapse is defined in terms of the maximum story drift ratio. The median collapse capacity of the structure is determined as 3.97g, which means under the effect of an earthquake record set scaled to 3.97g, half of the earthquake records cause the structure to reach the collapse

point. MCE ground motion intensity is 2.05g as shown in the following sections; therefore, *CMR* is calculated as *CMR*=3.97/2.05=1.94. The allowable value of *CMR* is defined by specification depending on total system collapse uncertainty.

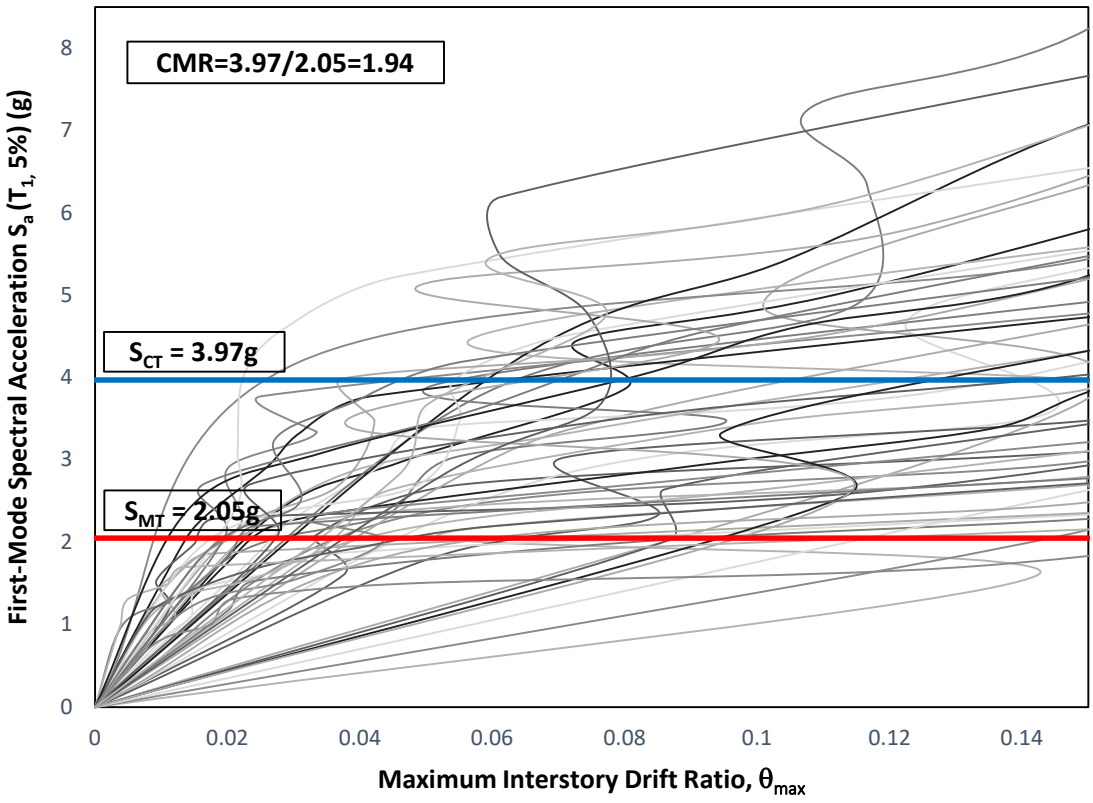

Figure 2.5. Determination of collapse margin ratio according to IDA.

2.4.2. Development of Fragility Curve

There are two parameters necessary for the construction of a fragility curve, which are median value and standard deviation.

The median value of a fragility function of a structure against collapse can be said to be equal to the median collapse capacity of that structure, corresponding to a 50% probability of collapse.

Some uncertainties in the analysis are reflected in the fragility curve by means of standard deviation value. The slope of the fragility curve is indicative of the standard deviation. To assess this value, the procedure categorizes uncertainties according to sources and assigns a value for each category. After all, it achieves standard deviation by combining each system uncertainty.

2.4.2.1. Record-to-record uncertainty, β_{RTR} This type of uncertainty is caused by both dynamic characteristics and frequency content of selected records and variations in hazard characteristics. For the record set employed in this study, this uncertainty is calculated as 0.37, 0.28 and 0.16 for Building-1, Building-2 and Building-3, respectively. The methodology assumes $\beta_{RTR} = 0.4$ for structures with period-based ductility, $\mu_T \geq 3$ based on studies conducted by Haselton and Baker, 2006 [23]; Ibarra and Krawinkler, 2005 [14] and Zareian, 2006 [24]. Thus, for all buildings, $\beta_{RTR} = 0.4$ is employed in this study.

2.4.2.2. Design requirements uncertainty, β_{DR} This type of uncertainty is relevant to the confidence in the design requirements and rated by Table 2.1 given in the specification.

Table 2.1. Rates of uncertainty in terms of confidence in design requirements [3].

COMPLETENESS & ROBUSTNESS	CONFIDENCE IN BASIS OF DESIGN REQUIREMENTS		
	HIGH	MEDIUM	LOW
HIGH Extensive safeguards against unanticipated failure modes. All important design and quality assurance issues are addressed.	(A) Superior β_{DR}=0.10	(B) Good β_{DR}=0.20	(C) Fair β_{DR}=0.35
MEDIUM Reasonable safeguards against unanticipated failure modes. Most of the important design and quality assurance issues are addressed.	(B) Good β_{DR}=0.20	(C) Fair β_{DR}=0.35	(D) Poor β_{DR}=0.50
LOW Questionable safeguards against unanticipated failure modes. Many important design and quality assurance issues are not addressed.	(C) Fair β_{DR}=0.35	(D) Poor β_{DR}=0.50	---

2.4.2.3. Test data uncertainty, β_{TD} This type of uncertainty is relevant to the confidence in the test results and rated by Table 2.2 given in the specification.

Table 2.2. Rates of uncertainty in terms of confidence in test results [3].

COMPLETENESS & ROBUSTNESS	CONFIDENCE IN TEST RESULTS		
	HIGH	MEDIUM	LOW
HIGH Material, component, connection, assembly, and system behavior well understood and accounted for. All, or nearly all, important testing issues addressed.	(A) Superior β_{TD}=0.10	(B) Good β_{TD}=0.20	(C) Fair β_{TD}=0.35
MEDIUM Material, component, connection, assembly, and system behavior generally understood and accounted for. Most important testing issues addressed.	(B) Good β_{TD}=0.20	(C) Fair β_{TD}=0.35	(D) Poor β_{TD}=0.50
LOW Material, component, connection, assembly, and system behavior fairly understood and accounted for. Several important testing issues not addressed.	(C) Fair β_{TD}=0.35	(D) Poor β_{TD}=0.50	---

2.4.2.4. Modeling uncertainty, β_{MDL} This type of uncertainty is relevant to the compatibility of structural model with the actual structural response characteristics and rated by Table 2.3 given in the specification.

Table 2.3. Rates of uncertainty in terms of accuracy of models [3].

REPRESENTATION of COLLAPSE CHARACTERISTICS	ACCURACY ROBUSTNESS OF MODELS		
	HIGH	MEDIUM	LOW
HIGH Index models capture the full range of the archetype design space and structural behavioral effects that contribute to collapse.	(A) Superior β_{MDL}=0.10	(B) Good β_{MDL}=0.20	(C) Fair β_{MDL}=0.35
MEDIUM Index models are generally comprehensive and representative of the design space and behavioral effects that contribute to collapse.	(B) Good β_{MDL}=0.20	(C) Fair β_{MDL}=0.35	(D) Poor β_{MDL}=0.50
LOW Significant aspects of the design space and/or collapse behavior are not captured in the index models.	(C) Fair β_{MDL}=0.35	(D) Poor β_{MDL}=0.50	---

2.4.2.5. Total system uncertainty, β_{TOT} It is a combination of all uncertainties. This value is the standard deviation of the lognormal cumulative distribution function (fragility function) and defined as

$$\beta_{TOT} = \sqrt{\beta_{RTR}^2 + \beta_{DR}^2 + \beta_{TD}^2 + \beta_{MDL}^2}\,. \tag{2.5}$$

2.4.3. Evaluation of Performance of Building

In the calculation of the Collapse Margin Ratio, *CMR*, a modification factor is used to consider spectral shape (frequency content) called Spectral Shape Factor, *SSF*. The spectral shape of rear earthquakes tends to have a peak in a narrow period range and decreases rapidly for longer or shorter periods, which is dissimilar to the design spectrum. Thus, if the building has enough ductility to oscillate and go through inelastic deformations, for periods other than the first period, only rare earthquakes give less damage to the structure than expected since ground motion intensities used in the analysis are determined according to fundamental period. To deal with this issue, different earthquake record sets should be chosen for each unique building depending on the period, soil class, and hazard level. Since buildings differ in numerous types, to overcome this situation, specification introduces a simplified procedure. Depending on the fundamental period, seismic design category, and ductility of the structure, the procedure gives *SSF*s to increase the collapse margin ratio or median collapse capacity of the structure. Table 2.4 shows spectral shape factors given for seismic design category SDC B, SDC C, SDC D_{min}, and SDC D_{max}.

Table 2.4. Spectral shape factor (SSF) for (a) SDC B, SDC C, or SDC D_{min}, (b) SDC D_{max} given by FEMA P-695 procedure [3].

(a)

T	PERIOD-BASED DUCTILITY, μ_T							
(sec.)	1.0	1.1	1.5	2	3	4	6	≥ 8
≤ 0.5	1.00	1.02	1.04	1.06	1.08	1.09	1.12	1.14
0.6	1.00	1.02	1.05	1.07	1.09	1.11	1.13	1.16
0.7	1.00	1.03	1.06	1.08	1.10	1.12	1.15	1.18
0.8	1.00	1.03	1.06	1.08	1.11	1.14	1.17	1.20
0.9	1.00	1.03	1.07	1.09	1.13	1.15	1.19	1.22
1.0	1.00	1.04	1.08	1.10	1.14	1.17	1.21	1.25
1.1	1.00	1.04	1.08	1.11	1.15	1.18	1.23	1.27
1.2	1.00	1.04	1.09	1.12	1.17	1.20	1.25	1.30
1.3	1.00	1.05	1.10	1.13	1.18	1.22	1.27	1.32
1.4	1.00	1.05	1.10	1.14	1.19	1.23	1.30	1.35
≥ 1.5	1.00	1.05	1.11	1.15	1.21	1.25	1.32	1.37

(b)

T	PERIOD-BASED DUCTILITY, μ_T							
(sec.)	1.0	1.1	1.5	2	3	4	6	≥ 8
≤ 0.5	1.00	1.05	1.10	1.13	1.18	1.22	1.28	1.33
0.6	1.00	1.05	1.11	1.14	1.20	1.24	1.30	1.36
0.7	1.00	1.06	1.11	1.15	1.21	1.25	1.32	1.38
0.8	1.00	1.06	1.12	1.16	1.22	1.27	1.35	1.41
0.9	1.00	1.06	1.13	1.17	1.24	1.29	1.37	1.44
1.0	1.00	1.07	1.13	1.18	1.25	1.31	1.39	1.46
1.1	1.00	1.07	1.14	1.19	1.27	1.32	1.41	1.49
1.2	1.00	1.07	1.15	1.20	1.28	1.34	1.44	1.52
1.3	1.00	1.08	1.16	1.21	1.29	1.36	1.46	1.55
1.4	1.00	1.08	1.16	1.22	1.31	1.38	1.49	1.58
≥ 1.5	1.00	1.08	1.17	1.23	1.32	1.40	1.51	1.61

The Adjust Collapse Margin Ratio (*ACMR*) employed in the evaluation is given as

$$ACMR = SSF \; x \; CMR. \tag{2.6}$$

For the evaluation of R factors, acceptable values of $ACMR$ based on system uncertainty are given in the methodology for different collapse probabilities such as 10% and 20%. In the methodology, it is suggested that collapse probability under the MCE record set should not exceed 10% based on engineering judgment for structures in concern designed according to the R factors given in the Code. Alternatively, validity of the R factor used in the design can be approved to be acceptable with the condition of

$$ACMR \geq ACMR10\% \,. \tag{2.7}$$

The values of $ACMR10\%$ depending on the system uncertainty is given below.

Table 2.5. "Acceptable values of adjusted collapse margin ratio (ACMR10% and ACMR20%)" [3].

TOTAL SYSTEM COLLAPSE UNCERTAINTY	COLLAPSE PROBABILITY				
	5%	10% ($ACMR_{10\%}$)	15%	20% ($ACMR_{20\%}$)	25%
0.275	1.57	1.42	1.33	1.26	1.20
0.300	1.64	1.47	1.36	1.29	1.22
0.325	1.71	1.52	1.40	1.31	1.25
0.350	1.78	1.57	1.44	1.34	1.27
0.375	1.85	1.62	1.48	1.37	1.29
0.400	1.93	1.67	1.51	1.40	1.31
0.425	2.01	1.72	1.55	1.43	1.33
0.450	2.10	1.78	1.59	1.46	1.35
0.475	2.18	1.84	1.64	1.49	1.38
0.500	2.28	1.90	1.68	1.52	1.40
0.525	2.37	1.96	1.72	1.56	1.42
0.550	2.47	2.02	1.77	1.59	1.45
0.575	2.57	2.09	1.81	1.62	1.47
0.600	2.68	2.16	1.86	1.66	1.50
0.625	2.80	2.23	1.91	1.69	1.52
0.650	2.91	2.30	1.96	1.73	1.55
0.675	3.04	2.38	2.01	1.76	1.58
0.700	3.16	2.45	2.07	1.80	1.60
0.725	3.30	2.53	2.12	1.84	1.63
0.750	3.43	2.61	2.18	1.88	1.66
0.775	3.58	2.70	2.23	1.92	1.69
0.800	3.73	2.79	2.29	1.96	1.72
0.825	3.88	2.88	2.35	2.00	1.74
0.850	4.05	2.97	2.41	2.04	1.77
0.875	4.22	3.07	2.48	2.09	1.80
0.900	4.39	3.17	2.54	2.13	1.83
0.925	4.58	3.27	2.61	2.18	1.87
0.950	4.77	3.38	2.68	2.22	1.90

3. METHODOLOGY

3.1. Building Information

Three different special concentrically braced frame buildings are investigated in this study. All the buildings have the same plan and section views with different building heights. There are 7 and 3 bays in the X and Y directions, respectively. All the bays have the same span length of 8 m. SCBFs are located at the perimeter of the buildings. In the X direction, 2x3 braced frames, and in the Y direction, 2x2 braced frames are designed based on earthquake demand calculated according to the Turkish Seismic Code [1] to resist lateral loads. Story height is 4 m for all buildings and building heights are 12 m (3-story), 24 m (6-story), and 36 m (9-story). Secondary beams are placed with 2 m spacing to transfer gravity loads. A 15 cm thick reinforced concrete slab is used as a diaphragm. Typical plan views and section views for Building-2 are given in the following figures. The other buildings have the same configuration except for story height.

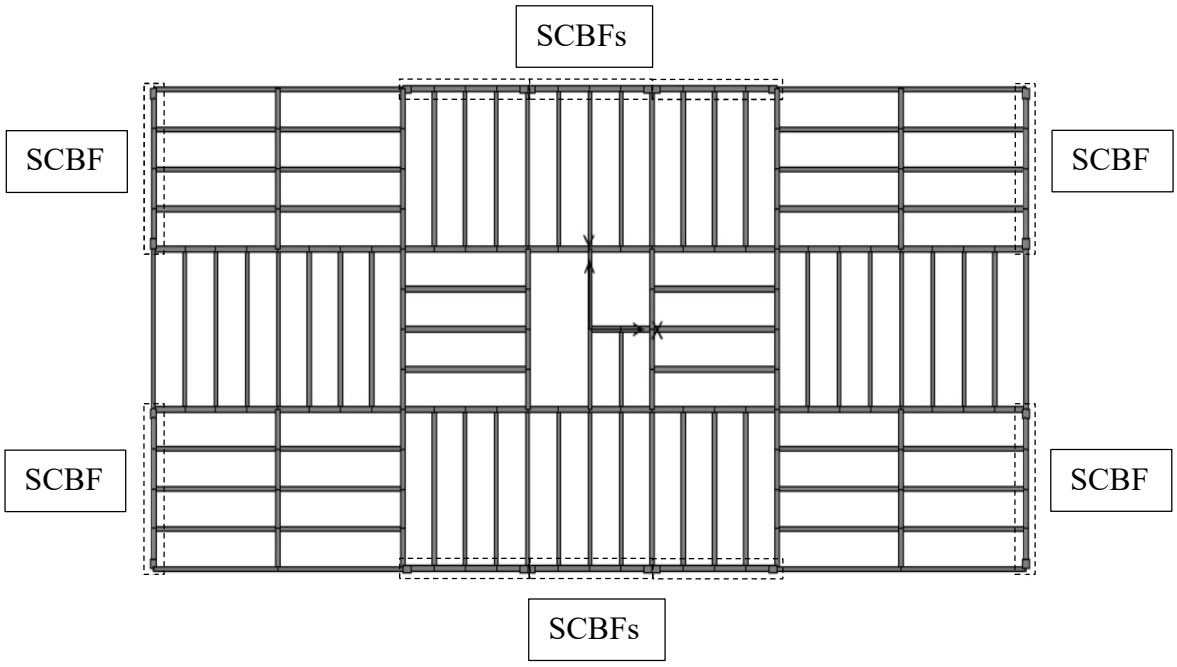

Figure 3.1. Typical plan view of buildings.

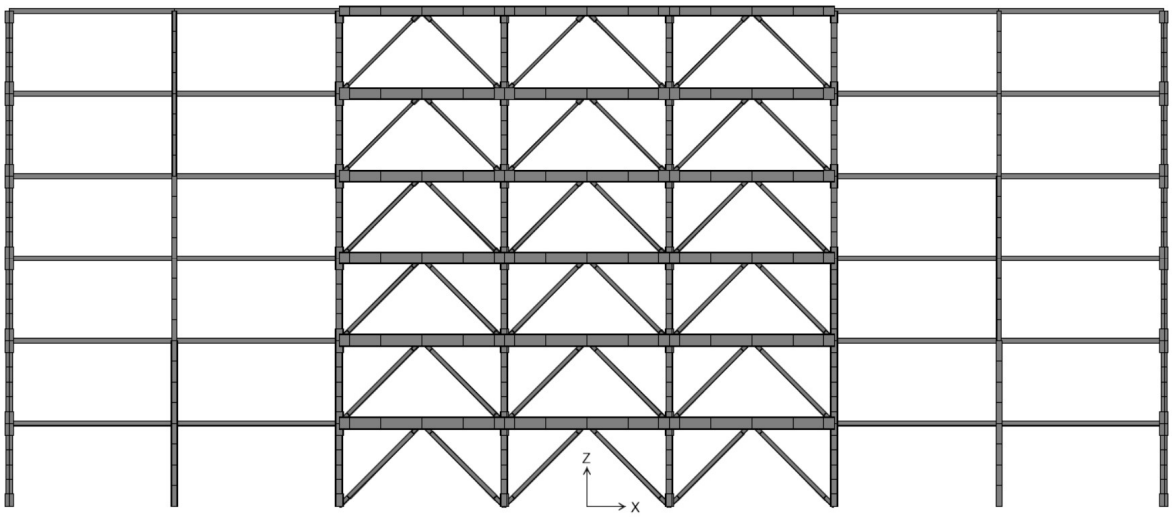

Figure 3.2. Section view of building-2 in X-direction.

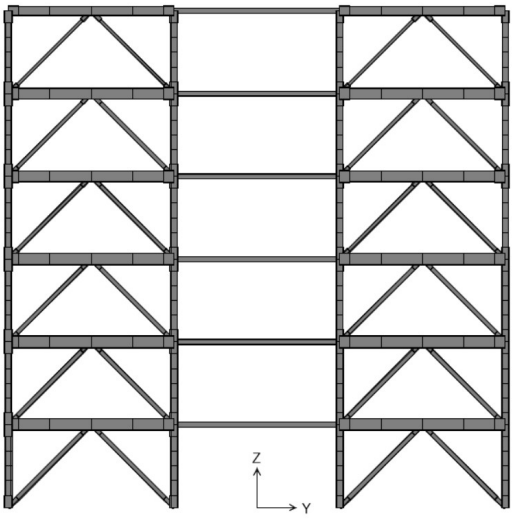

Figure 3.3. Section view of building-2 in Y-direction.

Since in practice, only braced frames are designed to resist lateral loads and other structural members are considered to resist only gravity loads, all the beams except braced frame beams are connected as a pinned connection. Columns except frame columns are designed as gravity columns with zero contribution to lateral loads. The connection of all columns to the base is designed as a pinned connection. A brace-to-beam and column connection is provided with fillet welds between the brace and gusset plate as a pinned

connection. Braces are designed to buckle out of the plane direction. A 2.5t allowance is supplied for the buckling area in the gusset plate. In Turkish Seismic Code Section 9.6.5 [1], the connection of the beam to the column in SCBFs can be applied as either a rigid connection or a simple connection. The connection of brace beams to columns is designed as a fully rigid connection since load transfer from only the beam web is quite hard because of the high unbalanced axial forces on beams and connections.

3.2. Linear Elastic Design

To determine the acting forces on structural members under gravity and seismic loads, CSI-SAP2000 software is utilized for linear elastic modeling of all buildings. Finite element method is utilized in this software to determine deformations and stresses on the members. Modal analysis is performed for all buildings to obtain the modal characteristics and periods of structures.

All the steel members are modeled with frame elements and the concrete slab is modeled with membrane (no bending rigidity) elements. Material properties and sections are introduced to software to calculate the stiffness matrix of the structure. Rigid end zones for frame beams, columns, and braces are modeled by dividing frame elements manually. End zone elements are modeled to have very large axial and bending stiffness properties. The length of the braces is taken as the actual length of the brace as shown in the following figure.

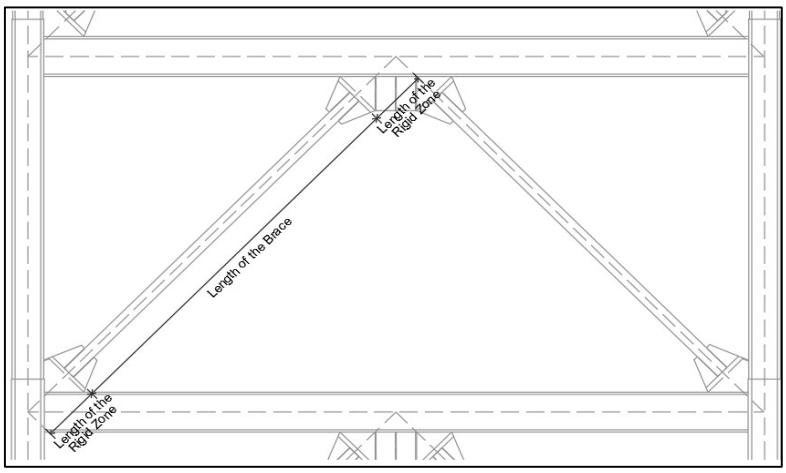

Figure 3.4. Considered length of the braces.

To transfer earthquake loads to braced frames rigid diaphragm is assigned to joints on each floor level. Secondary beams are included in the structural model. The rigidity of the connections is neglected, and connections are assumed as perfectly pinned or fully rigid. No modification to the stiffness properties of the structure is applied. Gravity forces on all the elements and axial forces on braces caused by seismic loads are obtained from this structural analysis.

3.2.1. Materials

Two different material grades are used in the design based on strength requirements: S275 and S355. 275 and 355 MPa of yielding strength and 430 and 510 MPa of ultimate strength is considered in the design for S275 and S355 materials, respectively. Elasticity modulus is taken as 200000 MPa and shear modulus is calculated for all members. The specific weight of steel members is taken as $\gamma_s = 77\ kN/m^3$ and the specific weight of the concrete slab is taken as $\gamma_c = 25\ kN/m^3$.

3.2.2. Gravity Loads

Gravity loads can be divided into three different actions, which are dead loads, superimposed dead loads, and live loads. Dead loads are calculated based on the specific weight of materials and included in the structural model implicitly. Superimposed dead loads are determined as 3.5 kN/m^2 considering weight of both architectural layers on slab and non-structural wall. Live loads are determined as 2 kN/m^2 considering building occupancy type as office according to TS498 [25].

3.2.3. Earthquake Loads

The buildings in concern are located in Avcılar, Istanbul. The soil class of the site is assumed to be ZC by considering soil conditions of the location. Seismic loads acting on the structure are determined according to the Turkish Seismic Code. Mapped values of short-period spectral acceleration, S_S, and 1-second spectral acceleration, S_1 are obtained from the TEHM website [4]. The response spectrum for the site is given in Figure 3.5 for the DD2

earthquake level. The equivalent seismic force approach is adopted in linear design. The structural behavior factor, *R*, and overstrength factor, *D* are taken as 5 and 2, respectively based on structural system type of buildings according to the code [1].

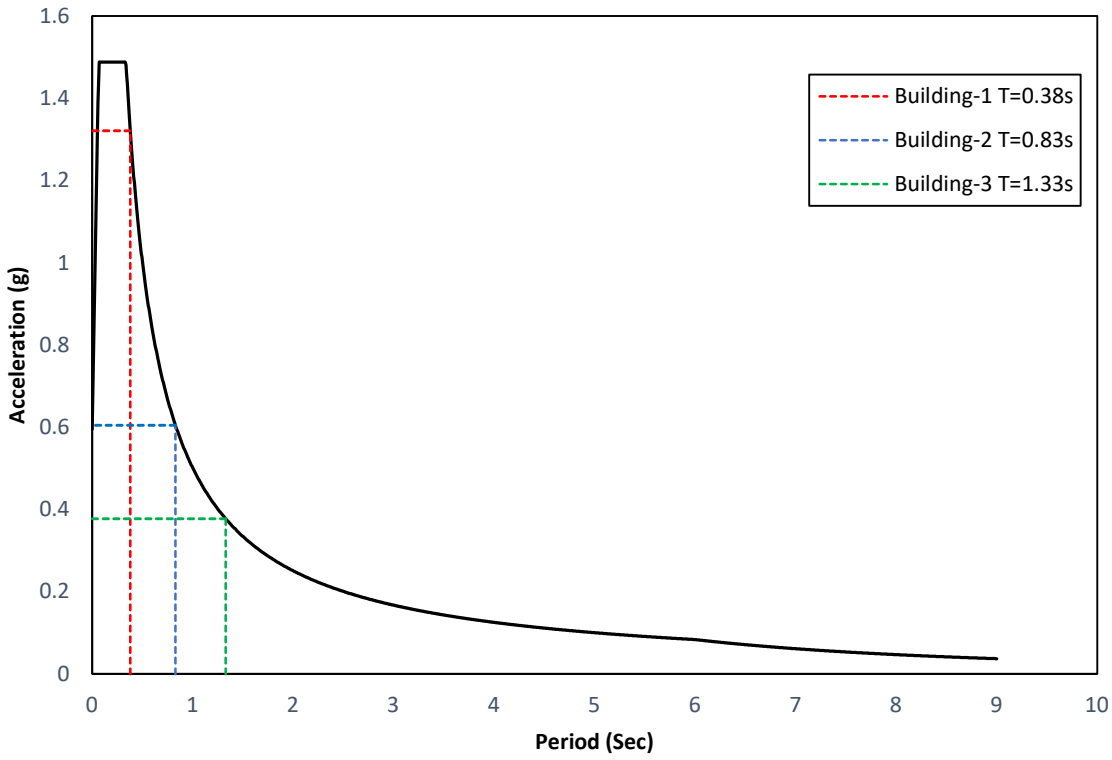

Figure 3.5. Elastic response spectrum for the site.

To consider the vertical impact of the earthquake, dead loads and superimposed dead loads are increased by 20% according to the code as

$$E_d^{(Z)} = \frac{2}{3} S_{DS} G. \tag{3.1}$$

All dead loads and superimposed dead loads are included in the seismic mass. Besides, 30 % of the live load is taken into consideration according to the TSC [1]. Seismic mass is modeled as lumped mass at the centroid of each story level. According to the Turkish Seismic Code, 5% modal damping is applied.

3.2.4. Determination of the Dimensions of Structural Members

3.2.4.1. Braces. Acting forces on braces are calculated from the combination of reduced earthquake forces and gravity forces. As a result of capacity design principles, the strength of braces specifies the dimensions of columns and beams. Thus, in common practice, the demand/capacity ratios of braces are kept high. In this study, this attitude is carried on. In the following tables, the dimensions of braces and the demand/capacity ratios are given for all three studied buildings.

Table 3.1. Demand/capacity ratios of braces for building-1.

STORY	X Direction		Y Direction	
	Section	D/C	Section	D/C
1	HSS190x190x12	0.98	HSS230x230x13	0.96
2	HSS160x160x13	1.00	HSS200x200x13	0.95
3	HSS130x130x12	1.00	HSS160x160x12	0.94

Table 3.2. Demand/capacity ratios of braces for building-2.

STORY	X Direction		Y Direction	
	Section	D/C	Section	D/C
1	HSS210x210x12	0.98	HSS210x210x13	1.00
2	HSS200x200x12	0.97	HSS200x200x13	0.99
3	HSS190x190x13	0.95	HSS190x190x13	1.00
4	HSS180x180x12	0.93	HSS180x180x13	0.98
5	HSS150x150x12	0.94	HSS160x160x12	0.97
6	HSS130x130x9	0.94	HSS130x130x12	0.96

Table 3.3. Demand/capacity ratios of braces for building-3.

STORY	X Direction		Y Direction	
	Section	D/C	Section	D/C
1	HSS210x210x12	0.95	HSS210x210x12	1.00
2	HSS200x200x12	0.95	HSS200x200x12	0.99
3	HSS190x190x13	0.96	HSS190x190x13	0.99
4	HSS190x190x13	0.94	HSS190x190x13	0.96
5	HSS180x180x13	0.95	HSS180x180x13	0.97
6	HSS170x170x13	0.94	HSS170x170x13	0.96
7	HSS150x150x13	0.97	HSS150x150x13	1.00
8	HSS140x140x12	0.91	HSS140x140x12	0.96
9	HSS120x120x10	0.93	HSS120x120x11	0.97

3.2.4.2. Beams. Seismic design forces of beams of SCBF are calculated from unbalanced forces at the middle of the beam due to buckling and post-buckling mechanisms of braces as shown in Figure 3.6. For dimensioning of the beams, brace strengths are determined with expected material strengths per TSC [1]. Finally, the gravity forces are added to those unbalanced forces. For performance evaluation of buildings, demand/capacity ratios are suggested to be high, which is taken into consideration. The material type used in the beams is S355. In the following tables, the dimensions of beams and demand/capacity ratios are given for all three buildings.

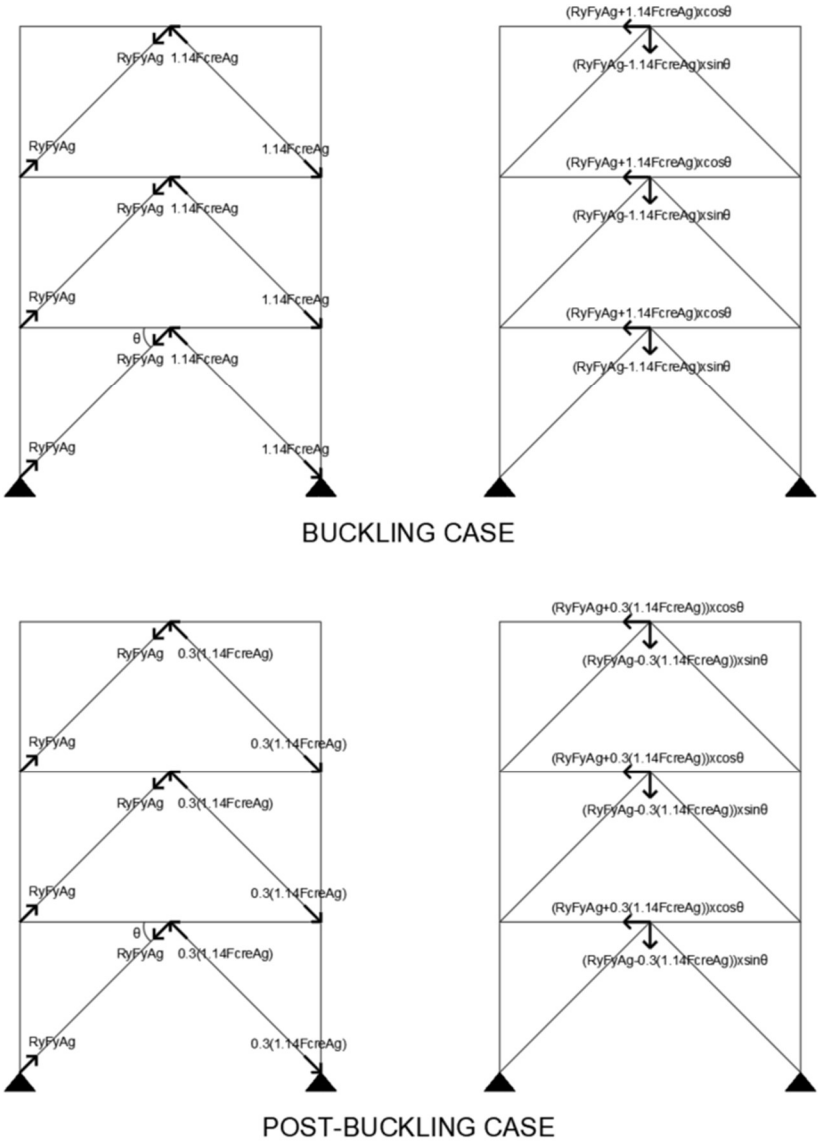

Figure 3.6. Acting forces on beams due to buckling and post-buckling mechanisms.

Table 3.4. Demand/capacity ratios of beams for building-1.

STORY	X Direction		Y Direction	
	Section	D/C	Section	D/C
1	HE 550 B	0.97	HE 650 B	0.94
2	HE 550 B	0.90	HE 600 B	0.94
3	HE 450 B	1.00	HE 500 B	0.98

Table 3.5. Demand/capacity ratios of beams for building-2.

STORY	X Direction		Y Direction	
	Section	D/C	Section	D/C
1	HE 600 B	0.92	HE 600 B	0.98
2	HE 600 B	0.89	HE 600 B	0.94
3	HE 600 B	0.90	HE 600 B	0.90
4	HE 550 B	0.93	HE 550 B	0.99
5	HE 550 B	0.80	HE 550 B	0.85
6	HE 450 B	0.82	HE 450 B	1.00

Table 3.6. Demand/capacity ratios of beams for building-3.

STORY	X Direction		Y Direction	
	Section	D/C	Section	D/C
1	HE 600 B	0.92	HE 600 B	0.92
2	HE 600 B	0.89	HE 600 B	0.89
3	HE 600 B	0.90	HE 600 B	0.90
4	HE 600 B	0.90	HE 600 B	0.90
5	HE 550 B	0.99	HE 550 B	0.99
6	HE 550 B	0.94	HE 550 B	0.94
7	HE 500 B	0.99	HE 500 B	0.99
8	HE 500 B	0.88	HE 500 B	0.88
9	HE 450 B	0.84	HE 450 B	0.89

3.2.4.3. Columns. In SCBF columns, the seismic design forces are calculated based on unbalanced forces caused by buckling and post-buckling mechanisms as shown in Figure 3.7. Brace strength is determined with expected material strengths according to TSC for column dimensioning. Gravity forces are then added to those unbalanced forces. The demand/capacity ratios of columns are determined to be high for collapse assessment. The material type used in the columns is S275 and S355. For all three buildings, the dimensions of columns and demands/capacity ratios are presented in the following tables.

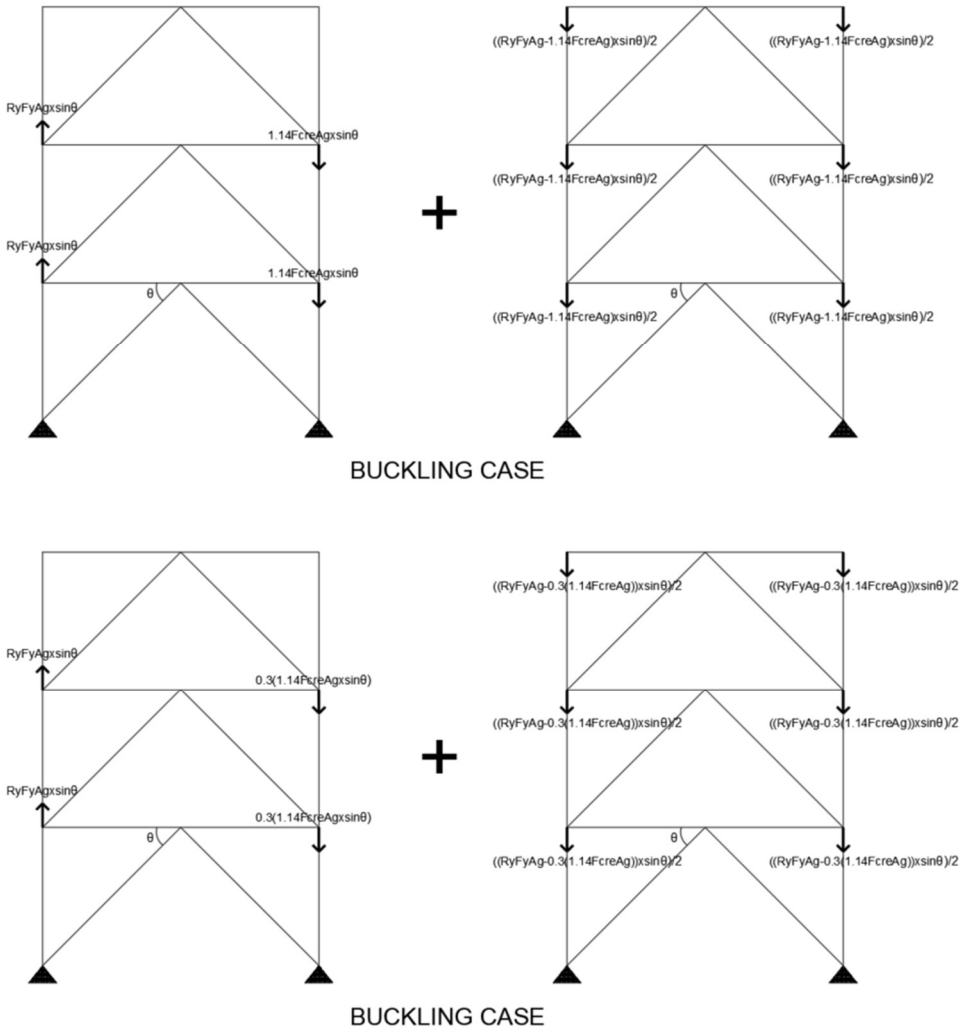

Figure 3.7. Acting forces on columns due to buckling and post-buckling mechanisms.

Table 3.7. Demand/capacity ratios of columns for building-1.

STORY	X Direction		Y Direction	
	Section	D/C	Section	D/C
1	HD 320 X 158	0.92	HD 320 X 158	0.96
2	HD 320 X 158	0.52	HD 320 X 158	0.52
3	HD 320 X 158	0.20	HD 320 X 158	0.19

Table 3.8. Demand/capacity ratios of columns for building-2.

STORY	X Direction		Y Direction	
	Section	D/C	Section	D/C
1	HD 320 X 300 (S355)	0.92	HD 320 X 300 (S355)	0.90
2	HD 320 X 245 (S355)	0.87	HD 320 X 245 (S355)	0.85
3	HD 320 X 198	0.95	HD 320 X 198	0.95
4	HD 320 X 127	0.93	HD 320 X 127	0.94
5	HD 320 X 127	0.52	HD 320 X 127	0.53
6	HD 320 X 127	0.20	HD 320 X 127	0.21

Table 3.9. Demand/capacity ratios of columns for building-3.

STORY	X Direction		Y Direction	
	Section	D/C	Section	D/C
1	HD 400 X 551	0.94	HD 400 X 509	0.99
2	HD 400 X 463	0.96	HD 400 X 463	0.93
3	HD 400 X 382	0.97	HD 400 X 382	0.94
4	HD 400 X 314	0.95	HD 400 X 287	1.00
5	HD 400 X 237	0.96	HD 400 X 237	0.93
6	HD 400 X 216	0.75	HD 400 X 187	0.84
7	HD 400 X 187	0.57	HD 400 X 187	0.55
8	HD 400 X 187	0.32	HD 400 X 187	0.32
9	HD 400 X 187	0.13	HD 400 X 187	0.13

3.2.5. Modal Analysis

Natural vibration periods and corresponding mode shapes are obtained by using Ritz vectors to prevent local modes. For two fundamental periods of the buildings are Tx=0.33s, Ty=0.38s for Building-1; Tx=0.61s, Ty=0.83s for Building-2; and Tx=0.91s, Ty=1.33s for Building-3. In the following figures, the first three modes and corresponding effective mass factors are given for all three building models. As given in the following tables, each building satisfies 95% of the mass participation requirement given by the TSC.

Table 3.10. Modal participation mass ratios for building-1.

Mode	Period	UX	UY	UZ	SumUX	SumUY	SumUZ	RX	RY	RZ	SumRX	SumRY	SumRZ
Number	Sec	Unitless	Unitless	Unitless	Unitless	Unitless	Unitless	Unitless	Unitless	Unitless	Unitless	Unitless	Unitless
1	0.44	8.48E-13	4.25E-16	3.26E-02	8.48E-13	4.25E-16	3.26E-02	1.01E-05	1.41E-05	4.99E-16	1.01E-05	1.41E-05	4.99E-16
2	0.44	3.37E-18	0.00E+00	3.19E-03	8.48E-13	4.25E-16	3.58E-02	1.23E-06	1.57E-06	0.00E+00	1.13E-05	1.56E-05	4.99E-16
3	0.44	4.21E-20	0.00E+00	9.50E-04	8.48E-13	4.25E-16	3.67E-02	3.73E-07	4.72E-07	3.68E-18	1.17E-05	1.61E-05	5.02E-16
4	0.38	6.54E-12	8.33E-01	3.91E-13	7.39E-12	8.33E-01	3.67E-02	2.12E-02	2.86E-14	2.49E-07	2.12E-02	1.61E-05	2.49E-07
5	0.35	2.49E-03	2.07E-12	4.76E-02	2.49E-03	8.33E-01	8.43E-02	3.43E-07	1.76E-01	1.84E-10	2.12E-02	1.76E-01	2.49E-07
6	0.35	4.20E-04	7.28E-10	2.82E-01	2.90E-03	8.33E-01	3.66E-01	5.43E-08	2.90E-02	7.83E-09	2.12E-02	2.05E-01	2.57E-07
7	0.35	7.79E-09	9.90E-04	1.06E-07	2.90E-03	8.34E-01	3.66E-01	1.37E-01	2.27E-07	1.28E-10	1.59E-01	2.05E-01	2.57E-07
8	0.34	3.00E-03	2.16E-08	2.50E-04	5.90E-03	8.34E-01	3.66E-01	2.08E-06	1.44E-01	6.61E-09	1.59E-01	3.49E-01	2.64E-07
9	0.34	6.93E-05	5.04E-07	3.43E-02	5.97E-03	8.34E-01	4.01E-01	2.90E-04	1.62E-03	6.12E-07	1.59E-01	3.51E-01	8.76E-07
10	0.34	3.03E-07	4.12E-03	8.15E-06	5.97E-03	8.38E-01	4.01E-01	1.52E-03	1.66E-06	2.70E-09	1.60E-01	3.51E-01	8.79E-07
11	0.34	6.05E-02	4.96E-08	5.60E-04	6.64E-02	8.38E-01	4.01E-01	3.22E-05	1.41E-03	6.63E-09	1.60E-01	3.52E-01	8.85E-07
12	0.34	1.35E-05	4.80E-04	2.97E-05	6.64E-02	8.39E-01	4.01E-01	5.20E-03	1.44E-05	2.12E-09	1.66E-01	3.52E-01	8.87E-07
13	0.34	8.02E-02	2.43E-07	4.70E-04	1.47E-01	8.39E-01	4.02E-01	3.30E-04	2.83E-02	9.14E-07	1.66E-01	3.80E-01	1.80E-06
14	0.34	1.47E-02	1.28E-05	2.62E-05	1.61E-01	8.39E-01	4.02E-01	2.83E-03	4.80E-04	1.24E-06	1.69E-01	3.81E-01	3.04E-06
15	0.34	9.17E-05	2.74E-03	3.21E-05	1.61E-01	8.42E-01	4.02E-01	2.13E-02	1.61E-05	5.28E-09	1.90E-01	3.81E-01	3.05E-06
16	0.34	1.20E-04	2.60E-04	2.30E-04	1.62E-01	8.42E-01	4.02E-01	8.12E-06	7.03E-05	2.04E-08	1.90E-01	3.81E-01	3.07E-06
17	0.34	2.20E-04	8.05E-07	1.75E-03	1.62E-01	8.42E-01	4.04E-01	6.16E-03	4.20E-04	1.56E-06	1.96E-01	3.81E-01	4.63E-06
18	0.33	7.16E-01	1.37E-11	7.02E-07	8.78E-01	8.42E-01	4.04E-01	3.07E-08	1.40E-04	5.83E-07	1.96E-01	3.82E-01	5.22E-06
19	0.32	9.14E-06	1.20E-10	8.74E-05	8.78E-01	8.42E-01	4.04E-01	1.76E-05	9.78E-02	9.99E-08	1.96E-01	4.79E-01	5.31E-06
20	0.32	1.20E-11	1.20E-04	8.29E-10	8.78E-01	8.42E-01	4.04E-01	9.33E-02	1.07E-07	3.88E-11	2.90E-01	4.79E-01	5.31E-06
21	0.32	4.56E-06	2.11E-14	1.33E-02	8.78E-01	8.42E-01	4.17E-01	3.02E-05	1.09E-03	1.28E-07	2.90E-01	4.80E-01	5.44E-06
22	0.31	1.84E-08	1.85E-12	1.45E-03	8.78E-01	8.42E-01	4.19E-01	7.30E-04	2.04E-02	2.62E-06	2.90E-01	5.01E-01	8.07E-06
23	0.31	8.59E-12	3.66E-09	5.62E-06	8.78E-01	8.42E-01	4.19E-01	1.15E-02	2.94E-05	7.67E-09	3.02E-01	5.01E-01	8.07E-06
24	0.31	1.22E-12	4.07E-09	2.32E-06	8.78E-01	8.42E-01	4.19E-01	2.97E-03	6.60E-06	2.97E-09	3.05E-01	5.01E-01	8.08E-06
25	0.29	7.33E-12	7.27E-16	2.60E-04	8.78E-01	8.42E-01	4.19E-01	1.58E-03	1.26E-03	1.72E-05	3.06E-01	5.02E-01	2.53E-05
26	0.29	2.84E-08	2.56E-12	1.30E-02	8.78E-01	8.42E-01	4.32E-01	1.80E-04	7.30E-04	3.19E-09	3.07E-01	5.03E-01	2.53E-05
27	0.28	1.10E-10	5.31E-11	3.80E-04	8.78E-01	8.42E-01	4.32E-01	7.67E-03	5.76E-06	2.51E-12	3.14E-01	5.03E-01	2.53E-05
28	0.27	4.99E-15	6.32E-19	4.64E-03	8.78E-01	8.42E-01	4.37E-01	2.74E-03	1.80E-04	2.05E-05	3.17E-01	5.03E-01	4.58E-05
29	0.25	1.65E-11	3.71E-13	1.84E-02	8.78E-01	8.42E-01	4.55E-01	3.10E-04	5.84E-06	1.25E-13	3.17E-01	5.03E-01	4.58E-05
30	0.24	5.06E-16	1.71E-18	1.91E-03	8.78E-01	8.42E-01	4.57E-01	1.30E-04	2.86E-05	1.61E-06	3.17E-01	5.03E-01	4.74E-05
31	0.22	7.80E-07	2.40E-07	1.45E-13	8.78E-01	8.42E-01	4.57E-01	9.05E-09	2.27E-09	8.46E-01	3.17E-01	5.03E-01	8.46E-01
32	0.14	7.75E-13	1.33E-01	6.01E-15	8.78E-01	9.75E-01	4.57E-01	1.21E-01	2.39E-13	3.26E-08	4.38E-01	5.03E-01	8.46E-01
33	0.13	1.00E-01	1.48E-12	5.68E-12	9.78E-01	9.75E-01	4.57E-01	8.52E-13	3.12E-02	1.63E-07	4.38E-01	5.34E-01	8.46E-01
34	0.10	5.04E-10	1.95E-06	2.63E-06	9.78E-01	9.75E-01	4.57E-01	1.20E-04	7.66E-07	1.31E-05	4.39E-01	5.34E-01	8.46E-01
35	0.10	7.29E-06	7.74E-09	3.59E-07	9.78E-01	9.75E-01	4.57E-01	6.32E-06	1.26E-05	2.28E-06	4.39E-01	5.34E-01	8.46E-01
36	0.10	3.87E-08	5.80E-06	1.16E-05	9.78E-01	9.75E-01	4.57E-01	6.69E-03	4.29E-06	9.48E-05	4.45E-01	5.34E-01	8.47E-01
37	0.09	2.28E-05	1.02E-07	1.13E-05	9.78E-01	9.75E-01	4.57E-01	2.87E-05	3.20E-04	4.72E-05	4.45E-01	5.35E-01	8.47E-01
38	0.09	9.58E-08	9.00E-04	2.19E-06	9.78E-01	9.76E-01	4.57E-01	6.30E-04	1.82E-06	5.84E-05	4.46E-01	5.35E-01	8.47E-01
39	0.09	1.98E-07	2.13E-02	6.36E-07	9.78E-01	9.98E-01	4.57E-01	1.65E-02	6.45E-06	1.67E-07	4.62E-01	5.35E-01	8.47E-01
40	0.09	1.61E-05	2.00E-04	2.84E-05	9.78E-01	9.98E-01	4.57E-01	3.30E-04	5.30E-04	5.20E-04	4.63E-01	5.35E-01	8.47E-01
41	0.08	1.98E-02	1.14E-12	4.33E-09	9.98E-01	9.98E-01	4.57E-01	3.59E-09	4.30E-03	3.41E-08	4.63E-01	5.39E-01	8.47E-01
42	0.06	4.00E-09	6.77E-07	5.00E-05	9.98E-01	9.98E-01	4.57E-01	1.29E-03	9.25E-08	4.70E-04	4.64E-01	5.39E-01	8.48E-01
43	0.06	1.64E-05	7.46E-10	1.67E-06	9.98E-01	9.98E-01	4.57E-01	3.77E-08	1.54E-02	4.59E-06	4.64E-01	5.55E-01	8.48E-01
44	0.05	9.33E-09	9.85E-06	4.55E-05	9.98E-01	9.98E-01	4.57E-01	5.12E-08	9.09E-06	4.12E-05	4.64E-01	5.55E-01	8.48E-01
45	0.04	4.70E-05	2.66E-08	5.64E-06	9.98E-01	9.98E-01	4.57E-01	6.95E-07	1.40E-04	8.08E-06	4.64E-01	5.55E-01	8.48E-01
46	0.03	4.69E-08	1.40E-04	4.55E-05	9.98E-01	9.98E-01	4.57E-01	3.30E-04	4.31E-06	6.40E-05	4.64E-01	5.55E-01	8.48E-01
47	0.02	8.83E-06	3.30E-04	4.42E-05	9.98E-01	9.98E-01	4.57E-01	9.40E-04	3.92E-06	4.21E-05	4.65E-01	5.55E-01	8.48E-01
48	0.02	2.00E-04	1.45E-05	1.54E-06	9.98E-01	9.98E-01	4.57E-01	7.14E-05	2.82E-09	1.61E-05	4.65E-01	5.55E-01	8.48E-01
49	0.01	5.90E-04	1.44E-07	6.69E-06	9.99E-01	9.98E-01	4.57E-01	3.72E-06	3.50E-04	4.23E-06	4.65E-01	5.55E-01	8.48E-01
50	0.01	2.02E-07	4.00E-04	5.17E-05	9.99E-01	9.99E-01	4.57E-01	9.56E-05	7.34E-06	6.65E-05	4.66E-01	5.55E-01	8.48E-01

Table 3.11. Modal participation mass ratios for building-2.

Mode	Period	UX	UY	UZ	SumUX	SumUY	SumUZ	RX	RY	RZ	SumRX	SumRY	SumRZ
Number	Sec	Unitless	Unitless	Unitless	Unitless	Unitless	Unitless	Unitless	Unitless	Unitless	Unitless	Unitless	Unitless
1	0.83	1.19E-12	7.56E-01	7.89E-20	1.19E-12	7.56E-01	7.89E-20	1.11E-01	5.01E-14	1.79E-07	1.11E-01	5.01E-14	1.79E-07
2	0.61	8.09E-01	2.87E-12	9.08E-14	8.09E-01	7.56E-01	9.08E-14	3.63E-13	3.19E-02	1.87E-06	1.11E-01	3.19E-02	2.05E-06
3	0.46	2.04E-06	1.62E-07	1.39E-11	8.09E-01	7.56E-01	1.40E-11	2.58E-08	7.59E-08	7.59E-01	1.11E-01	3.19E-02	7.59E-01
4	0.45	3.08E-10	6.54E-14	4.46E-02	8.09E-01	7.56E-01	4.46E-02	5.35E-06	1.27E-05	2.59E-10	1.11E-01	3.19E-02	7.59E-01
5	0.44	2.08E-15	0.00E+00	3.80E-03	8.09E-01	7.56E-01	4.84E-02	9.01E-07	1.63E-06	3.23E-13	1.11E-01	3.20E-02	7.59E-01
6	0.44	2.97E-19	0.00E+00	1.83E-03	8.09E-01	7.56E-01	5.02E-02	5.58E-07	1.94E-06	1.52E-09	1.11E-01	3.20E-02	7.59E-01
7	0.44	0.00E+00	0.00E+00	1.90E-04	8.09E-01	7.56E-01	5.04E-02	2.52E-10	2.06E-06	2.10E-08	1.11E-01	3.20E-02	7.59E-01
8	0.37	2.80E-04	2.80E-11	9.56E-02	8.10E-01	7.56E-01	1.46E-01	1.17E-07	1.55E-01	1.03E-09	1.11E-01	1.87E-01	7.59E-01
9	0.37	1.00E-04	1.50E-09	2.61E-01	8.10E-01	7.56E-01	4.07E-01	1.03E-06	5.56E-02	7.70E-10	1.11E-01	2.42E-01	7.59E-01
10	0.37	2.18E-09	4.60E-04	1.76E-06	8.10E-01	7.56E-01	4.07E-01	1.02E-01	1.27E-06	8.03E-07	2.12E-01	2.42E-01	7.59E-01
11	0.37	1.69E-09	1.60E-07	1.11E-05	8.10E-01	7.56E-01	4.07E-01	7.55E-06	1.13E-06	2.31E-03	2.12E-01	2.42E-01	7.62E-01
12	0.36	4.30E-05	8.69E-08	2.49E-02	8.10E-01	7.56E-01	4.32E-01	2.54E-06	7.56E-02	2.98E-09	2.12E-01	3.18E-01	7.62E-01
13	0.36	6.43E-05	5.25E-07	2.63E-02	8.10E-01	7.56E-01	4.58E-01	2.93E-06	8.10E-02	8.42E-09	2.12E-01	3.99E-01	7.62E-01
14	0.35	3.86E-08	1.36E-03	4.64E-05	8.10E-01	7.57E-01	4.58E-01	1.58E-05	1.04E-05	1.71E-09	2.12E-01	3.99E-01	7.62E-01
15	0.35	2.20E-04	1.71E-07	1.14E-02	8.10E-01	7.57E-01	4.69E-01	6.62E-07	3.03E-03	5.89E-07	2.12E-01	4.02E-01	7.62E-01
16	0.34	2.30E-04	2.10E-05	5.36E-03	8.10E-01	7.57E-01	4.75E-01	1.40E-04	3.00E-05	1.38E-06	2.13E-01	4.02E-01	7.62E-01
17	0.34	8.80E-06	3.40E-04	2.40E-04	8.10E-01	7.58E-01	4.75E-01	1.88E-03	1.90E-04	7.15E-06	2.14E-01	4.02E-01	7.62E-01
18	0.34	8.66E-07	1.30E-04	1.61E-05	8.10E-01	7.58E-01	4.75E-01	5.68E-03	3.80E-04	2.60E-05	2.20E-01	4.02E-01	7.62E-01
19	0.34	1.65E-03	1.90E-04	1.17E-07	8.12E-01	7.58E-01	4.75E-01	1.60E-04	1.39E-02	1.94E-07	2.20E-01	4.16E-01	7.62E-01
20	0.34	1.30E-04	2.50E-03	3.13E-07	8.12E-01	7.61E-01	4.75E-01	2.31E-03	1.11E-03	4.30E-08	2.23E-01	4.17E-01	7.62E-01
21	0.33	3.37E-05	5.61E-08	3.11E-05	8.12E-01	7.61E-01	4.75E-01	8.31E-07	7.08E-03	4.20E-06	2.23E-01	4.24E-01	7.62E-01
22	0.33	1.82E-10	9.50E-04	3.11E-08	8.12E-01	7.62E-01	4.75E-01	5.28E-02	1.75E-07	5.47E-09	2.75E-01	4.25E-01	7.62E-01
23	0.33	2.32E-06	9.40E-10	2.70E-04	8.12E-01	7.62E-01	4.75E-01	6.22E-06	1.22E-02	1.22E-05	2.75E-01	4.37E-01	7.62E-01
24	0.32	6.51E-06	2.59E-10	6.42E-03	8.12E-01	7.62E-01	4.82E-01	1.61E-06	1.50E-04	1.02E-06	2.75E-01	4.37E-01	7.62E-01
25	0.32	3.47E-11	5.94E-08	2.82E-06	8.12E-01	7.62E-01	4.82E-01	6.61E-03	1.00E-04	2.05E-06	2.82E-01	4.37E-01	7.62E-01
26	0.31	1.76E-13	1.92E-07	8.20E-07	8.12E-01	7.62E-01	4.82E-01	6.30E-04	7.81E-06	2.49E-07	2.83E-01	4.37E-01	7.62E-01
27	0.29	9.94E-07	9.62E-07	1.13E-02	8.12E-01	7.62E-01	4.93E-01	2.40E-04	4.30E-04	1.42E-09	2.83E-01	4.37E-01	7.62E-01
28	0.29	4.39E-12	1.72E-01	8.87E-08	8.12E-01	9.33E-01	4.93E-01	2.41E-01	3.29E-09	3.23E-08	5.24E-01	4.37E-01	7.62E-01
29	0.29	1.88E-08	1.72E-06	3.70E-04	8.12E-01	9.33E-01	4.94E-01	3.91E-03	1.23E-05	8.83E-11	5.28E-01	4.37E-01	7.62E-01
30	0.28	1.12E-11	2.83E-11	2.17E-03	8.12E-01	9.33E-01	4.96E-01	1.48E-05	8.10E-04	6.52E-07	5.28E-01	4.38E-01	7.62E-01
31	0.25	1.25E-09	1.08E-10	1.06E-02	8.12E-01	9.33E-01	5.06E-01	1.00E-04	8.77E-07	2.00E-12	5.28E-01	4.38E-01	7.62E-01
32	0.23	1.27E-01	8.41E-13	8.34E-10	9.39E-01	9.33E-01	5.06E-01	1.34E-11	8.55E-02	3.65E-07	5.28E-01	5.24E-01	7.62E-01
33	0.17	2.24E-07	5.00E-08	8.22E-10	9.39E-01	9.33E-01	5.06E-01	6.75E-08	1.34E-07	1.67E-01	5.28E-01	5.24E-01	9.28E-01
34	0.16	1.43E-13	4.14E-02	4.00E-13	9.39E-01	9.75E-01	5.06E-01	6.43E-02	1.34E-13	1.62E-08	5.93E-01	5.24E-01	9.28E-01
35	0.14	3.39E-02	3.32E-13	3.11E-11	9.73E-01	9.75E-01	5.06E-01	2.25E-13	1.87E-02	4.60E-08	5.93E-01	5.42E-01	9.28E-01
36	0.12	4.28E-12	6.08E-05	4.14E-07	9.73E-01	9.75E-01	5.06E-01	3.32E-03	1.91E-07	8.78E-09	5.96E-01	5.42E-01	9.28E-01
37	0.12	4.64E-13	1.41E-02	3.28E-09	9.73E-01	9.89E-01	5.06E-01	2.82E-02	1.98E-09	3.69E-09	6.24E-01	5.42E-01	9.28E-01
38	0.11	5.36E-06	9.77E-09	1.81E-05	9.73E-01	9.89E-01	5.06E-01	1.89E-05	9.71E-05	3.04E-07	6.24E-01	5.43E-01	9.28E-01
39	0.10	2.00E-04	1.32E-05	8.82E-06	9.73E-01	9.89E-01	5.06E-01	6.94E-03	7.85E-05	5.29E-07	6.31E-01	5.43E-01	9.28E-01
40	0.10	1.57E-02	1.77E-07	3.04E-07	9.89E-01	9.89E-01	5.06E-01	8.80E-05	1.05E-02	3.51E-08	6.31E-01	5.53E-01	9.28E-01
41	0.09	9.01E-10	6.81E-03	1.69E-08	9.89E-01	9.96E-01	5.06E-01	1.09E-02	2.91E-08	1.52E-08	6.42E-01	5.53E-01	9.28E-01
42	0.08	1.33E-03	5.22E-08	4.46E-05	9.90E-01	9.96E-01	5.06E-01	1.69E-06	1.70E-03	5.30E-05	6.42E-01	5.55E-01	9.28E-01
43	0.08	5.94E-03	5.70E-08	1.08E-05	9.96E-01	9.96E-01	5.06E-01	1.12E-07	2.60E-03	1.14E-05	6.42E-01	5.57E-01	9.28E-01
44	0.08	4.33E-08	2.73E-03	9.79E-09	9.96E-01	9.99E-01	5.06E-01	5.32E-03	2.08E-08	5.29E-08	6.47E-01	5.57E-01	9.28E-01
45	0.07	2.60E-03	1.28E-11	3.78E-07	9.99E-01	9.99E-01	5.06E-01	1.68E-09	1.05E-03	7.72E-07	6.47E-01	5.59E-01	9.28E-01
46	0.04	3.25E-09	1.21E-05	5.19E-06	9.99E-01	9.99E-01	5.06E-01	1.94E-03	4.90E-06	5.23E-05	6.49E-01	5.59E-01	9.28E-01
47	0.03	9.55E-05	3.47E-08	3.97E-06	9.99E-01	9.99E-01	5.06E-01	1.15E-09	2.13E-05	7.95E-09	6.49E-01	5.59E-01	9.28E-01
48	0.03	2.05E-08	2.60E-04	1.99E-06	9.99E-01	9.99E-01	5.06E-01	1.34E-03	1.77E-06	9.06E-06	6.51E-01	5.59E-01	9.28E-01
49	0.01	3.90E-04	1.78E-06	4.32E-06	9.99E-01	9.99E-01	5.06E-01	5.80E-09	2.10E-04	5.32E-07	6.51E-01	5.59E-01	9.28E-01
50	0.01	2.56E-06	2.70E-04	6.06E-06	9.99E-01	9.99E-01	5.06E-01	3.51E-05	1.18E-06	1.79E-05	6.51E-01	5.59E-01	9.28E-01

Table 3.12. Modal participation mass ratios for building-3.

Mode	Period	UX	UY	UZ	SumUX	SumUY	SumUZ	RX	RY	RZ	SumRX	SumRY	SumRZ
Number	Sec	Unitless	Unitless	Unitless	Unitless	Unitless	Unitless	Unitless	Unitless	Unitless	Unitless	Unitless	Unitless
1	1.33	7.04E-13	7.23E-01	0.00E+00	7.04E-13	7.23E-01	0.00E+00	1.81E-01	6.51E-14	1.50E-07	1.81E-01	6.51E-14	1.50E-07
2	0.91	7.87E-01	2.47E-12	4.11E-15	7.87E-01	7.23E-01	4.11E-15	6.63E-13	6.38E-02	3.18E-06	1.81E-01	6.38E-02	3.33E-06
3	0.72	3.50E-06	1.32E-07	1.09E-14	7.87E-01	7.23E-01	1.50E-14	4.07E-08	2.40E-07	7.36E-01	1.81E-01	6.38E-02	7.36E-01
4	0.45	1.06E-09	3.05E-10	6.48E-02	7.87E-01	7.23E-01	6.48E-02	2.23E-06	9.85E-06	4.29E-11	1.81E-01	6.38E-02	7.36E-01
5	0.45	1.74E-13	1.90E-01	2.46E-10	7.87E-01	9.14E-01	6.48E-02	2.76E-01	2.32E-14	2.88E-08	4.57E-01	6.38E-02	7.36E-01
6	0.44	5.87E-16	1.50E-17	3.85E-03	7.87E-01	9.14E-01	6.87E-02	5.48E-07	1.33E-06	3.19E-13	4.57E-01	6.38E-02	7.36E-01
7	0.44	2.07E-17	1.64E-20	1.27E-03	7.87E-01	9.14E-01	6.99E-02	2.25E-07	5.27E-07	7.23E-12	4.57E-01	6.38E-02	7.36E-01
8	0.40	6.30E-04	2.17E-11	3.27E-02	7.88E-01	9.14E-01	1.03E-01	2.53E-07	1.94E-01	5.19E-10	4.57E-01	2.58E-01	7.36E-01
9	0.39	6.05E-05	3.95E-09	3.39E-01	7.88E-01	9.14E-01	4.41E-01	2.71E-06	1.84E-02	5.30E-10	4.57E-01	2.76E-01	7.36E-01
10	0.38	6.79E-09	2.90E-04	6.09E-06	7.88E-01	9.14E-01	4.41E-01	9.62E-02	2.47E-06	9.19E-08	5.53E-01	2.76E-01	7.36E-01
11	0.38	5.92E-11	4.13E-08	1.94E-05	7.88E-01	9.14E-01	4.41E-01	4.59E-05	3.61E-05	7.90E-04	5.53E-01	2.76E-01	7.37E-01
12	0.37	2.80E-04	3.98E-09	9.42E-03	7.88E-01	9.14E-01	4.51E-01	1.83E-09	8.95E-02	1.14E-09	5.53E-01	3.66E-01	7.37E-01
13	0.37	1.30E-04	1.68E-07	3.51E-02	7.89E-01	9.14E-01	4.86E-01	2.12E-06	2.67E-02	1.60E-08	5.53E-01	3.92E-01	7.37E-01
14	0.37	2.60E-07	1.90E-04	7.79E-05	7.89E-01	9.14E-01	4.86E-01	1.78E-03	5.18E-06	1.28E-09	5.55E-01	3.92E-01	7.37E-01
15	0.37	1.07E-07	1.01E-09	2.76E-06	7.89E-01	9.14E-01	4.86E-01	1.40E-04	2.00E-04	4.66E-06	5.55E-01	3.93E-01	7.37E-01
16	0.36	1.61E-03	2.32E-08	1.22E-02	7.90E-01	9.14E-01	4.98E-01	7.68E-07	1.20E-04	2.95E-08	5.55E-01	3.93E-01	7.37E-01
17	0.35	3.23E-03	8.73E-07	8.37E-03	7.93E-01	9.14E-01	5.06E-01	2.34E-05	8.50E-04	2.29E-09	5.55E-01	3.94E-01	7.37E-01
18	0.35	9.61E-05	1.41E-05	1.83E-05	7.93E-01	9.14E-01	5.06E-01	8.59E-05	1.57E-05	4.59E-07	5.55E-01	3.94E-01	7.37E-01
19	0.34	2.33E-02	2.71E-06	1.00E-04	8.17E-01	9.14E-01	5.07E-01	2.40E-03	5.31E-02	1.48E-06	5.58E-01	4.47E-01	7.37E-01
20	0.34	7.91E-03	1.39E-05	7.80E-04	8.25E-01	9.14E-01	5.07E-01	8.07E-03	1.78E-02	2.13E-06	5.66E-01	4.65E-01	7.37E-01
21	0.34	5.10E-05	4.40E-04	3.26E-05	8.25E-01	9.15E-01	5.07E-01	5.60E-04	8.97E-05	1.25E-07	5.66E-01	4.65E-01	7.37E-01
22	0.34	3.83E-05	1.70E-04	1.09E-08	8.25E-01	9.15E-01	5.07E-01	8.15E-03	2.07E-05	1.09E-08	5.75E-01	4.65E-01	7.37E-01
23	0.33	1.00E-04	3.70E-06	3.40E-04	8.25E-01	9.15E-01	5.08E-01	1.12E-03	1.70E-05	1.24E-06	5.76E-01	4.65E-01	7.37E-01
24	0.33	2.84E-03	7.19E-10	2.90E-03	8.28E-01	9.15E-01	5.11E-01	5.30E-05	2.56E-03	1.57E-08	5.76E-01	4.67E-01	7.37E-01
25	0.32	9.64E-02	4.42E-12	1.50E-04	9.24E-01	9.15E-01	5.11E-01	2.49E-07	9.02E-02	4.52E-07	5.76E-01	5.57E-01	7.37E-01
26	0.32	5.03E-08	8.18E-07	2.97E-05	9.24E-01	9.15E-01	5.11E-01	5.95E-03	4.44E-05	9.95E-08	5.82E-01	5.57E-01	7.37E-01
27	0.31	1.46E-07	7.83E-09	1.60E-03	9.24E-01	9.15E-01	5.12E-01	3.94E-03	2.42E-03	3.94E-06	5.86E-01	5.60E-01	7.37E-01
28	0.30	1.73E-05	5.99E-09	8.58E-03	9.24E-01	9.15E-01	5.21E-01	2.40E-04	7.60E-05	1.91E-08	5.86E-01	5.60E-01	7.37E-01
29	0.29	4.38E-07	3.24E-08	7.10E-04	9.24E-01	9.15E-01	5.22E-01	2.25E-03	2.92E-05	9.89E-09	5.88E-01	5.60E-01	7.37E-01
30	0.26	8.04E-12	1.98E-10	7.13E-03	9.24E-01	9.15E-01	5.29E-01	9.14E-06	8.11E-05	4.03E-06	5.88E-01	5.60E-01	7.37E-01
31	0.25	4.03E-07	3.98E-08	9.21E-08	9.24E-01	9.15E-01	5.29E-01	6.44E-08	4.91E-07	1.75E-01	5.88E-01	5.60E-01	9.12E-01
32	0.24	9.05E-14	4.58E-02	1.94E-11	9.24E-01	9.61E-01	5.29E-01	9.07E-02	5.93E-13	8.06E-09	6.79E-01	5.60E-01	9.12E-01
33	0.19	3.75E-02	2.35E-13	6.31E-11	9.62E-01	9.61E-01	5.29E-01	1.41E-13	3.23E-02	9.62E-08	6.79E-01	5.92E-01	9.12E-01
34	0.17	5.54E-14	1.83E-02	2.55E-12	9.62E-01	9.79E-01	5.29E-01	4.41E-02	2.59E-11	4.01E-09	7.23E-01	5.92E-01	9.12E-01
35	0.15	6.89E-08	5.13E-07	4.48E-05	9.62E-01	9.79E-01	5.29E-01	2.69E-03	2.40E-05	1.91E-05	7.26E-01	5.92E-01	9.12E-01
36	0.14	3.57E-06	2.02E-06	1.39E-05	9.62E-01	9.79E-01	5.29E-01	1.91E-03	4.60E-04	2.96E-09	7.27E-01	5.93E-01	9.12E-01
37	0.13	1.68E-02	2.88E-09	8.79E-09	9.78E-01	9.79E-01	5.29E-01	5.11E-07	1.97E-02	7.38E-08	7.27E-01	6.13E-01	9.12E-01
38	0.13	4.43E-09	9.34E-03	4.05E-09	9.78E-01	9.88E-01	5.29E-01	2.11E-02	5.14E-07	6.26E-08	7.49E-01	6.13E-01	9.12E-01
39	0.11	7.48E-05	4.72E-03	1.17E-06	9.78E-01	9.93E-01	5.29E-01	1.04E-02	1.30E-04	7.56E-07	7.59E-01	6.13E-01	9.12E-01
40	0.11	9.12E-03	5.58E-05	1.18E-07	9.88E-01	9.93E-01	5.29E-01	1.60E-04	8.57E-03	9.71E-08	7.59E-01	6.21E-01	9.12E-01
41	0.10	2.20E-04	1.25E-03	3.18E-05	9.88E-01	9.94E-01	5.29E-01	5.17E-03	2.59E-05	1.34E-05	7.64E-01	6.21E-01	9.12E-01
42	0.09	2.41E-03	1.25E-03	4.38E-06	9.90E-01	9.95E-01	5.29E-01	2.45E-03	3.00E-03	1.69E-06	7.67E-01	6.24E-01	9.12E-01
43	0.09	2.46E-03	1.44E-03	1.28E-05	9.93E-01	9.97E-01	5.29E-01	2.33E-03	3.49E-03	3.02E-06	7.69E-01	6.28E-01	9.12E-01
44	0.08	2.16E-03	5.80E-04	1.94E-06	9.95E-01	9.97E-01	5.29E-01	1.41E-03	1.18E-03	5.03E-07	7.71E-01	6.29E-01	9.12E-01
45	0.07	7.90E-04	1.24E-03	5.21E-06	9.96E-01	9.99E-01	5.29E-01	3.64E-03	4.30E-04	1.30E-06	7.74E-01	6.29E-01	9.12E-01
46	0.07	2.22E-03	1.00E-04	5.79E-06	9.98E-01	9.99E-01	5.29E-01	1.80E-04	3.08E-03	9.20E-07	7.74E-01	6.32E-01	9.12E-01
47	0.05	9.40E-04	5.75E-06	1.10E-05	9.99E-01	9.99E-01	5.29E-01	2.14E-06	8.00E-04	8.33E-07	7.74E-01	6.33E-01	9.12E-01
48	0.03	7.95E-06	1.00E-04	2.25E-05	9.99E-01	9.99E-01	5.29E-01	2.57E-05	7.30E-04	1.39E-06	7.74E-01	6.34E-01	9.12E-01
49	0.02	8.85E-05	3.00E-04	2.18E-05	9.99E-01	9.99E-01	5.29E-01	1.38E-03	1.50E-04	2.18E-06	7.76E-01	6.34E-01	9.12E-01
50	0.02	2.80E-04	9.64E-05	1.45E-06	9.99E-01	9.99E-01	5.29E-01	5.70E-04	9.90E-04	3.97E-09	7.76E-01	6.35E-01	9.12E-01

Effective Mass Factor: 0.83 (Y Direction)

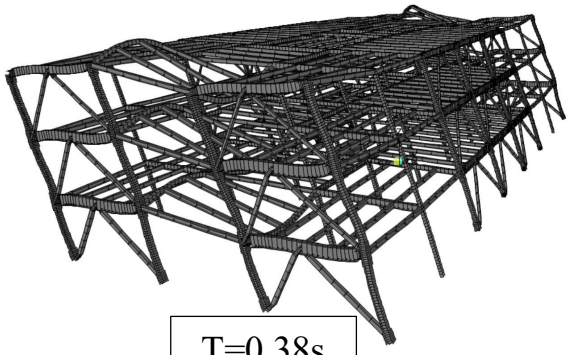

Effective Mass Factor: 0.72 (X Direction)

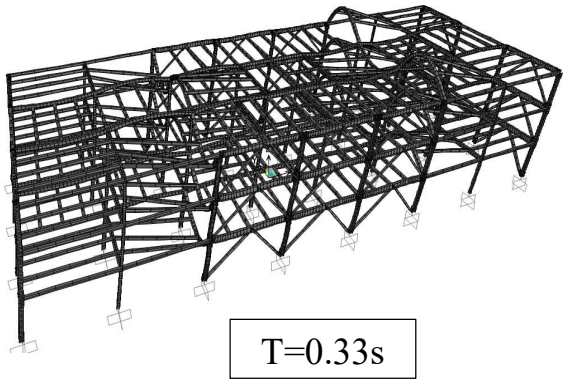

Effective Mass Factor: 0.85 (Torsion)

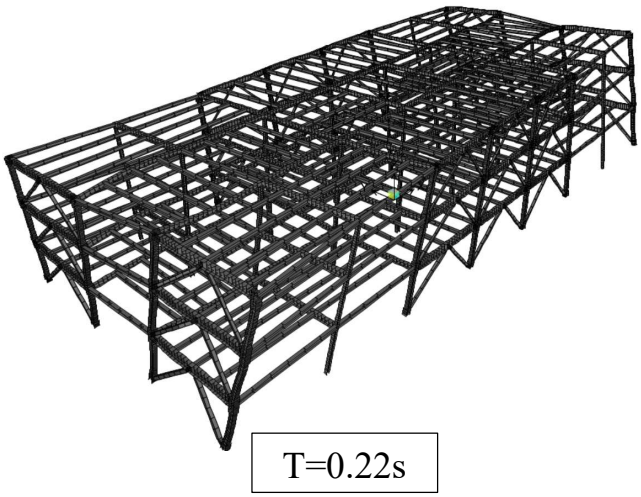

Figure 3.8. Three major modes of building-1.

Effective Mass Factor: 0.76 (Y Direction)

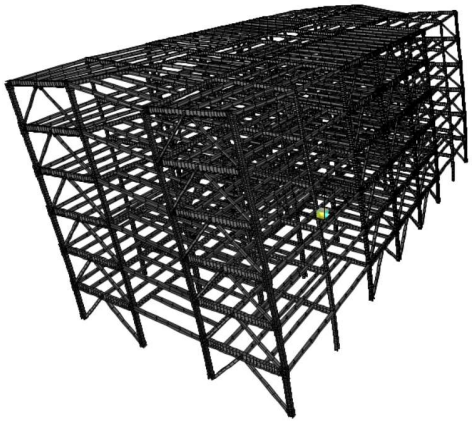

T=0.83s

Effective Mass Factor: 0.81 (X Direction)

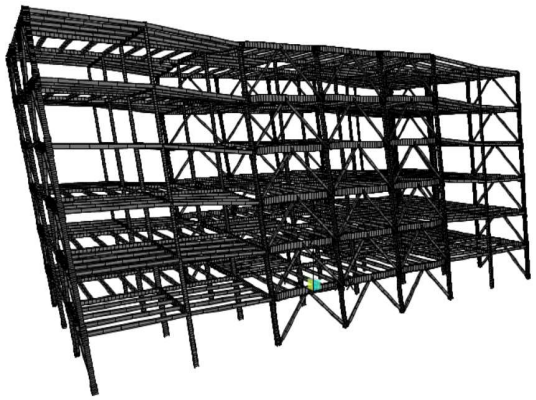

T=0.61s

Effective Mass Factor: 0.76 (Torsion)

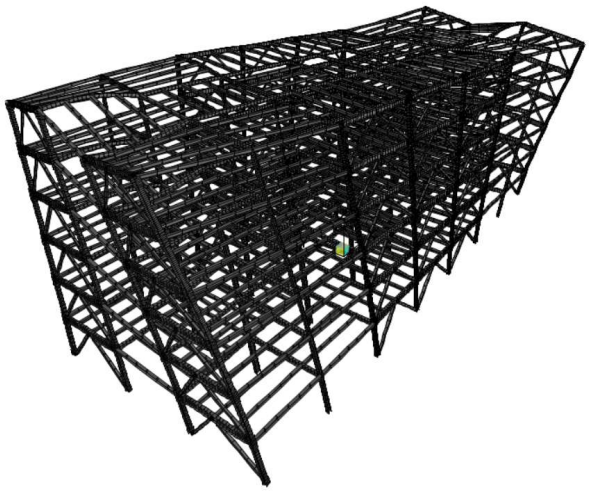

T=0.46s

Figure 3.9. Three major modes of building-2.

Effective Mass Factor: 0.72 (Y Direction)

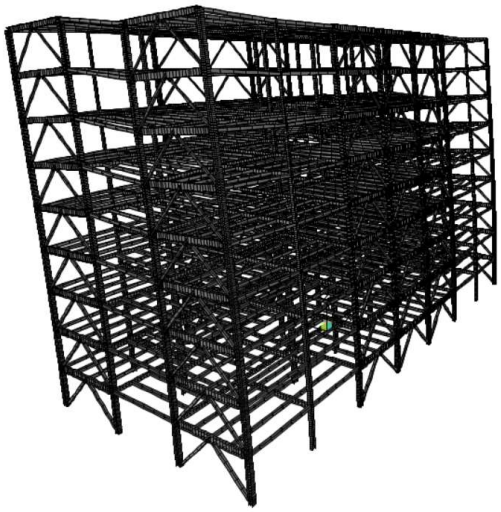

T=1.33s

Effective Mass Factor: 0.79 (X Direction)

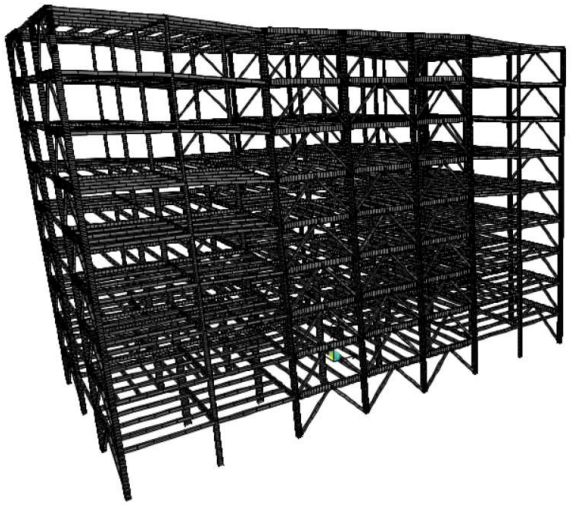

T=0.91s

Effective Mass Factor: 0.74 (Torsion)

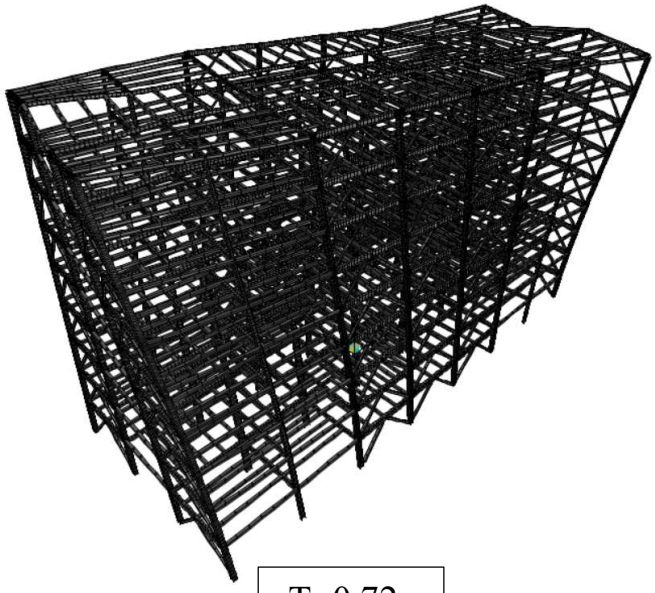

T=0.72s

Figure 3.10. Three major modes of building-3.

3.3. Nonlinear Analysis Model

Since it is more stable software for collapse analysis and mostly does not have convergence problems when we compare other nonlinear structural analysis software, CSI-PERFORM 3D [26] is utilized for the nonlinear analysis of structures.

All the members contributing to the seismic resistance of the structure should be included in the structural model. However, nonlinear analysis is a quite computationally time-consuming process. Therefore, some simplifications are applied for large scaled structural models such as excluding secondary beams from the structural model and instead considering only the weights of these beams.

In this study, three different buildings are analyzed with increasing earthquake demand until the collapse occurs for each, separately. For computational efficiency, each building is modeled and analyzed in two dimensions considering the fundamental period and critical direction only. Since the modes of each structure are almost uncoupled which means the first mode is triggered by pure movement in the Y direction with negligible effect of the X direction and the same with the second mode, the results of modal and linear analysis differ slightly. A comparison of fundamental periods obtained from linear and nonlinear analysis models for each building is given in Section 3.4. Besides, this 2D modeling approach is thought to give more realistic results since scaling of earthquake records and development of fragility curve is performed according to the fundamental period only in the procedure followed by FEMA-P695.

In the 2D modeling approach, the earthquake characteristics of each building are represented by a concentrically braced frame and a P-Delta column. Figure 3.11 shows the 2D frame model of Building-2 as an example. Since the first mod is in the Y direction, SCBF in this direction is modeled with a P-Delta column which is not fixed at the base.

The P-Delta column is intended to transfer the additional moment caused by the mass of the structure times lateral deformation to the main lateral load-resisting system. To include P-Delta analysis of the whole structure, the P-Delta column is modeled with an elastic bar

element having no lateral resistance. Equal displacement is given to the end of the elastic bar element and the left column of the frame at each story level. Section property of the elastic bar element is determined such that it is not exposed to excessive vertical deformation for the accuracy of the analysis. Since there are four SCBFs in the Y direction, a fourth of the seismic weight of the structure is applied at the end joints of elastic bar elements as point loads in order to consider P-Delta effects.

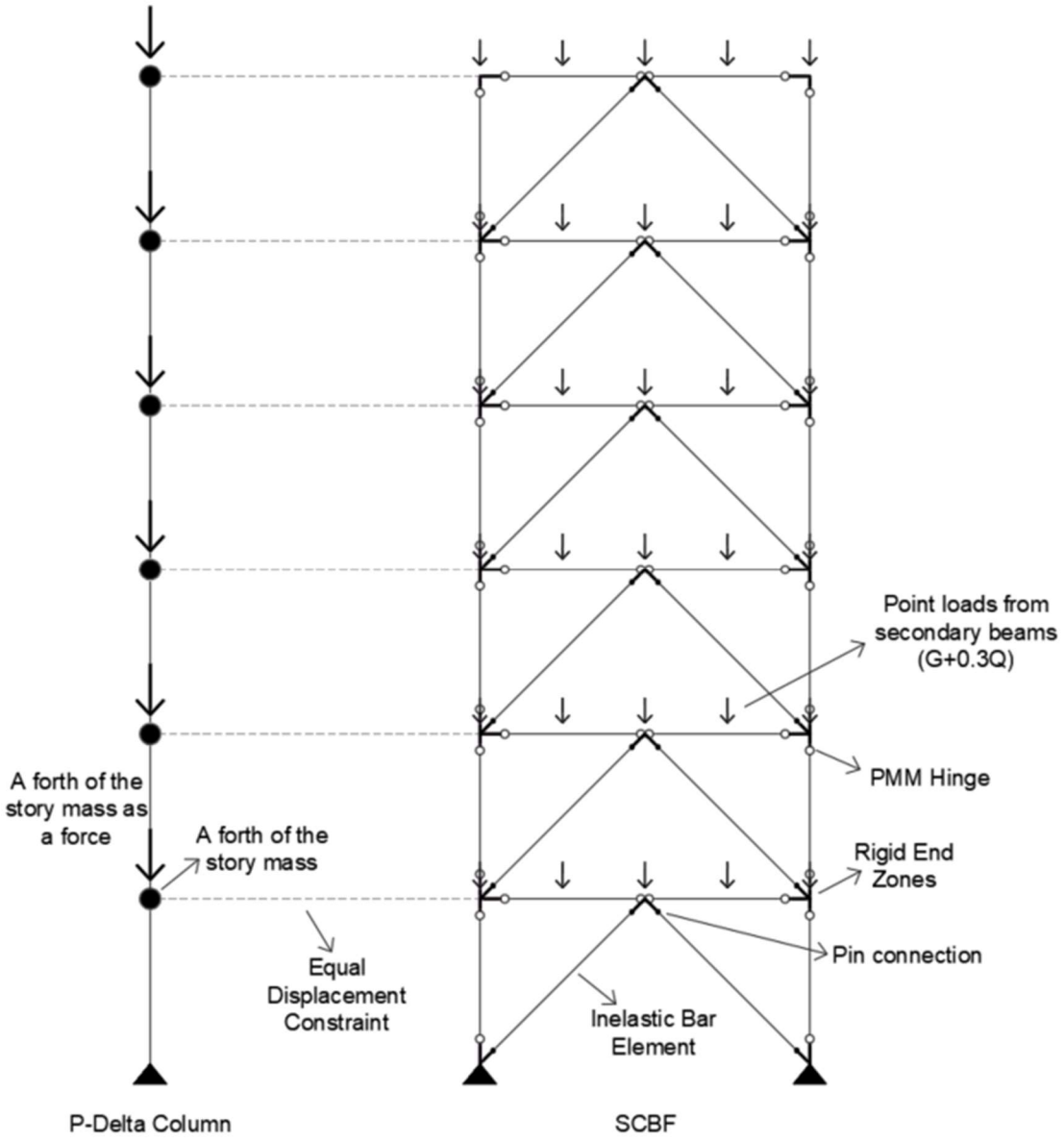

Figure 3.11. 2D model of building-2.

When a brace is designed such that buckling occurs out-of-plane direction, the in-plane deformation of the gusset plate remains so small. To represent this rigidity, three different rigid end zones are defined. The first one starts from the working point and extends to starting of the brace member. The second one starts from the working point and extends to the end of the gusset plate along the column direction, and to allow some limited deformation within the rigid zone, the third one starts from the working point and extends to 75% of the gusset plate length along the beam direction. This limited deformation in-plane direction results from diagonal stress fields. This modeling approach proposed by Hsiao et al. (2012, 2013a) [27] matches best with experiment results performed in a research program started at the University of Washington in 2005.

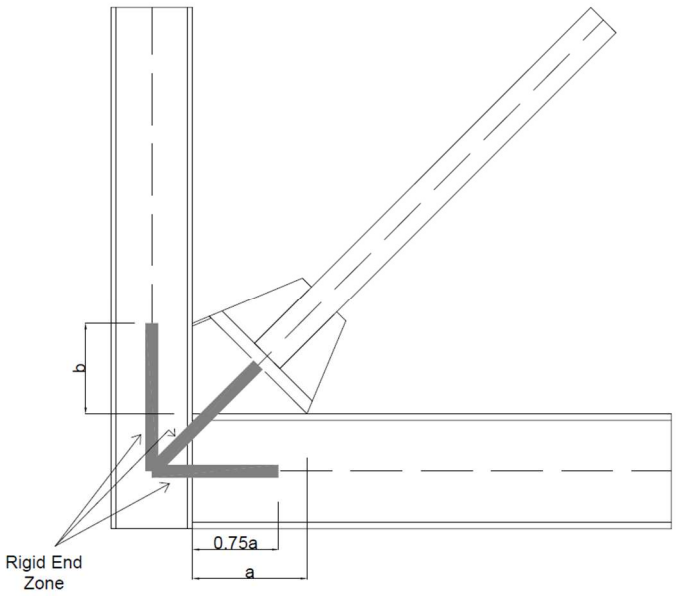

Figure 3.12. Connection detail identifying rigid zone lengths (Hsiao et al. 2012).

3.3.1. Materials

According to the Turkish Seismic Code, for the design of new buildings, expected material strengths shall be used in nonlinear structural analysis. The following table shows the expected material strengths of the structural steel material grades taken from the TSC [1]. Elasticity and shear modulus properties of materials remain the same.

Table 3.13. Structural steel expected strengths [1].

Structural Steel Grade	Expected Material Strength (Mpa)
S235	352.5
S275	357.5
S355	390.5

3.3.2. Gravity Loads

In the analysis model, acting gravity forces on SCBF are applied as point loads at the joints which secondary beams are connected to. Before seismic analysis, a nonlinear static analysis is performed to analyze the earthquake behavior of the deformed structure under gravity loads. The load combination to be used in nonlinear static analysis is compatible with the definition of the seismic mass.

3.3.3. Earthquake Loads

Seismic load acting on the structures is defined via earthquake records. After the static nonlinear analysis, a nonlinear time history analysis is adopted. For each building, 22 earthquake records are employed per direction. Since the 2D modeling approach is adopted, earthquake records in both directions are applied to the structure separately as a different record according to the FEMA P-695. In other words, for each building, 44 different earthquake records are applied to the structure.

Collapse analysis of the structures is performed according to DD1 level earthquake, mentioned as the maximum considered earthquake in this study. Maximum considered earthquake is defined as an earthquake level of 2% exceedance probability in 50 years with a return period of 2475 years.

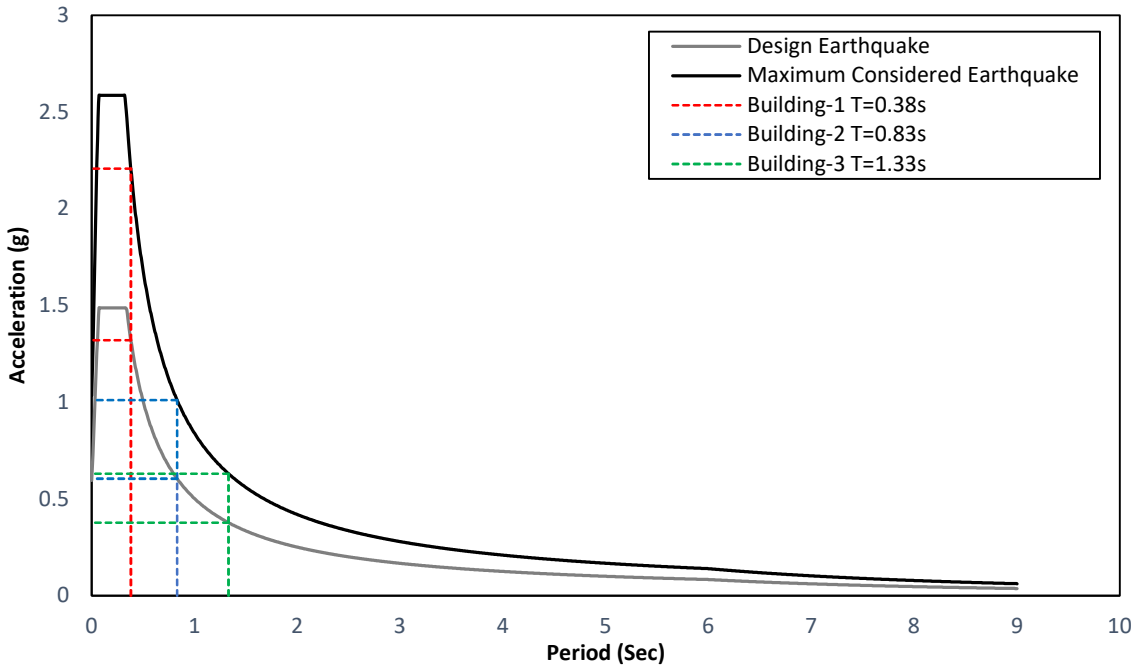

Figure 3.13. Design and maximum considered earthquake (DD-1) elastic response spectrums.

Selection and scaling of earthquake records are given in detail in Section 3.5.

3.3.4. Seismic Mass

The components of seismic mass in nonlinear modeling are the same in linear modeling that is all of the dead and super dead loads with some portion of the live load. According to the Turkish Seismic Code, the live load participation factor shall be taken as 0.3.

Since there are four SCBFs in the Y direction, seismic mass is divided into four for the 2D structural model and defined as joint mass at the ends of P-Delta columns at every story level.

3.3.5. Damping

According to the TSC, 5% modal damping is assumed for all modes. In Perform 3D, if only modal damping is utilized in the analysis, many displaced shapes remain undamped

because modal damping applies only defined mode shapes [26]. Even if a limited number of mode shapes are defined, many other remains to exist in the analysis. Thus, to ensure the damping of these higher modes, and sake of the analysis, a small amount of Rayleigh damping is additionally employed in the analysis.

3.3.6. Modeling of Structural Members

To reduce computational demands, secondary beams and gravity columns are assumed to remain elastic and the contribution of these members to the capacity of the structure is neglected. Thus, the only lateral load-resisting system in which nonlinear deformations are expected is SCBF included in the structural model as shown in Figure 3.11.

According to ASCE 41-17 [28], actions are classified as force-controlled and deformation-controlled actions. Force-controlled actions are defined for actions that acceptance criteria and component testing are not specified in the standard. For deformation-controlled actions, the standard defines a generalized force-deformation relationship given in Figure 3.14 and designates each parameter in this relationship depending on the member type. Parameters a, b and c indicate total plastic deformation without strength loss, total deformation and residual strength, respectively. In this study, only deformation-controlled actions are defined for the members of concentrically braced frames based on the ASCE 41-17 [28].

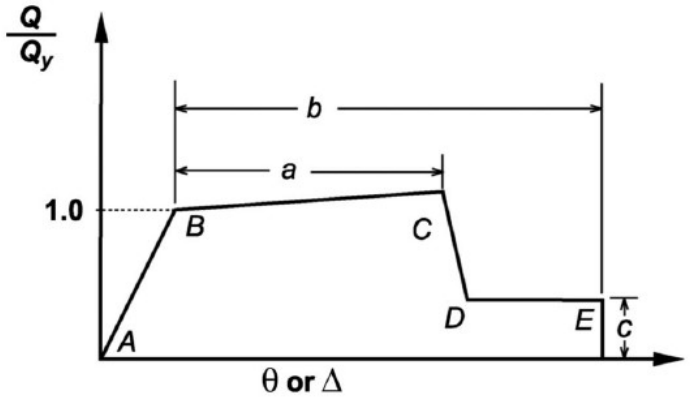

Figure 3.14. Generalized force-deformation relation for steel elements or component according to the ASCE 41-17 [28].

3.3.6.1. Braces. In special concentrically braced systems, the most nonlinearity is expected to occur in the braces. Under earthquake loading, braces dissipate energy by yielding under tensile loads and buckling under compressive loads. To observe this behavior on braces, inelastic bar elements are introduced in Perform 3D model.

For inelastic bar elements, a backbone curve is developed according to ASCE 41-17. The yielding deformation of the braces under compressive is determined by

$$\Delta_c = \frac{P_c L}{EA}, \tag{3.2}$$

and under tensile stresses is determined by

$$\Delta_T = \frac{P_T L}{EA}. \tag{3.3}$$

The yielding deformation is represented by Δ_c and Δ_T, while the compressive and tensile strengths are represented by P_c and P_T, respectively, and the elasticity modulus, the area of the section, and the length of the member are represented by E, A, and L.

The yielding strength of members under compressive is determined by

$$P_c = min\left(1.14 F_{CRE} A, R_y F_y A\right), \tag{3.4}$$

and tensile stresses is determined by

$$P_T = R_y F_y A, \tag{3.5}$$

where F_{CRE}, R_y and F_y refer to expected critical buckling strength, the ratio between expected yield strength to characteristic yield strength, and the characteristic yield strength, respectively. According to the Turkish seismic code, the value of R_y is taken as 1.3 and 1.1 for S275 and S355 material grades, respectively.

Parameters to define the force-deformation relation of braces change according to the slenderness of the brace sections. To illustrate an example, calculated parameters of Figure 3.14, and developed backbone curve is given below for HSS210X210X13 section in the first story. The parameters of a, b and c are given in ASCE 41-17 for braces defined as slender or stocky. For a brace whose slenderness is between two limits, interpolation between those values is permitted.

Table 3.14. Calculated parameters of figure 3.14 for force-deformation relation of steel brace HSS210X210X13.

Parameter:	**a**	**b**	**c**
Brace in Tension:	9.00	11.00	0.60
Brace in Compression, Slender:	0.50	9.00	0.30
Brace in Compression, Stocky:	1.00	7.00	0.50
Brace in Compression, Interpolated:	0.97	7.13	0.49

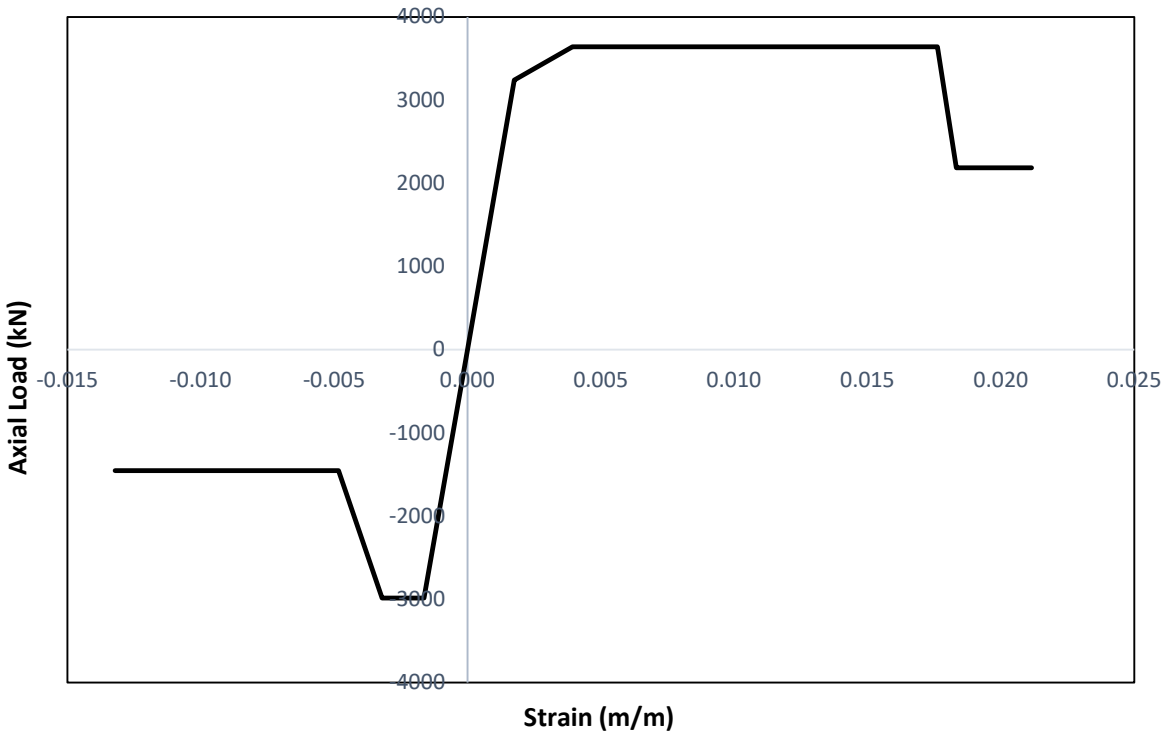

Figure 3.15. Sample brace backbone curve for HSS210X210X13 section.

In Figure 3.15, strength loss in the tension zone results from the deterioration of steel material whereas, in the compression zone, buckling of the brace causes strength degradation.

In the tension zone, a strain hardening slope equal to 10% of the elastic slope is used until the ultimate strength is reached whereas, in the compression zone, no strain hardening is considered. Also, the slope of degradation is taken as equal to the elastic slope according to FEMA P-2006 standard [29].

3.3.6.2. Beams and Columns. In this study, the beam-to-column connection is preferred as a fully rigid connection. This connection is designed such that the nonlinear behavior is expected to occur first in beams prior to the connection. Thus, in the nonlinear model moment rotation hinges are defined at the beam ends as well as at intersection points with braces.

Beams of chevron-type special concentrically braced frames experience large axial forces due to the unbalanced forces transferred by the braces, which may affect the nonlinear behavior of the beams. PMM hinges are therefore defined for those beams.

On the other hand, the columns of special concentrically braced frames are designed for axial forces only depending on buckling mechanisms. Yet, as the braces make large deformation, the structure starts to show a softening behavior, and the beam and columns of SCBFs begin to resist lateral loads as a moment frame if the connection is designed as a rigid connection. Since in this study buildings are subjected to increasing earthquake loads until collapse, the definition of PMM hinges of columns has an important role in the collapse capacity of the structures.

In the Perform 3D software, there are different options to define a PMM hinge. One can assume an elastic perfectly plastic behavior without or with strength loss or a trilinear behavior. The strength loss may or may not be dependent on the axial force. In this study, to decrease analysis time and represent softening of building in excessive loads, elastic perfectly plastic behavior with strength loss depending on the axial force level is employed.

According to the TSC, moment strength of members is calculated as

$$\theta_y = \frac{W_p F_{ye} L}{6EI}, \tag{3.6}$$

and yield rotation is calculated as

$$M_{pe} = W_p F_{ye}, \tag{3.7}$$

where θ_y, W_p and F_{ye} refer to yield rotation, plastic section modulus and expected yield strength, respectively.

For both beam and column members, to demonstrate strength loss behavior, two different axial force levels are introduced, and intermediate values are calculated with interpolation by software [26]. The upper value of axial force is taken as the compressive force capacity of the member and the lower value of axial force is taken as 0. For the upper value of axial force, strength degradation almost starts immediately after the yielding, and for the lower value of axial force, the force deformation relationship of the columns and beams is determined according to the given parameters for beams in ASCE41-17. For the upper value of axial force, the moment strength of the member is decreased to 10% of the initial strength after loss whereas, for lower values, it is decreased to 60% of the initial one. Parameters used in the analysis for P=0 are given in Table 3.15 and the backbone curve is given in Figure 3.16 for the HD320X300 column profile.

Table 3.15. Assigned parameters of figure 3.14 for force-deformation relation of steel beams and columns (for P=0).

a	b	c
9	11	0.6

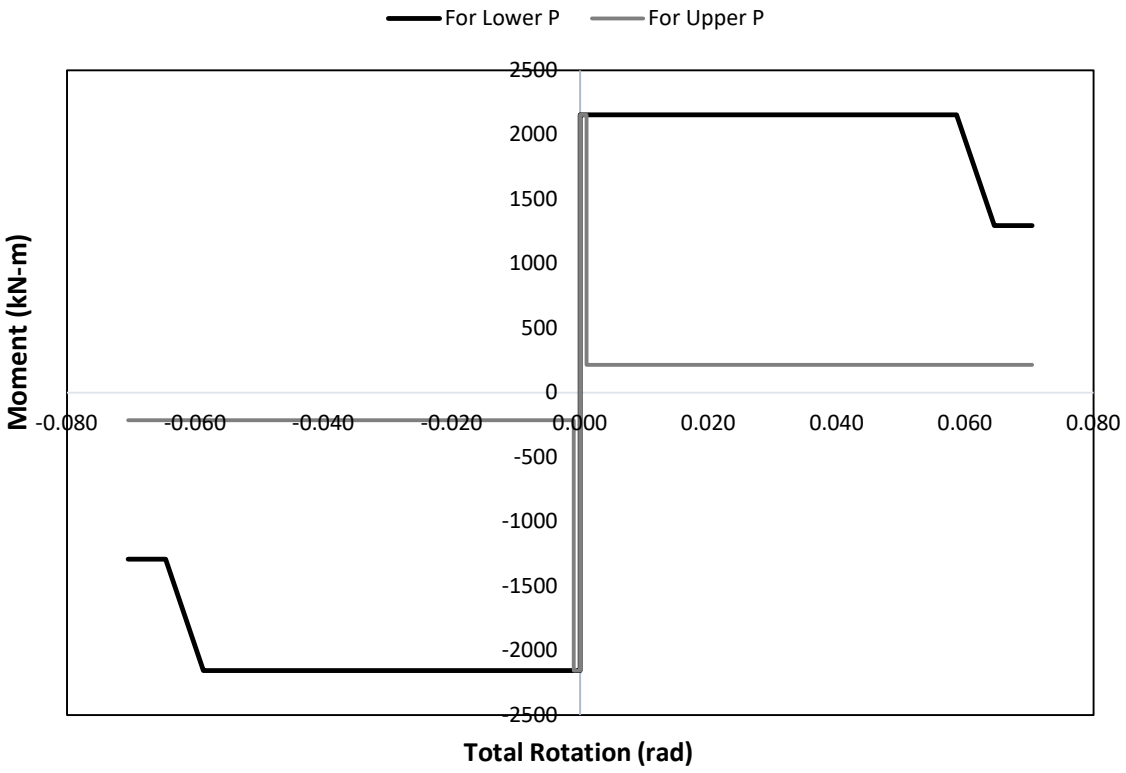

Figure 3.16. Sample column backbone curve for HD320X300 section.

The slope of degradation is taken as equal to the elastic slope according to FEMA P-2006 standard.

PMM yield surface employed by Perform 3D is similar to study conducted by El-Tawil and Deierlein [30]. To construct a PMM surface in Perform 3D, only a few parameters should be defined. Recommended values are used for these parameters and resulting yield surfaces are given below [31].

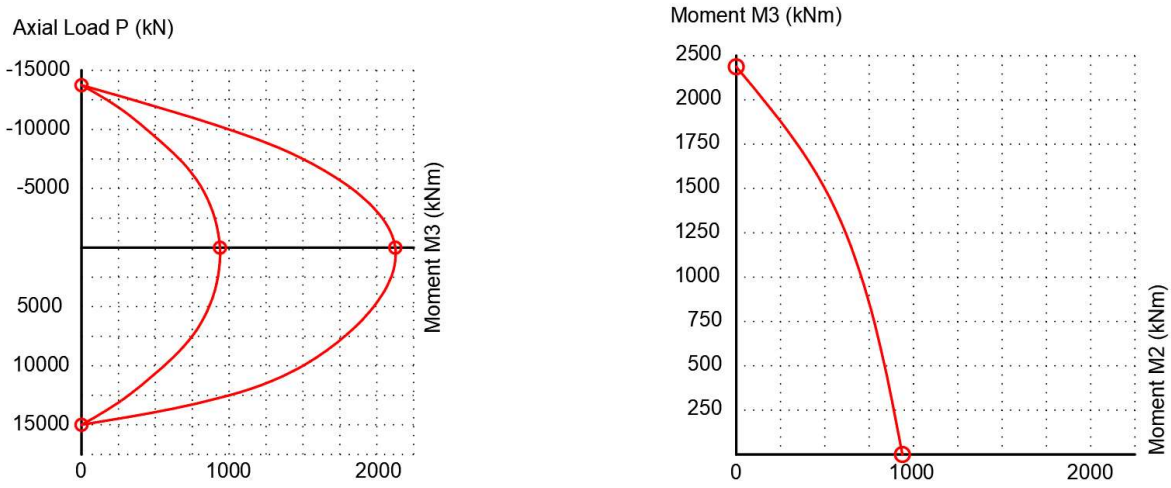

Figure 3.17. Yield surfaces for HD320X300 section from perform 3D.

3.4. Modal Analysis

Modal analysis of each frame is conducted before the nonlinear analysis in Perform 3D software. Mod shapes and natural periods of each frame are obtained, and the resulting is compared with the first mode of the corresponding 3D model for each building in Table 3.16. Fundamental periods of frames are achieved as 0.41 s, 0.88 s and 1.39 s for Building-1, Building-2 and Building-3, respectively. The first four mod shapes and effective mass factor for each mode are given in Figure 3.18, Figure 3.19 and Figure 3.20. Square dotes in these figures show start and end joints of each frame mesh.

Table 3.16. 3D model and frame model comparison in terms of fundamental periods

	3D Model	Frame Model	% Difference
Building-1	0.38	0.41	7
Building-2	0.83	0.88	6
Building-3	1.33	1.39	4

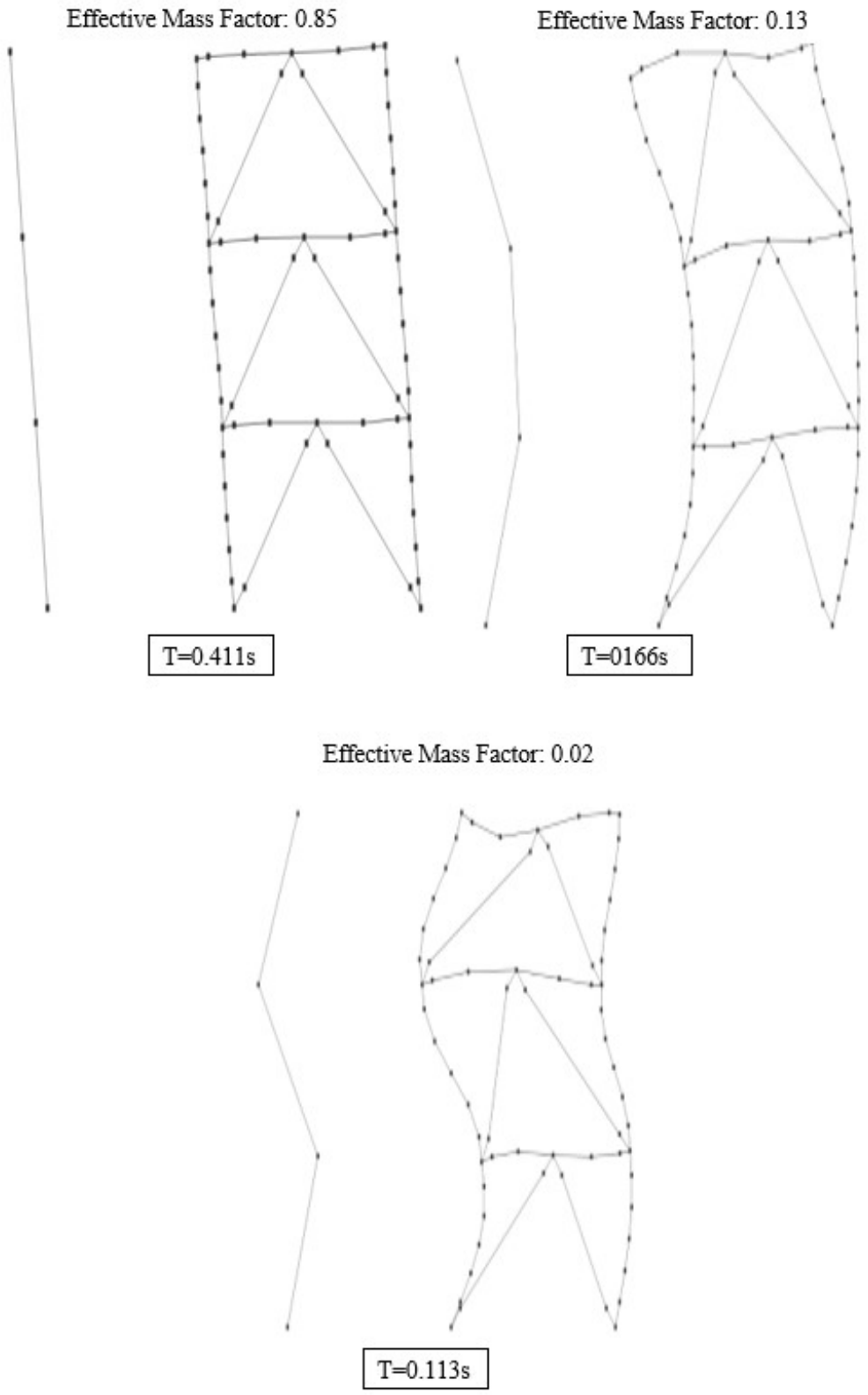

Figure 3.18. First three modes of building-1.

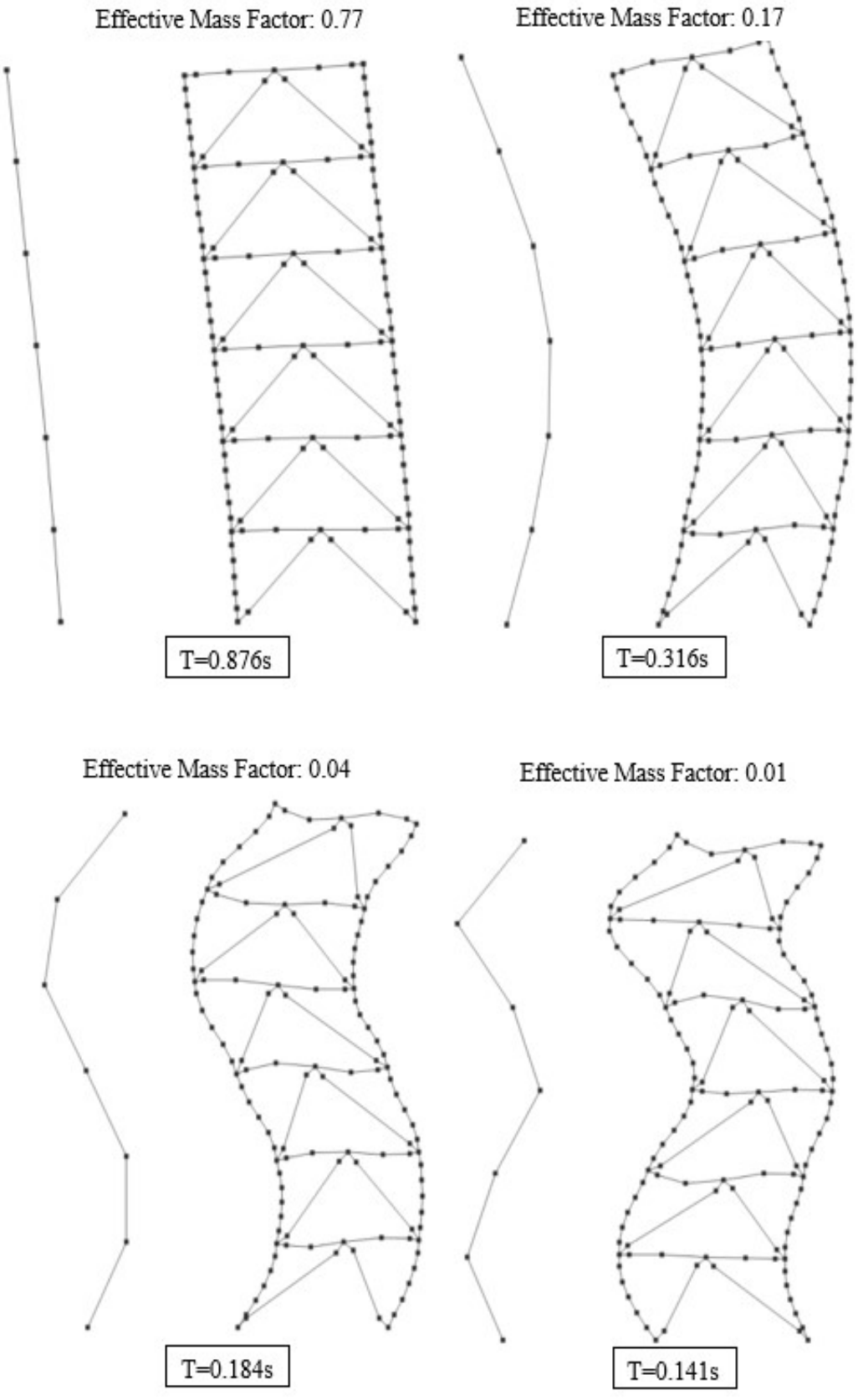

Figure 3.19. First four modes of building-2.

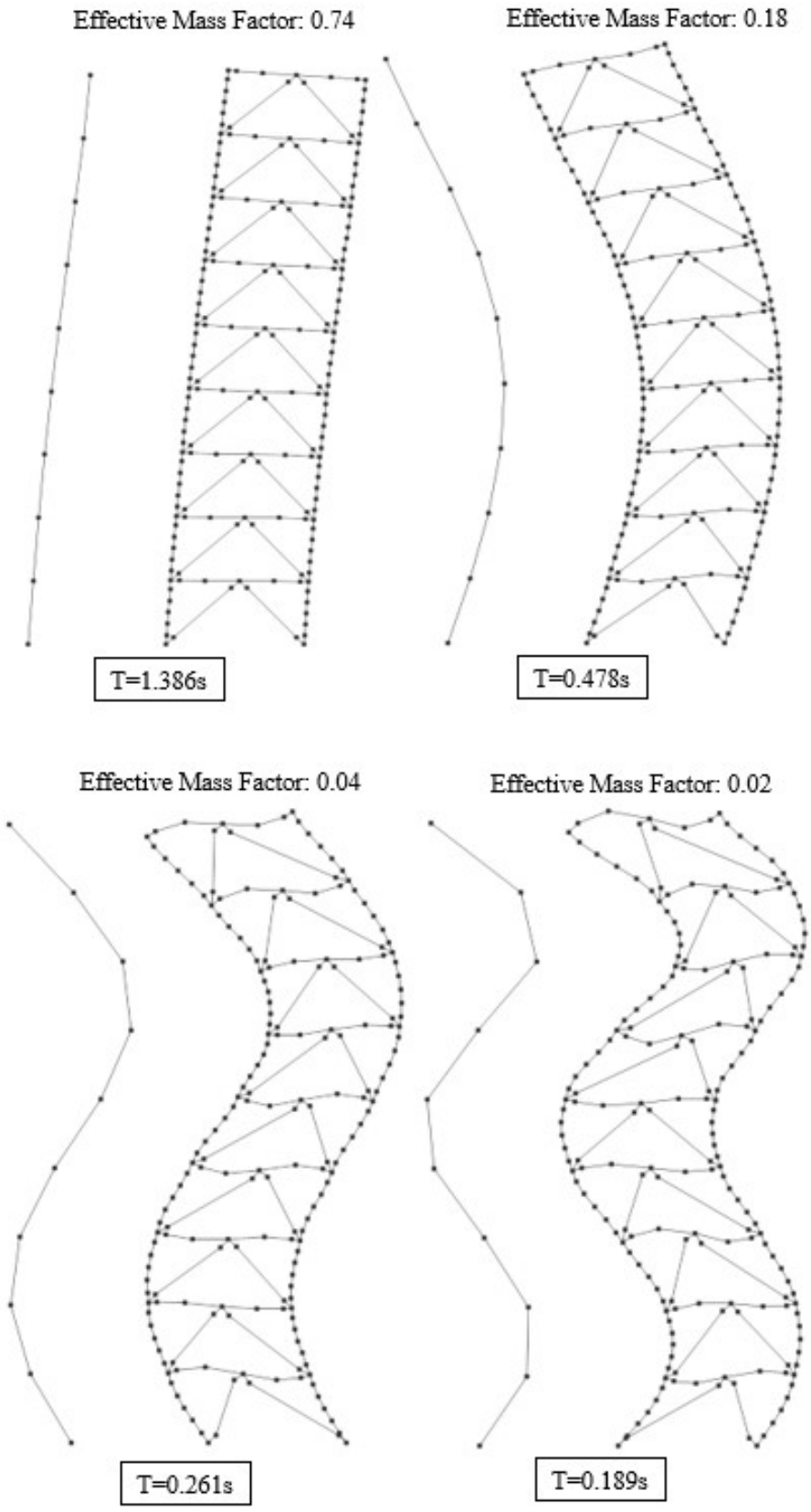

Figure 3.20. First four modes of building-3.

3.5. Selection and Scaling of Ground Motion Record Sets

The methodology followed requires a set of ground motion records for incremental dynamic analysis and the development of fragility curves. To conduct incremental dynamic analysis, a set of ground motions is scaled to the maximum considered earthquake (DD1 level earthquake for this study) intensity in the fundamental period of structure first. After the first analysis, the record set is scaled to gradually increasing intensities until half of the records cause the structure to reach the collapse point. The collapse is usually defined in terms of inter-story drifts. To estimate median collapse capacity with an acceptable deviation and consider the record-to-record variability, a sufficient number of ground motion records should be included in the set.

In the methodology, as a difference from incremental dynamic analysis procedure, median spectral acceleration, S_T of record set is used as intensity measure instead of separate acceleration values for each record.

3.5.1. Selection of Ground Motions

The selection of the records is quite important since this changes the analysis results directly. Some of the important factors regarding the selection of ground motion records are listed below.

- Ground motion requirements of code should be satisfied.
- Very strong ground motions should be represented with enough amounts of records.
- An adequate number of records should be employed to achieve reliable results.
- Records should be independent of the structural system of buildings and cover a wide range of different structural systems.
- Records should be independent of site and source conditions.

To meet methodology objectives, far-field records, which are defined as ground motions recorded at stations having a minimum distance of 10 km to the fault rupture,

recommended by FEMA P-695 are selected. PEER NGA database is used [32]. Since the database is updated, the ground motion parameters used in this study slightly differ from the set given in the methodology, but the overall content is pretty much the same. Some characteristics of selected records are summarized below.

Since the high magnitude of earthquakes causes more collapse risk by releasing high energy, earthquakes with $M > 6.8$ are selected. Records contain both strike-slip and reverse sources. Only earthquakes recorded in both soil classes C and D are used. All the records have a minimum of 10 km distance to the source. The distance measure is chosen to be the average of Joyner-Boore and Campbell distances. To prevent bias in favor of any earthquake record, a maximum of two of the same ground motion recorded at different stations are used. To permit variability in the record set, ground motions having a minimum of 0.2 g of *PGA* and 15 cm/sec of *PGV* are applied. Selected earthquake records and some characteristics are given in Table 3.17.

Table 3.17. Selected earthquake records from PEER.

ID No.	Earthquake				Site Data		Source (Fault Type)	Site-Source Distance	
	M	Year	Name	Recording Station	NEHRP Class	V_{s_30} (m/sec)		R_{jb} (km)	R_{rup} (km)
1	6.69	1994	Northridge	Beverly Hills	D	355.81	Reverse	9.44	17.15
2	6.69	1994	Northridge	Canyon Country	D	325.6	Reverse	11.39	12.44
3	7.14	1999	Duzce, Turkey	Bolu	D	293.57	Strike-slip	12.02	12.04
4	7.13	1999	Hector Mine	Hector	C	726	Strike-slip	10.35	11.66
5	6.53	1979	Imperial Valley	Delta	D	242.05	Strike-slip	22.03	22.03
6	6.53	1979	Imperial Valley	El Centro Array #11	D	196.25	Strike-slip	12.56	12.56
7	6.9	1995	Kobe, Japan	Nishi-Akashi	C	609	Strike-slip	7.08	7.08
8	6.9	1995	Kobe, Japan	Shin-Osaka	D	256	Strike-slip	19.14	19.15
9	7.51	1999	Kocaeli, Turkey	Duzce	D	281.86	Strike-slip	13.6	15.37
10	7.51	1999	Kocaeli, Turkey	Arcelik	C	523	Strike-slip	10.56	13.49
11	7.28	1992	Landers	Yermo Fire Stat.	D	353.63	Strike-slip	23.62	23.62
12	7.28	1992	Landers	Coolwater	D	352.98	Strike-slip	19.74	19.74
13	6.93	1989	Loma Prieta	Capitola	D	288.62	Strike-slip	8.65	15.23
14	6.93	1989	Loma Prieta	Gilroy Array #3	D	349.85	Strike-slip	12.23	12.82
15	7.37	1990	Manjil, Iran	Abbar	C	723.95	Strike-slip	12.55	12.55
16	6.54	1987	Superstition Hills	El Centro Imp. Co.	D	192.05	Strike-slip	18.2	18.2
17	6.54	1987	Superstition Hills	Poe Road (temp)	D	316.64	Strike-slip	11.16	11.16
18	7.01	1992	Cape Mendocino	Rio Dell Overpass	D	566.42	Reverse	8.49	12.24
19	7.62	1999	Chi-Chi, Taiwan	CHY101	D	258.89	Reverse Oblique	9.94	9.94
20	7.62	1999	Chi-Chi, Taiwan	TCU045	C	704.64	Reverse Oblique	26	26
21	6.61	1971	San Fernando	LA - Hollywood	D	316.46	Reverse	22.77	22.77
22	6.5	1976	Friuli, Italy	Tolmezzo	C	505.23	Reverse	14.97	15.82

3.5.2. Scaling of Ground Motions

In methodology, the scaling process of ground motions consists of two steps which are normalization based on velocity and direct scaling.

To minimize differences in earthquake records caused by characteristics of events such as type of the source, soil class, magnitude, etc., and ensure consistency, records are normalized with respect to the mean peak ground velocity of the record set. It should be emphasized that the normalization of records does not distort the content of earthquake events; thus, aleatory variability in records remains.

Normalization is performed by taking the geometric mean of *PGV* values of two different directions for each record. The normalization factor is calculated for each record with

$$NM = Median(PGV_{geomean})/PGV_{geomean}. \quad (3.8)$$

Herein, $Median(PGV_{geomean})$ represents the median of $PGV_{geomean}$ values in the record set. For each record, the same normalization factor is used for both directions to reserve disparity in intensity compared to each other.

Median value of record set is calculated as 40.33 cm/s. For each record in the set, normalization factors and normalized peak ground velocities are given in Table 3.18. Normalization factor applies to not only velocity values but also acceleration values.

For the scaling of the records, common practice is such that all the records are scaled to match target spectrum demand at the fundamental period, which results in different scale factors for each record. Instead, in this procedure, only the median value of the normalized record set scaled to target spectrum demand at the fundamental period. Table 3.19 demonstrates peak ground accelerations, acceleration at the fundamental period of Building-2, S_a, and normalized S_a values to illustrate an example.

Table 3.18. Recorded peak ground velocities and normalization factors.

ID No.	Earthquake				Recorded Velocities				Normalization Factor
	M	Year	Name	Recording Station	$PGV_{1\text{-}dir}$	$PGV_{2\text{-}dir}$	PGV_{max}	$PGV_{geomean}$	
1	6.69	1994	Northridge	Beverly Hills	59.27	66.68	66.68	62.87	0.64
2	6.69	1994	Northridge	Canyon Country	44.36	41.11	44.36	42.7	0.94
3	7.14	1999	Duzce, Turkey	Bolu	55.91	55.91	55.91	55.91	0.72
4	7.13	1999	Hector Mine	Hector	26	44.75	44.75	34.11	1.18
5	6.53	1979	Imperial Valley	Delta	26.31	32.98	32.98	29.46	1.37
6	6.53	1979	Imperial Valley	El Centro Array #11	36	44.59	44.59	40.07	1.01
7	6.9	1995	Kobe, Japan	Nishi-Akashi	46.8	38.24	46.8	42.3	0.95
8	6.9	1995	Kobe, Japan	Shin-Osaka	31.31	21.8	31.31	26.13	1.54
9	7.51	1999	Kocaeli, Turkey	Duzce	58.84	55.63	58.84	57.21	0.7
10	7.51	1999	Kocaeli, Turkey	Arcelik	13.95	40.05	40.05	23.64	1.71
11	7.28	1992	Landers	Yermo Fire Stat.	51.1	29.08	51.1	38.55	1.05
12	7.28	1992	Landers	Coolwater	27.6	43.4	43.4	34.61	1.17
13	6.93	1989	Loma Prieta	Capitola	38	29.6	38	33.54	1.2
14	6.93	1989	Loma Prieta	Gilroy Array #3	36.29	45.4	45.4	40.59	0.99
15	7.37	1990	Manjil, Iran	Abbar	42.44	50.56	50.56	46.32	0.87
16	6.54	1987	Superstition Hills	El Centro Imp. Co.	48.05	41.77	48.05	44.8	0.9
17	6.54	1987	Superstition Hills	Poe Road (temp)	41.15	29	41.15	34.54	1.17
18	7.01	1992	Cape Mendocino	Rio Dell Overpass	67.86	48.32	67.86	57.26	0.7
19	7.62	1999	Chi-Chi, Taiwan	CHY101	65	109	109	84.17	0.48
20	7.62	1999	Chi-Chi, Taiwan	TCU045	50.06	46.35	50.06	48.17	0.84
21	6.61	1971	San Fernando	LA - Hollywood	21.71	16.93	21.71	19.17	2.1
22	6.5	1976	Friuli, Italy	Tolmezzo	22.84	30.51	30.51	26.4	1.53

Table 3.19. Recorded peak ground accelerations and accelerations at fundamental period of building-2.

ID No.	Earthquake				Recorded Accelerations				For T=0.876 S_a (Normalized)
	M	Year	Name	Recording Station	PGA_{1dir}	PGA_{2dir}	PGA_{max}	For T=0.876 S_a	
1	6.69	1994	Northridge	Beverly Hills,	0.44	0.49	0.49	1.23	0.79
2	6.69	1994	Northridge	Canyon Country-	0.4	0.47	0.47	0.55	0.52
3	7.14	1999	Duzce, Turkey	Bolu	0.74	0.81	0.81	1.11	0.8
4	7.13	1999	Hector Mine	Hector	0.27	0.33	0.33	0.32	0.38
5	6.53	1979	Imperial Valley	Delta	0.24	0.35	0.35	0.46	0.62
6	6.53	1979	Imperial Valley	El Centro Array #11	0.37	0.38	0.38	0.28	0.28
7	6.9	1995	Kobe, Japan	Nishi-Akashi	0.48	0.46	0.48	0.47	0.45
8	6.9	1995	Kobe, Japan	Shin-Osaka	0.23	0.23	0.23	0.41	0.64
9	7.51	1999	Kocaeli, Turkey	Duzce	0.31	0.36	0.36	0.5	0.35
10	7.51	1999	Kocaeli, Turkey	Arcelik	0.21	0.13	0.21	0.17	0.29
11	7.28	1992	Landers	Yermo Fire Station	0.24	0.15	0.24	0.37	0.39
12	7.28	1992	Landers	Coolwater	0.28	0.42	0.42	0.45	0.53
13	6.93	1989	Loma Prieta	Capitola	0.51	0.44	0.51	0.5	0.61
14	6.93	1989	Loma Prieta	Gilroy Array #3	0.56	0.37	0.56	0.4	0.4
15	7.37	1990	Manjil, Iran	Abbar	0.51	0.5	0.51	0.47	0.41
16	6.54	1987	Superstition Hills	El Centro Imp. Co.	0.36	0.26	0.36	0.37	0.34
17	6.54	1987	Superstition Hills	Poe Road (temp)	0.47	0.29	0.47	0.36	0.42
18	7.01	1992	Cape Mendocino	Rio Dell Overpass	0.18	0.21	0.21	0.33	0.23
19	7.62	1999	Chi-Chi, Taiwan	CHY101	0.34	0.4	0.4	0.9	0.43
20	7.62	1999	Chi-Chi, Taiwan	TCU045	0.47	0.51	0.51	0.49	0.41
21	6.61	1971	San Fernando	LA - Hollywood	0.22	0.19	0.22	0.24	0.51
22	6.5	1976	Friuli, Italy	Tolmezzo	0.36	0.32	0.36	0.34	0.52

For T=0.876s, the median value of the normalized record set, S_{NRT} is calculated as 0.42g. Earthquake demand at the fundamental period of Building-2 is determined as 0.96g according to the DD1 earthquake level, and eventually, the scale factor to match MCE intensity is calculated as 2.26. The same procedure is applied to two other buildings and corresponding scale factors to match MCE are calculated as 2.43 and 2.12 for Building-1 and Building-3, respectively.

Table 3.20. Scale factors to match the record set to the MCE intensity.

	SF
Building-1	2.43
Building-2	2.26
Building-3	2.12

In the following figure, the response spectra of each normalized earthquake record by considering two components individually are given. The response spectra of each record are taken from the PEER NGA database [32] and a normalization factor is applied to each spectrum. Also, the median value of the 44-record set is indicated with a bold line.

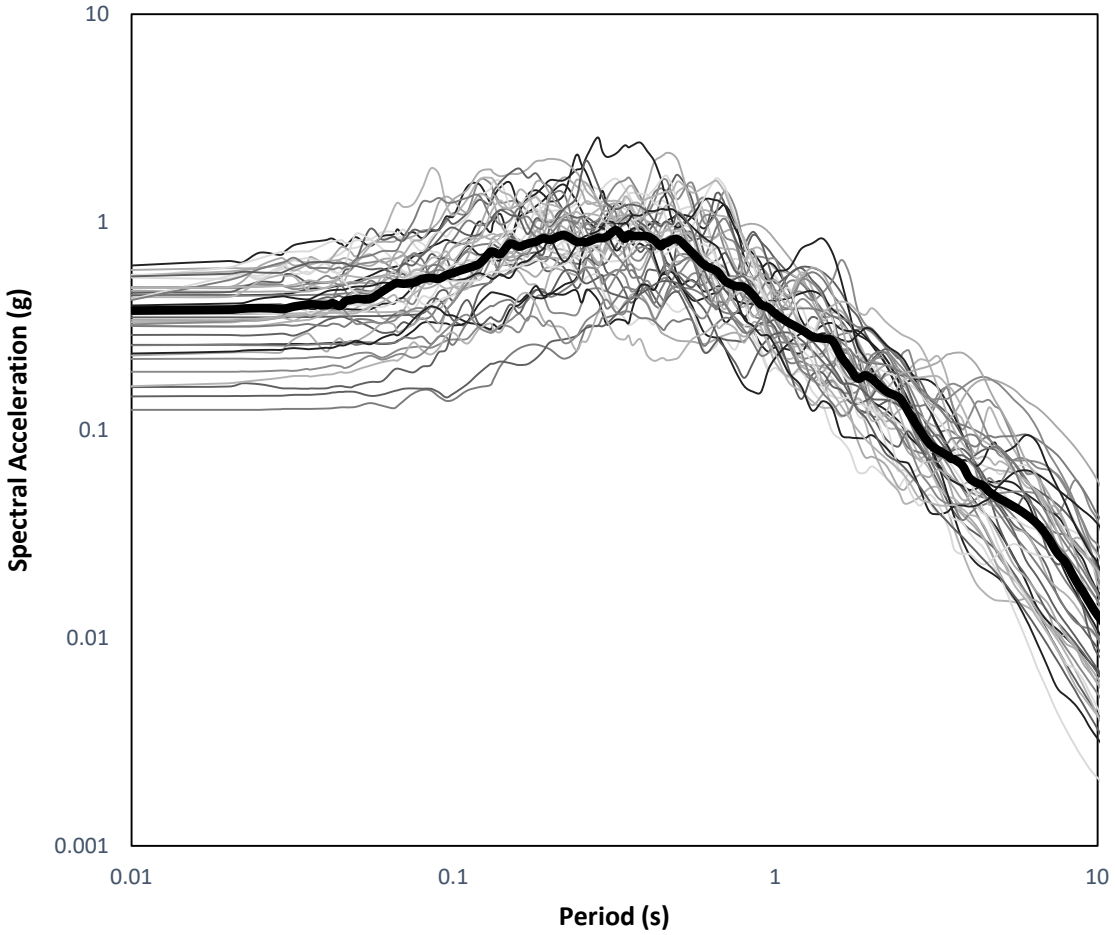

Figure 3.21. Response spectra of each normalized record and median value of 44-record set (log-log scale).

3.6. Hazard Curve

In Turkey, uniform hazard maps are available on the TEHM website [4]. For all locations, only four points of the hazard curve are provided corresponding to 2475 years, 475 years, 72 years, and 43 years return period. For the risk assessment, a complete form of hazard curve is required. According to the four points known, the hazard curve is completed from USGS Risk-Targeted Ground Motion Calculator [33] at fundamental periods of buildings. For all buildings, hazard curves are given in Figure 3.22.

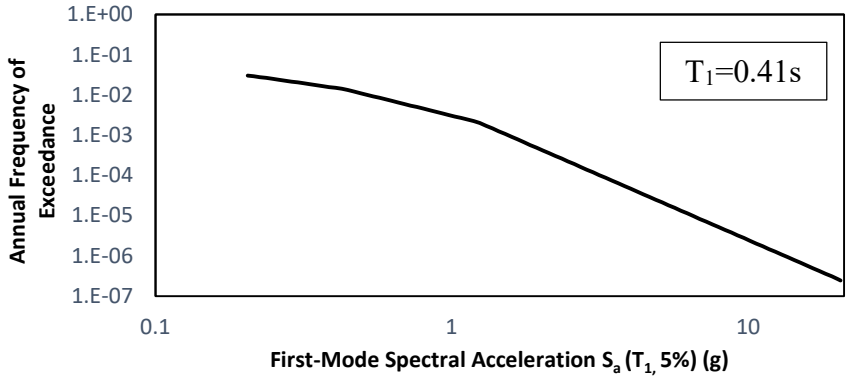

(a)

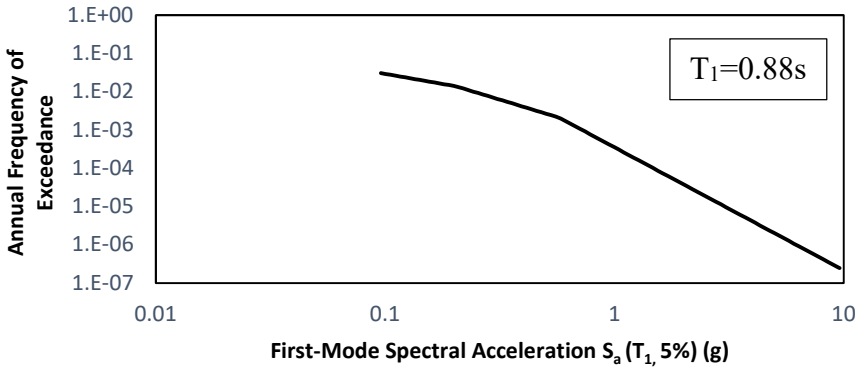

(b)

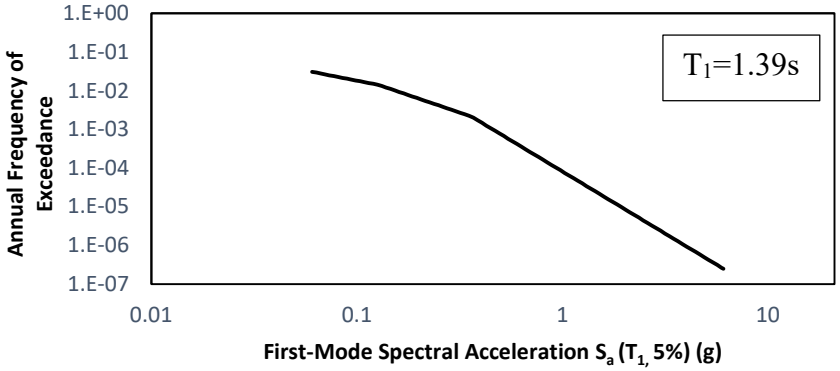

(c)

Figure 3.22. Hazard curve at fundamental period for (a) building-1, (b) building-2, (c) building-3.

4.ANALYSIS RESULTS

4.1. Nonlinear Static Push-over Analysis Result

A static push-over analysis is performed for each building to determine structural capacity and observe the behavior of the buildings under lateral loads. Prior to the lateral loads, a nonlinear static analysis is applied under gravity loads (G+0.3Q). One mode push-over analysis for the first mode is employed and lateral loads are introduced according to the first mode of the buildings. P-Delta effects are considered in the analysis and buildings are pushed until the inter-story drift ratio in any story reaches a value of 0.15.

Push-over analysis results shows that all buildings tend to have weak story behavior in different stories. It can be said that weak story mechanisms are those in which there are a lot of inelastic deformations concentrated in one story. While most of the structural system enables the distribution of deformation over the building height, special concentrically braced frames are the most vulnerable system to story mechanisms due to dramatic changes in the stiffness after buckling of the braces [34].

Figure 4.1 shows the hinge formation chronology for Building-1. First, the compression brace at the first story yields, and the yielding of the second story (compression) and first story (tension) brace follows. Yielding occurs first in the columns instead of beams due to lower moment capacities under the high level of axial forces. Push-over analysis reveals that the maximum drift ratio is obtained first at the first story and Building-1 tends to show a weak story mechanism.

Since the first story reaches the maximum drift ratio first, the drift ratio in the first story versus base shear is given for Building-1 in Figure 4.2. Hinges formed are indicated in this figure to show the sequence and location of events. With the buckling of the first story brace, the base shear capacity of the structure decreases significantly. After that, some part of strength is gained with the moment frame action. Sudden drops in this figure are the result of strength drops in the structural members.

Building-2 shows a similar behavior pattern to Building-1 and tends to have a weak story mechanism. On the other hand, in Building-3, plastic hinges form in the beams before the columns in the first and second stories. In this way, relatively a more ductile behavior is achieved in this building through energy dissipation in the beams and the maximum inter-story drift ratio is reached in the first and second stories at the same time. Plastic hinges at the top end of the second-story columns lead the structure to the collapse point in this building.

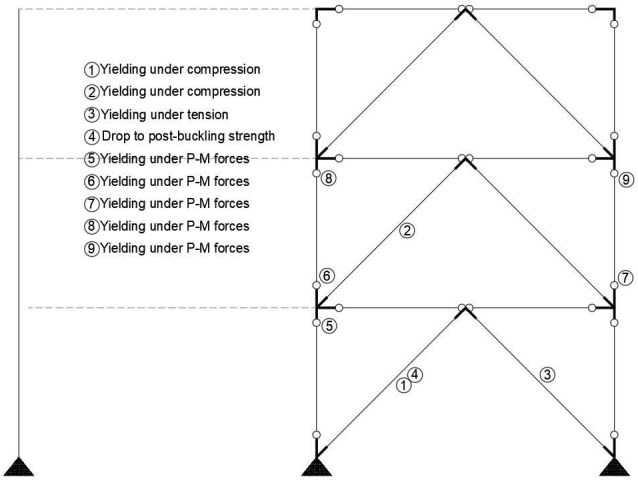

Figure 4.1. Hinge formation chronology for building-1.

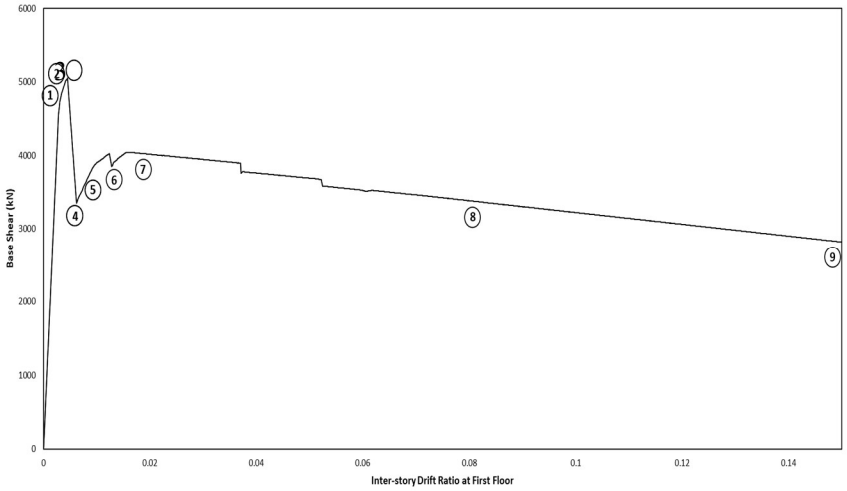

Figure 4.2. Pushover curve for building-1 according to first story drifts.

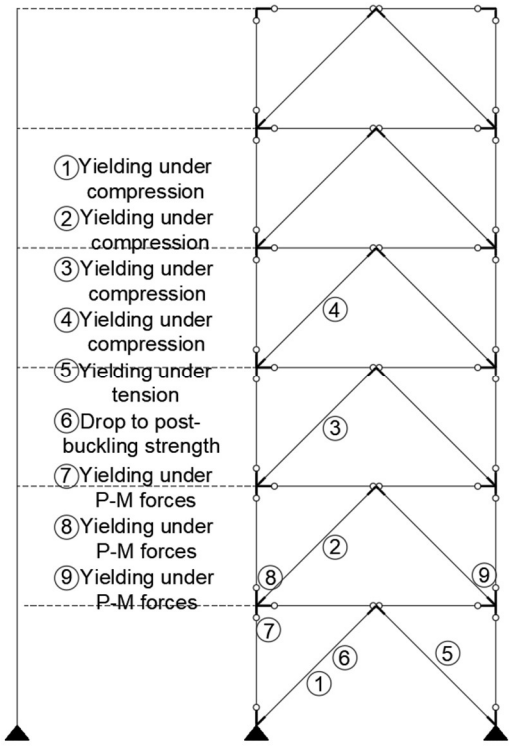

Figure 4.3. Hinge formation chronology for building-2.

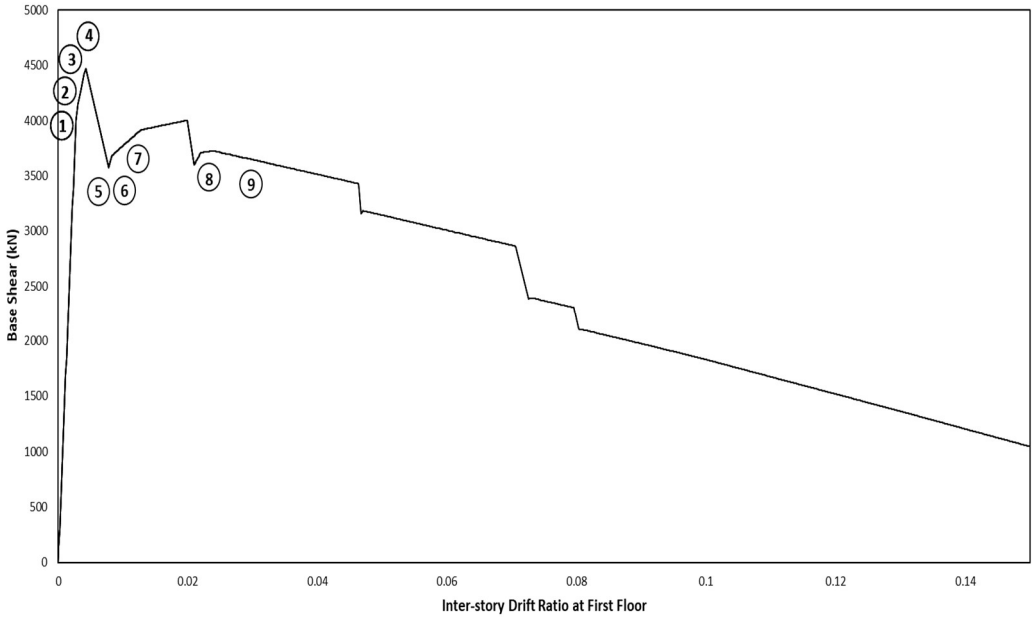

Figure 4.4. Pushover curve for building-2 according to first story drifts.

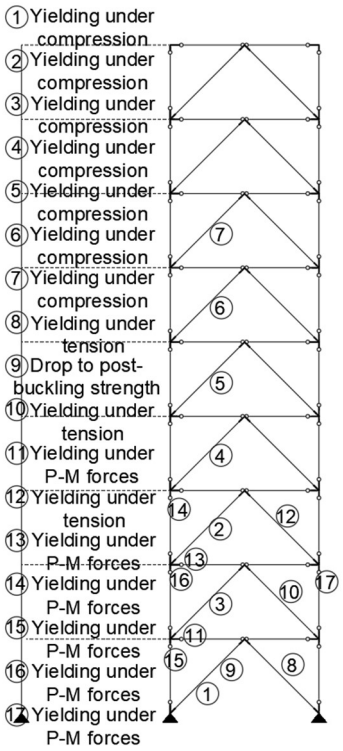

Figure 4.5. Hinge formation chronology for building-3.

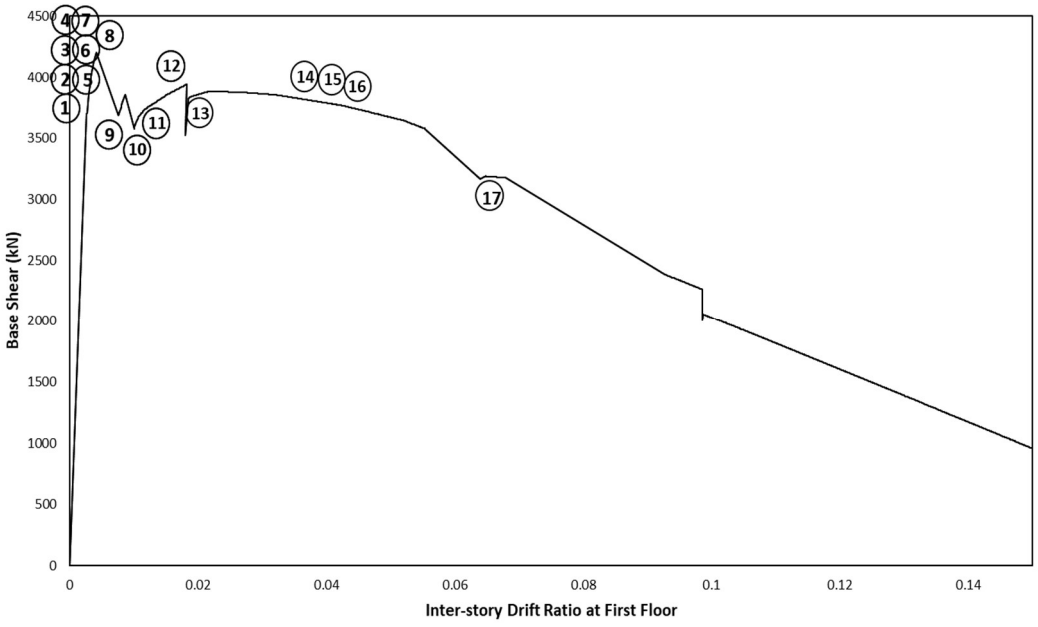

Figure 4.6. Pushover curve for building-3 according to first story drifts.

4.2. Incremental Dynamic Analysis Results

Nonlinear time history analysis is conducted for all buildings. To construct incremental dynamic analysis curves, each individual record is applied to structures with increasing intensities until collapse occurs. First, the record set is scaled to match the median value of the set with the MCE (DD1) acceleration value on the fundamental period of the structure in concern, and afterward, the scale factor is increased gradually. According to Vamvatsikos and Cornell (2002) [10], collapse can be defined as the point where structural analysis do not converge and instability occurs, or 10% of drift ratio can be employed instead.

For Building-1, the scale factor is calculated to be 2.43 for all normalized earthquake records in the set to match MCE intensity at the fundamental period. Under this earthquake record set, six of the records cause the structure to reach a collapse point. Table 4.1. summarizes scale factors and median acceleration values at the fundamental period of conducted analysis and number of records that causes collapses in the set for Building-1. Figure 4.7 represents incremental dynamic analysis curves of Building-1 under 22 earthquake pairs.

To match MCE intensity at the fundamental period, all normalized earthquake records in Building-2 are scaled with a factor of 2.26. A total of eight earthquake records cause Building-2 to collapse. Table 4.2. provides a summary of the scale factors and median acceleration value at the fundamental period and the number of records that cause collapses in Building 2. Figure 4.8 shows the incremental dynamics curves for Building-2 for 22 earthquake pairs.

For Building-3, the scale factor is calculated to be 2.12 for all normalized earthquake records in the set to match MCE intensity at the fundamental period. Under this earthquake record set, only one of the records causes the structure to reach the collapse point. Table 4.3. Summarizes scale and median acceleration value at fundamental period factors of conducted analysis and number of records that cause collapses in the set for Building-3. Figure 4.9 represents incremental dynamic analysis curves of Building-3 under 22 earthquake pairs.

Table 4.1. Summary of analysis for building-1.

SCALE FACTOR	MEDIAN ACCELERATION VALUE OF RECORD SET	# OF RECORDS CAUSES COLLAPSE
2.43	2.05	6
3.16	2.66	10
4.11	3.46	15
4.71	3.97	22
5.34	4.50	28

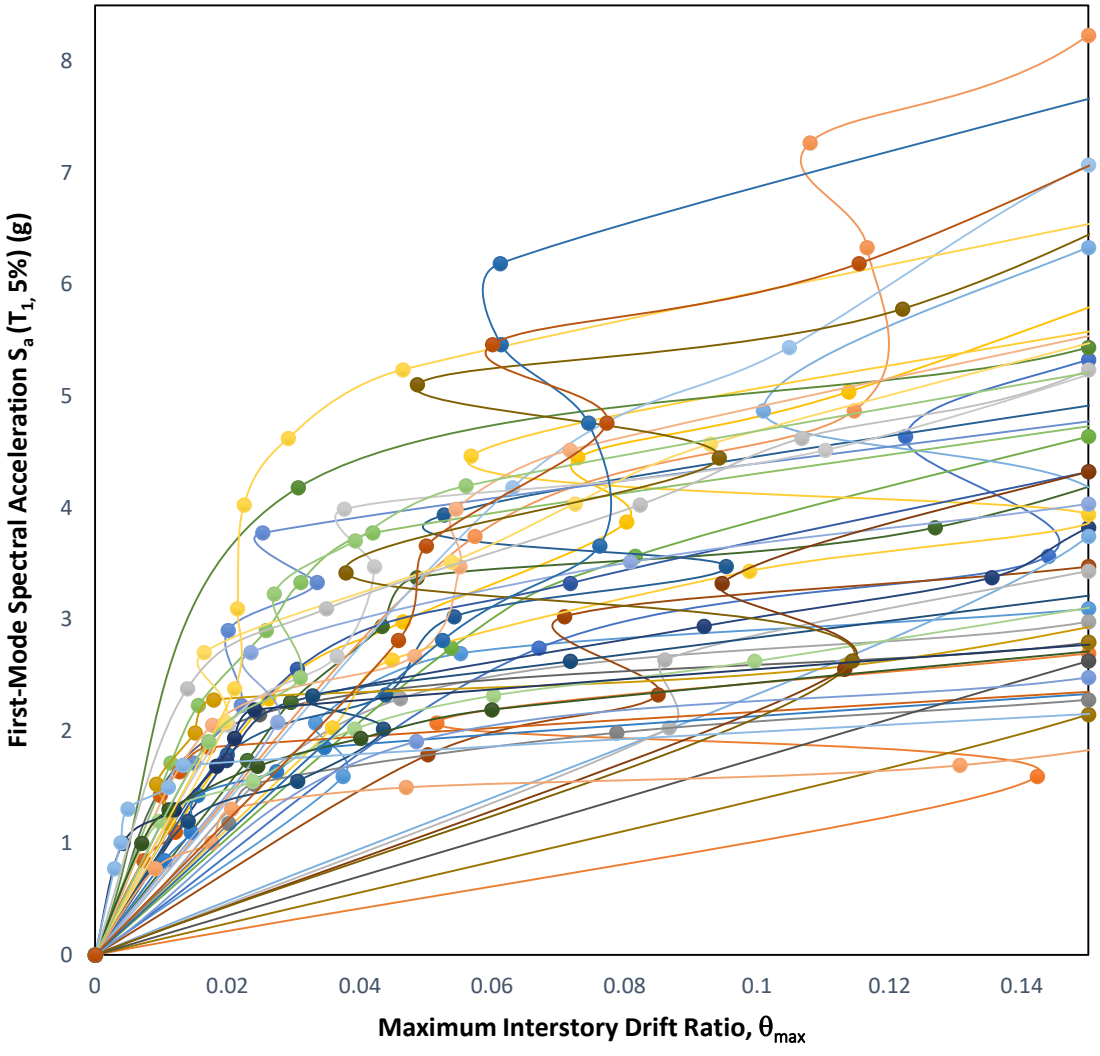

Figure 4.7. IDA curves of building-1 under 22 earthquake pairs.

Table 4.2. Summary of analysis for building-2.

SCALE FACTOR	MEDIAN ACCELERATION VALUE OF RECORD SET	# OF RECORDS CAUSES COLLAPSE
2.26	0.96	8
2.71	1.15	18
2.89	1.23	22
2.94	1.50	24

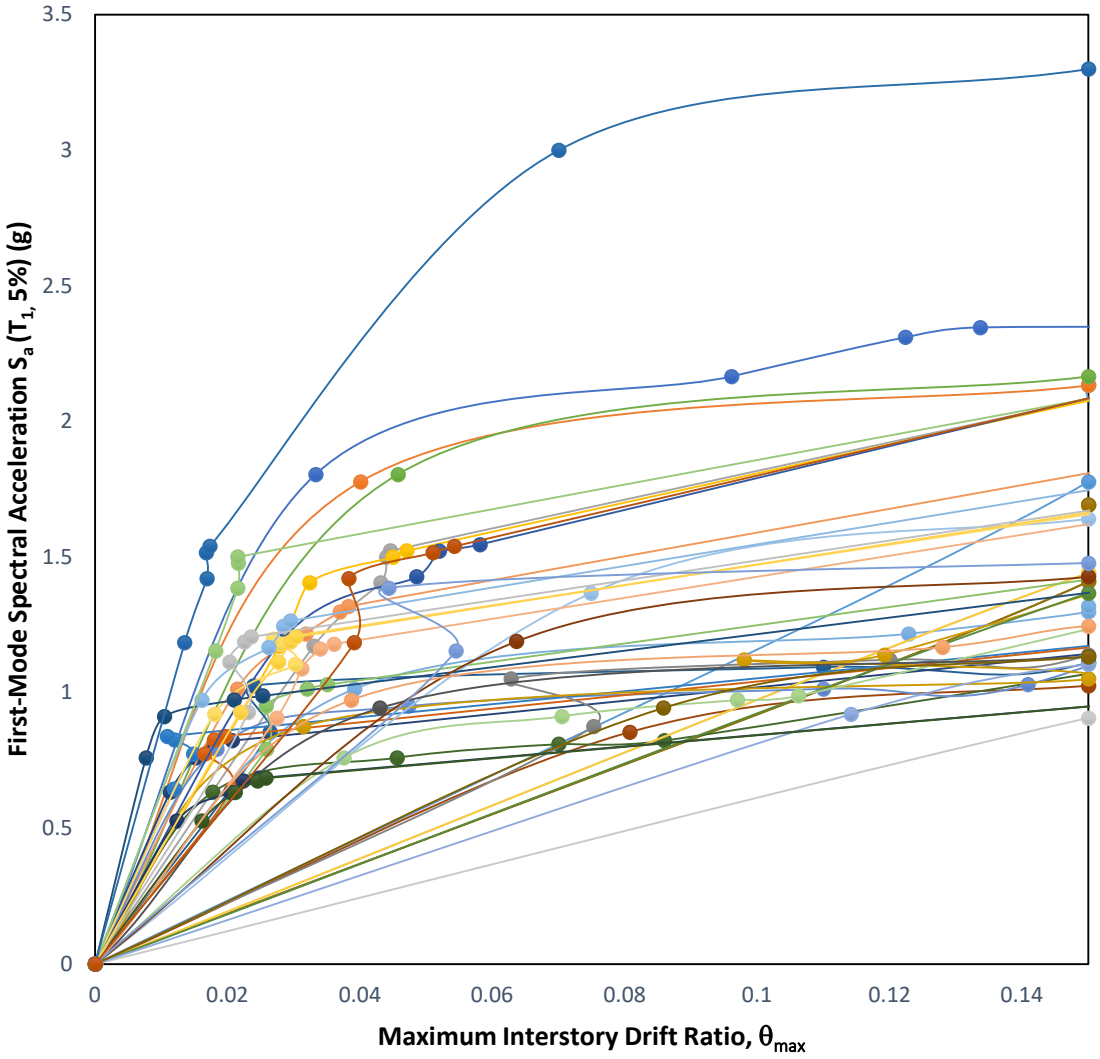

Figure 4.8. IDA curves of building-2 under 22 earthquake pairs.

Table 4.3. Summary of analysis for building-3.

SCALE FACTOR	MEDIAN ACCELERATION VALUE OF RECORD SET	# OF RECORDS CAUSES COLLAPSE
2.12	0.61	1
2.76	0.79	6
3.58	1.03	20
3.94	1.13	22

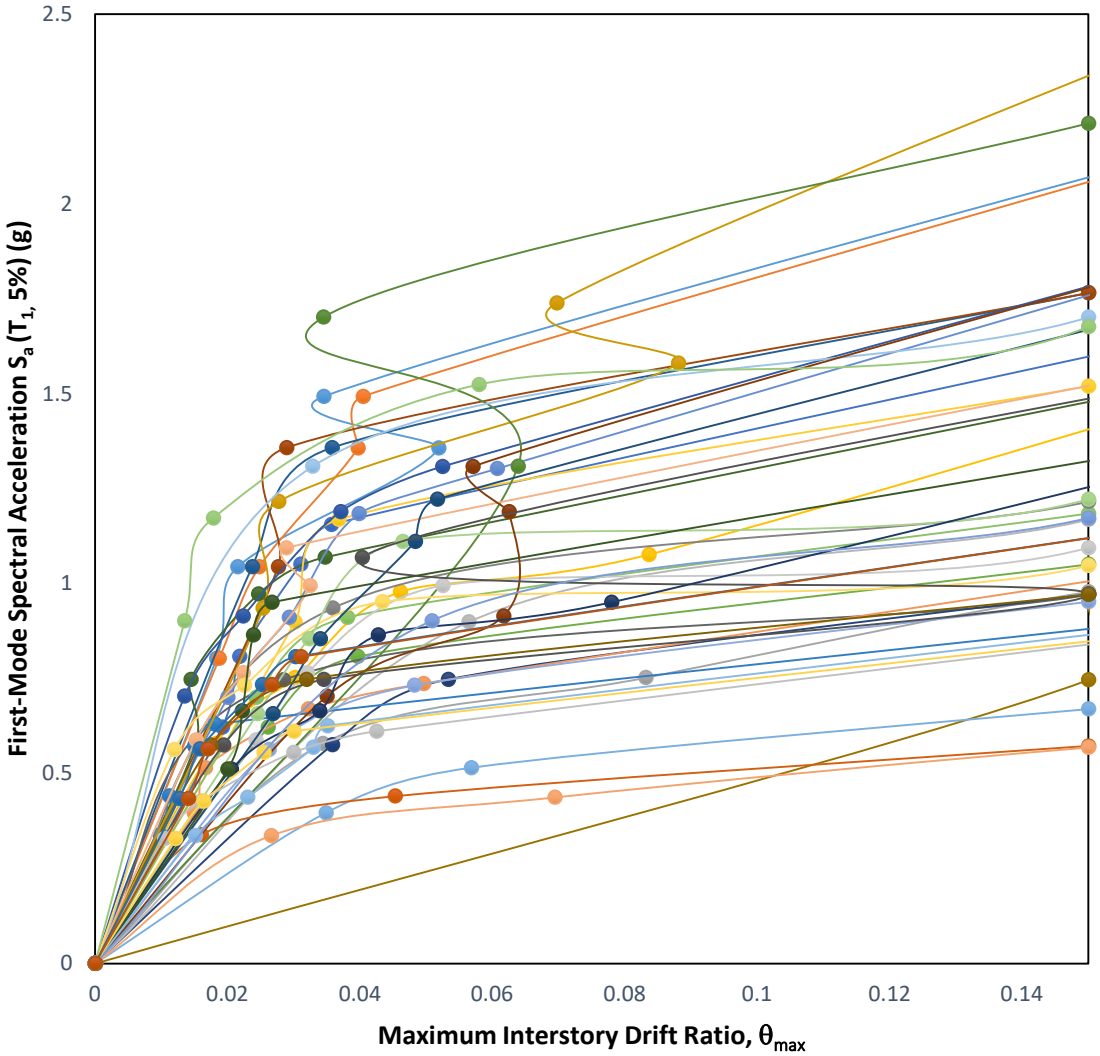

Figure 4.9. IDA curves of building-3 under 22 earthquake pairs.

4.3. Median Collapse Capacity and Collapse Margin Ratio

The median collapse capacity of the structure is identified as the median acceleration value of the record set at the fundamental period which causes the collapse of the structure under half of the records.

Figure 4.10, 4.11, and 4.12 shows the MCE intensity and median collapse capacity of Building 1, 2, and 3, respectively.

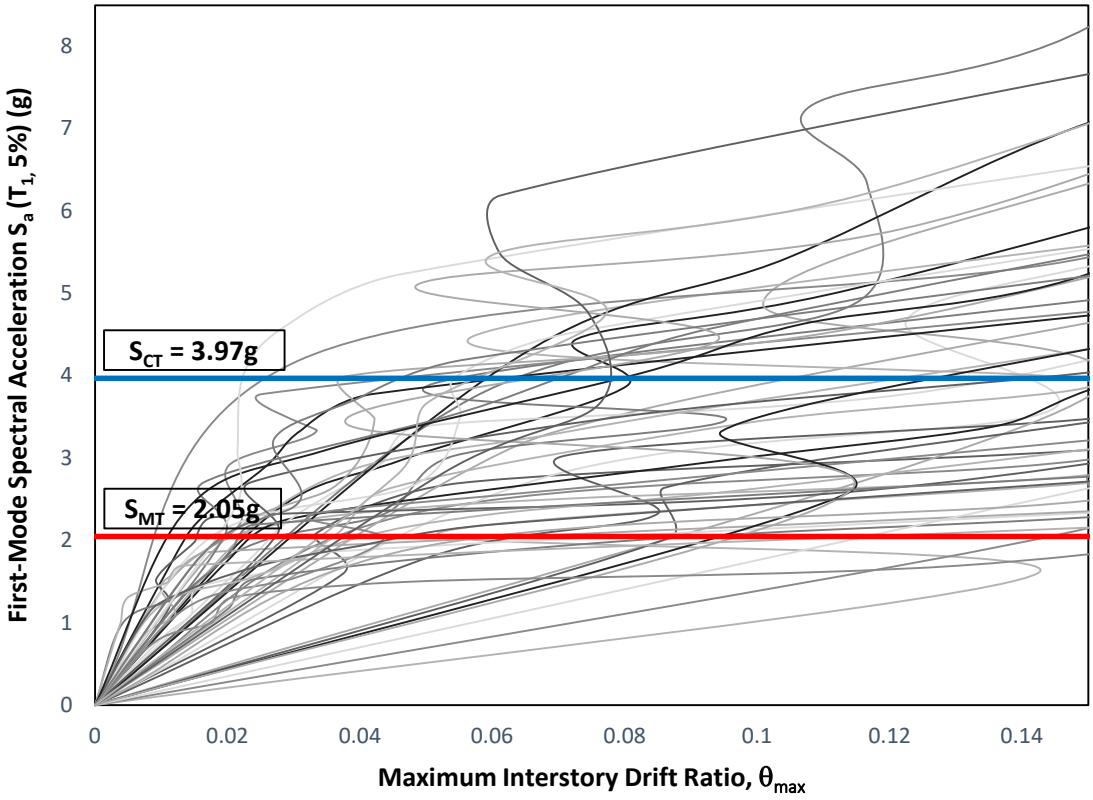

Figure 4.10. MCE intensity and median collapse capacity of building-1.

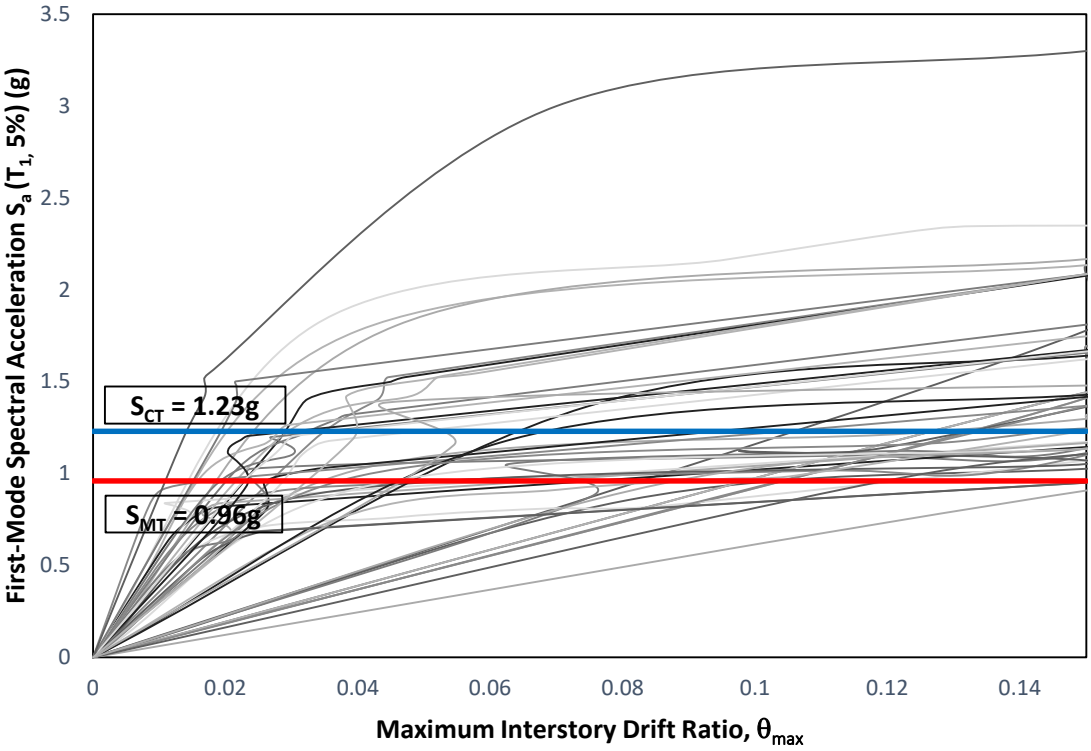

Figure 4.11. MCE intensity and median collapse capacity of building-2.

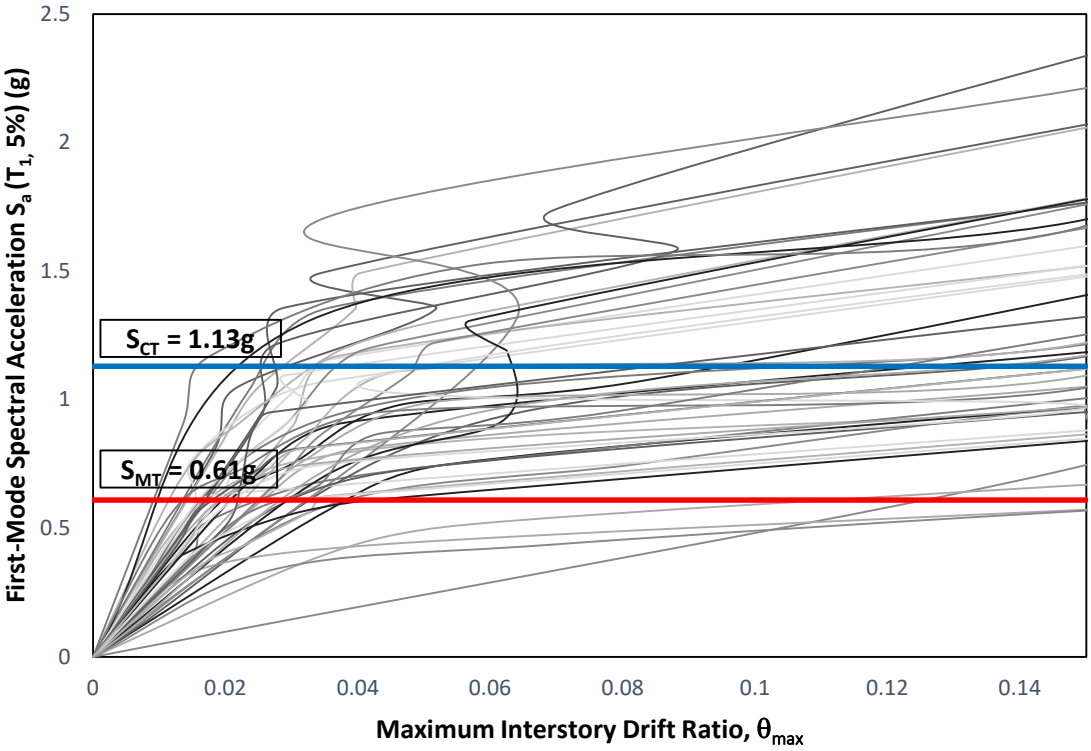

Figure 4.12. MCE intensity and median collapse capacity of building-3.

To consider the spectral shape effect of records, the median collapse capacity is increased by *SSF* given by FEMA-P695. Since spectral shape of rear earthquakes are such that it is most damaging for a narrow range of periods and drops rapidly at other periods, this factor accounts for the proper spectral shape of rare ground motions. *SSF* is decided as 1.30, 1.30, and 1.35 for Building-1, Building-2, and Building-3, respectively.

Adjusted collapse margin ratios for Building-1, Building-2 and Building-3 are

$$ACMR = \frac{1.30\ x\ 3.97g}{2.05g} = 2.52 \tag{4.1}$$

$$ACMR = \frac{1.30\ x\ 1.23g}{0.95g} = 1.68 \tag{4.2}$$

$$ACMR = \frac{1.35\ x\ 1.13g}{0.61g} = 2.50, \tag{4.3}$$

respectively.

Acceptability of the adjusted collapse margin ratio depends on the system uncertainty. Determination of total system uncertainty and evaluation of the performance of the building based on collapse margin ratios are given in the following sections.

4.4. Nonlinear Time History Analysis Results

Before going further, this section aims to give the reader a better insight into the behavior of relevant structural system members under seismic loads. Since Building-2 has the lowest *ACMR* and shows a weak story mechanism at the first story, hysteresis behavior model of brace and the variation of acting forces with time are represented for the first-story structural members drawn with red in Figure 4.13 of Building-2 under the Northridge (Beverly Hills) earthquake record scaled to MCE intensity. Also, inter-story drift ratios are given for all buildings.

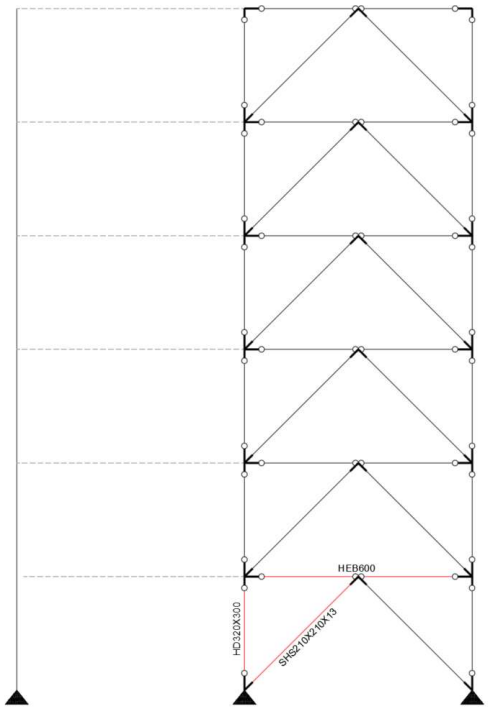

Figure 4.13. Structural members referred in sections 4.4.2, 4.4.3, 4.4.4 and 4.4.5.

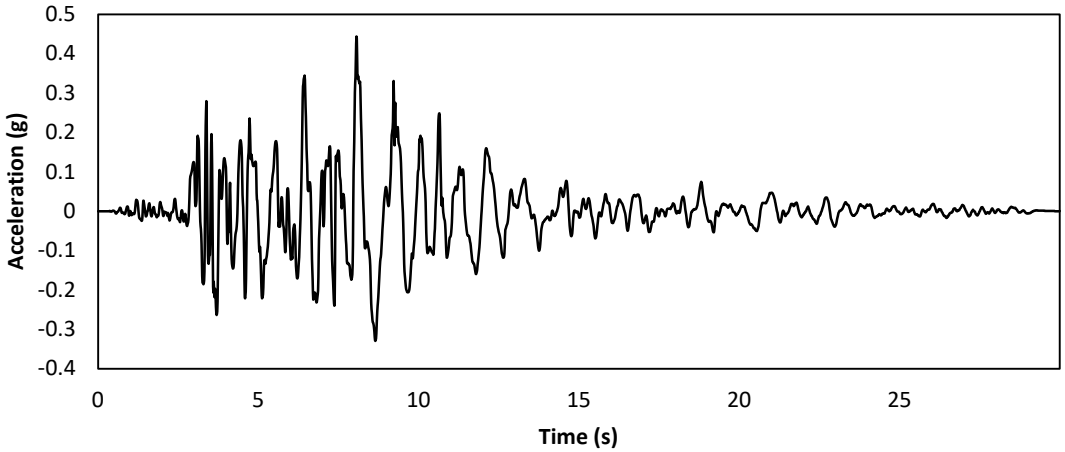

Figure 4.14. Northridge earthquake record (unscaled).

4.4.1. Inter-story Drift Ratios

Under the record set scaled to MCE intensity, inter-story drift ratios along the height of the structure are given for all three buildings in Figure 4.15.

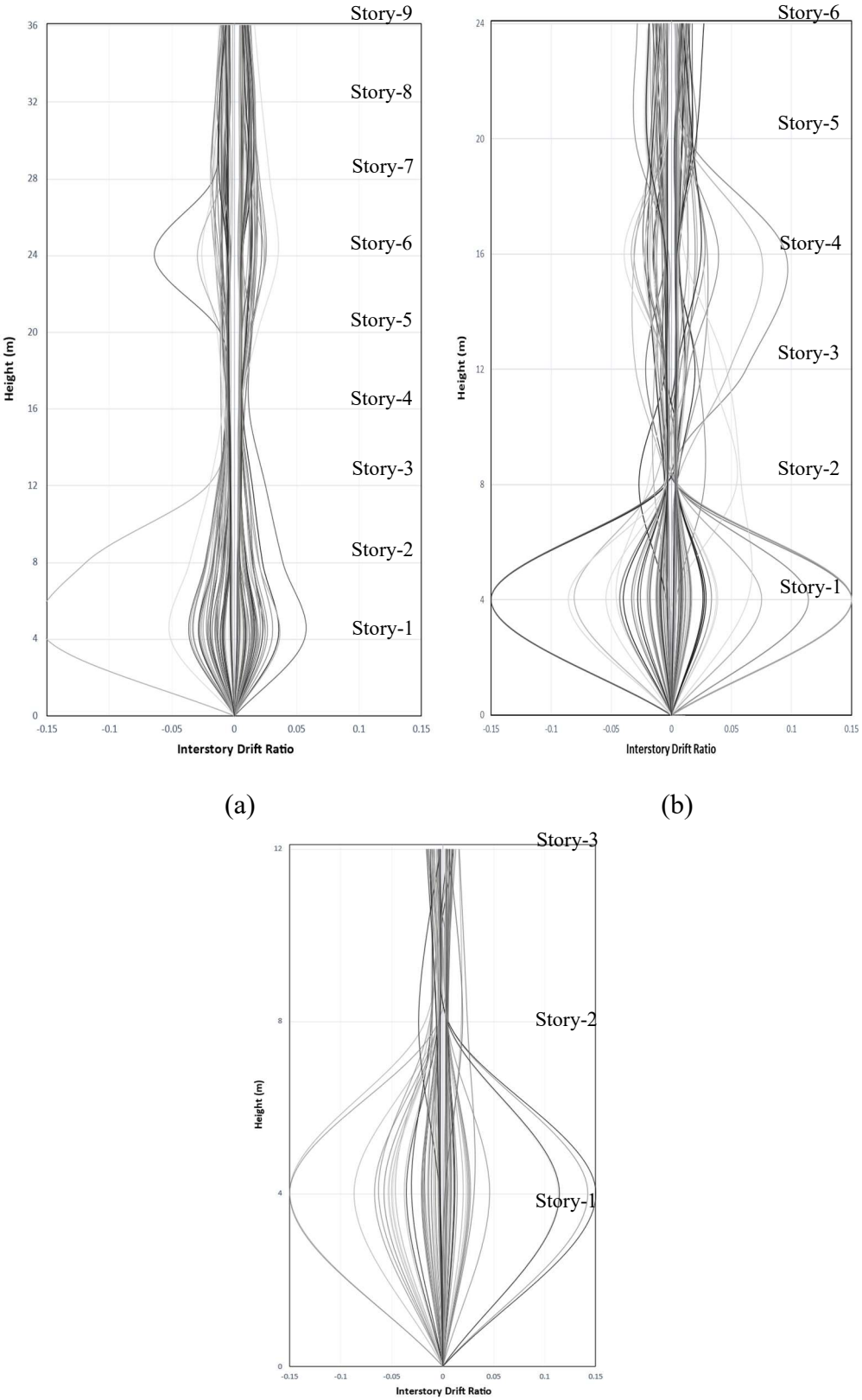

Figure 4.15. Intersory drift ratio distribution under MCE intensity for (a) building-3, (b) building-2, (c) building-1.

4.4.2. Behavior of the Braces

Braces of SCBFs are designed to buckle in compression and yield in tension to dissipate energy. Under each earthquake record, nonlinear behavior is observed in most of the braces while some remain elastic. The story of the initiation of nonlinear behavior depends on earthquake record content, though the first story often exhibits a weak story behavior. As a plastic hinge forms in a brace, other braces encounter more loads. Some braces experience strength loss after buckling phenomena while some only yield under compressive forces. Yielding in tension is observed in most of the braces; however, any brace is not subjected to strength degradation due to tensile loads.

Under some earthquake records, some braces experience excessive deformations that extend beyond the limits given in ASCE 41-17. For the sake of analysis, total strength loss is not considered. Figure 4.16 shows the hysteretic behavior of the first story brace of Building-2 under the Northridge earthquake record. As shown in the figure, after the buckling of the brace, the centroid of the hysteresis curve shifts significantly, and positive deformations cannot be achieved again. As the load continues to act on the brace, plastic deformations cumulatively increase at different times. In the subsequent chapters, this brace will also be used to represent the general behavior of frames that reach the collapse point. Thus, for integrity, its behavior is decided to be presented in this chapter.

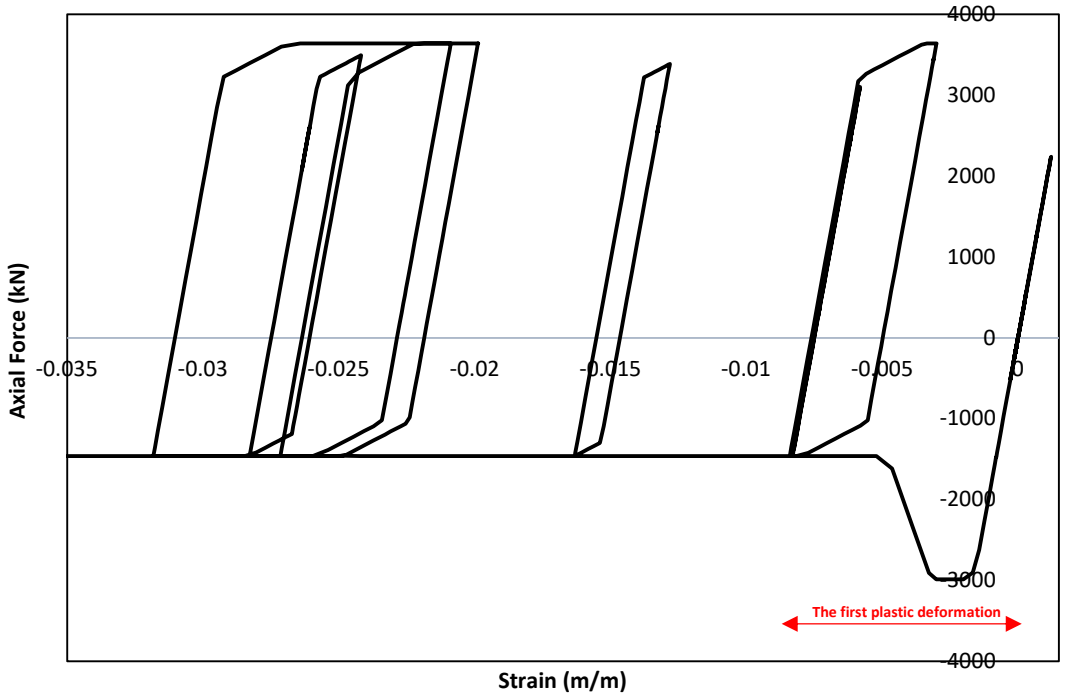

Figure 4.16. Hysteretic behavior of first story brace of building-2 under Northridge earthquake record scaled to MCE intensity level.

4.4.3. Behavior of Columns

Columns of SCBFs are dimensioned to remain elastic under the axial forces arising from bucking and post-bucking mechanisms in the design phase. For SCBFs whose beam-to-column connections are designed as a rigid connection, there is no additional clause to be considered in the design of those columns in TSC. Nonlinear analysis reveals that when the brace in a story deforms plastically, the beam and column end at that story begins to resist bending deformations by displaying a moment frame behavior. As a consequence of unbalanced forces on the beams and consideration of only axial forces in the design of the columns, most beams are concluded to have higher moment resistance than columns of chevron-type SCBFs. As a result, plastic hinge forms at the end of columns prior to beams due to the bending moments. Besides, if the axial capacity of the columns is kept to be close to the demand arising from gravity loads and buckling mechanisms of braces, strength degradation in bending occurs in the very early stages of the bending deformation of columns.

For the first story of Building-2, the column has a compression capacity of 13446 kN. At 5.42s of record, there is a degradation in column strength. At that moment, the acting axial force and bending moment on the column are 10673.9 kN and 873.1 kNm, respectively. At the same time, the acting axial load and axial strength of each brace that transfers loads to this column are given in the following table.

Table 4.4. Acting axial loads and axial strength of brace at 5.42s of Northridge record scaled to MCE intensity.

STORY	Axial Strength	Axial Load
1	-2986.76	-1463.55
2	-2766.03	-2484.66
3	-2543.87	-2526.95
4	-2320.34	-2320.30
5	-1750.27	-1733.39
6	-1123.26	-958.94

4.4.4. Behavior of Beams

Beams of SCBFs are dimensioned to remain elastic under the axial forces and bending moments caused by gravity forces and unbalanced forces due to the buckling and post-buckling mechanism of the braces. Since the flexural strength of columns is smaller than that of beams, there is no nonlinearity at the end of the beams.

In the design phase, since the beam-to-column connection is rigid, the acting moment at the middle of the beam is small compared to a simple beam. Nonlinear analysis indicates that when a hinge forms at the end of the column due to a high compressive load and associated small bending moment, the beam connected to this column is limited to transfer bending moments with the amount of flexural strength of this column. If the flexural strength of the column decreases due to increasing axial forces, the bending moment acting on the middle of the beam rises simultaneously. Thus, the design of the beams of rigid connected SCBFs should be performed with the assumption in the calculation of acting moments that the beam bends such a simple beam (zero moments at the end of the beams).

4.4.5. Behavior Pattern on the Collapse

If the behavior of structural members under earthquake records is examined, a similar behavior pattern is observed for all the buildings under each record on the way to collapse. For the purpose of illustrating this pattern, first story members of Building-2 under the Northridge earthquake record scaled to MCE intensity are dealt with solely because of its high inter-story drift ratio.

In the following figures, responses of first story members of Building 2 and variations of first story drift with time under the Northridge earthquake record are given. To make the behavior of frames reaching the collapse point clear, the time when the brace begins to experience a strength loss due to the compressive force is indicated with the red line.

After the bucking of the brace, moments at the end of columns increase rapidly as can be seen in figure 4.19. Axial loads acting on the column increase with respect to the rise in the acting compressive forces on the braces upstairs. At T=5.42s the column experiences strength degradation, but still resists some amount of bending deformation.

Figure 4.21 shows that subsequent to the strength loss of the brace, bending moments at the end of the beam increase in an obvious way. On the other hand, Figure 4.22 demonstrates that with axial force equaling the full compressive strength on the brace, axial loads on the beam increase accordingly. After buckling of the brace, axial loads remain high due to the tensile brace and moment frame behavior.

Figure 4.17 emphasizes that even though considerable strength and stiffness loss of the system is observed at the first 8s of record, the drift ratio does not get close to the collapse point. However, after the plastic hinge forms at the column end, frame members lose the ability to recycle under seismic loads and cannot fully reverse in another direction. At some point, second-order effects increase significantly, and the building eventually collapses.

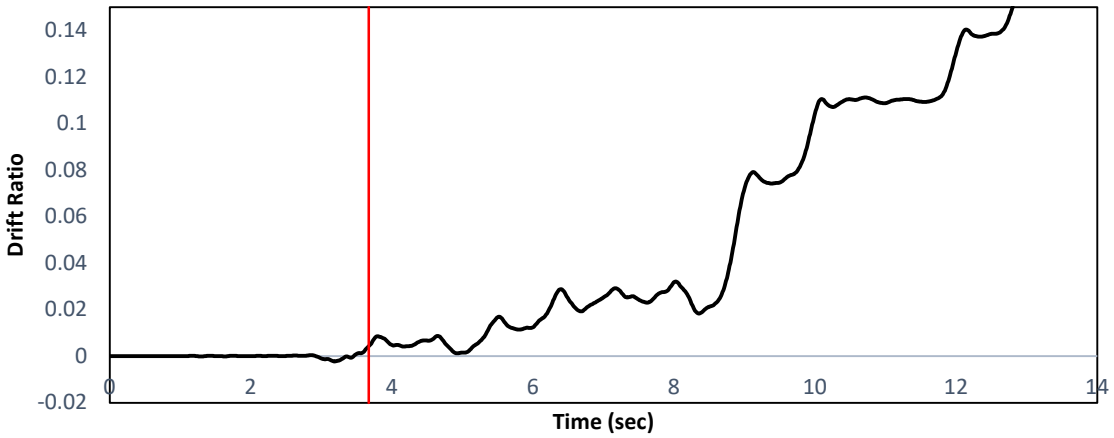

Figure 4.17. First story drift - time history.

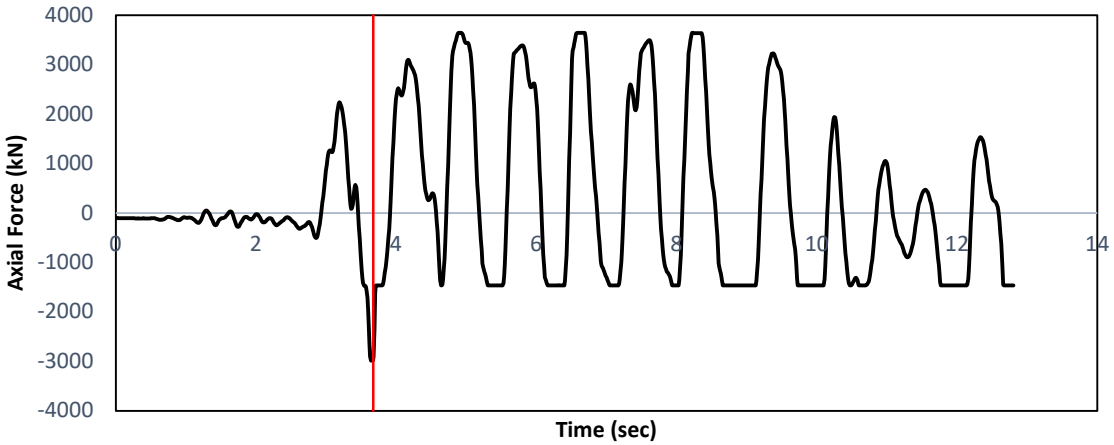

Figure 4.18. Axial forces in brace - time history.

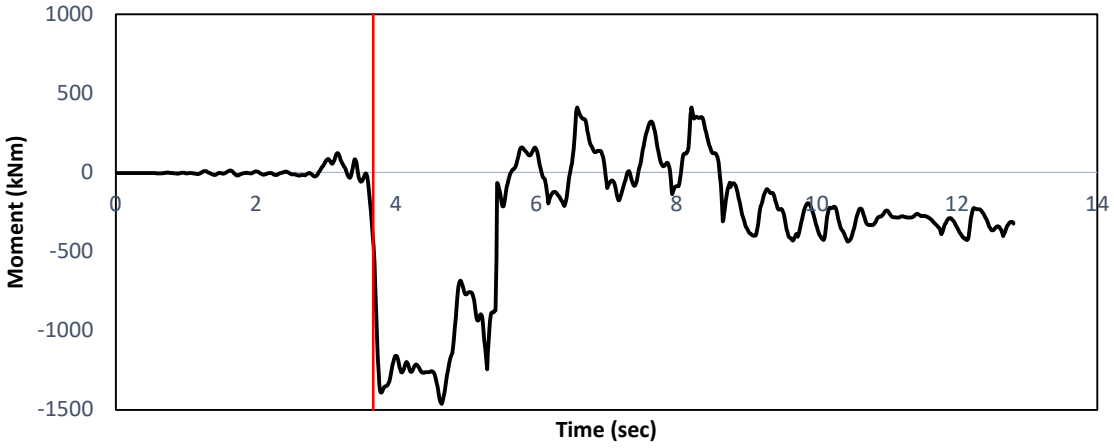

Figure 4.19. Bending moment in column - time history.

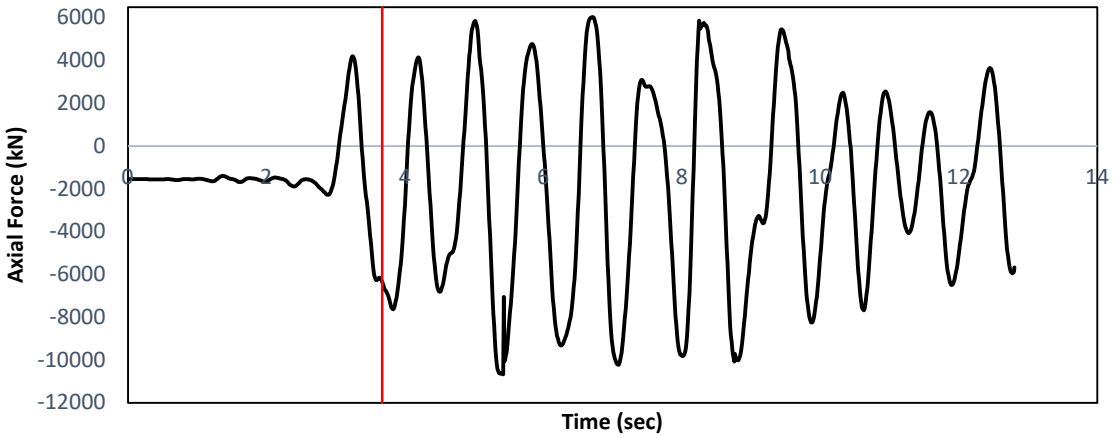

Figure 4.20. Axial forces in column - time history.

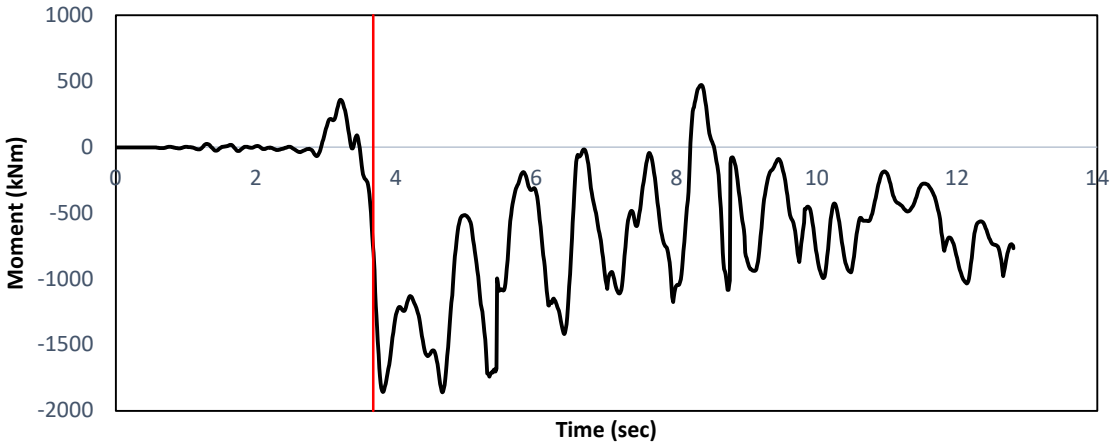

Figure 4.21. Bending moment in beam - time history.

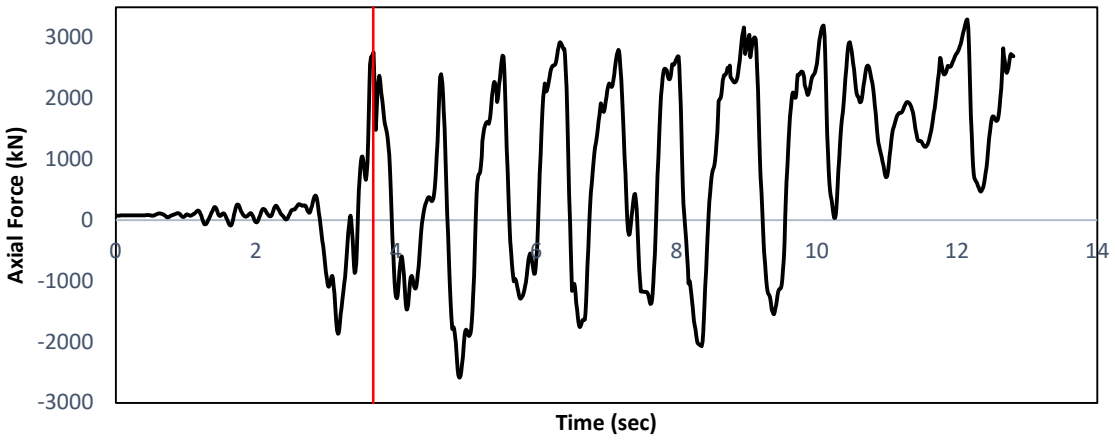

Figure 4.22. Axial forces in beam - time history.

To demonstrate the impact of second-order effects on collapse, the same story is employed to show the difference in the behavior between models in which P-Delta effects are included and excluded. Figure 4.23 shows that if P-Delta effects would not be taken into account, the structure stands still against the Northridge earthquake record, otherwise it collapses. Thus, it can be generalized that, in all the records that cause collapse, P-Delta effects rapids the collapse significantly. Recall that the reason why analysis with second-order effects does not continue till the end of the record is an assigned stop limit at 0.15 drift ratio in software.

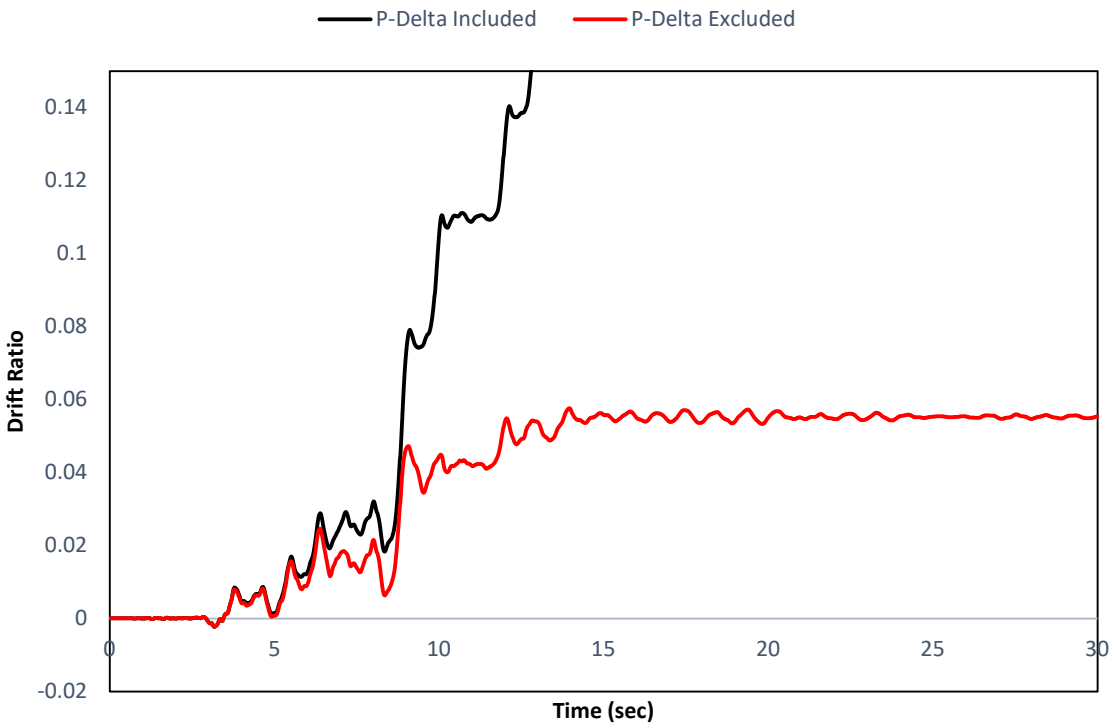

Figure 4.23. Impact of second order effects on collapse.

4.5. Fragility Functions

For the development of fragility curves which is defined in this study by a lognormal distribution function, there are two parameters to consider: median value and standard deviation. In this section, considered parameters and corresponding fragility functions for all buildings are introduced. The effect of standard deviation on the fragility curve is argued.

4.5.1. Median Value of Fragility Function

The median value is determined from the incremental dynamic analysis as the median collapse capacity of the structure increased by spectral shape factor. Calculated values of median values are given in Table 4.5 for all buildings.

Table 4.5. Median values of fragility functions.

Building	Median Value
Building-1	5.16g
Building-2	1.60g
Building-3	1.52g

4.5.2.Determination of System Uncertainty (Standard Deviation)

To determine the standard deviation of the fragility function, uncertainty is divided into components according to FEMA P-695 procedure. These uncertainties and considered values are given in Table 4.6.

Table 4.6. Considered uncertainties.

TYPE	VALUE
Record-to-Record Uncertainty, β_{RTR}	0.4
Design Requirement Uncertainty, β_{DR}	0.2
Test Data Uncertainty, β_{TD}	0.2
Modelin Uncertainty, β_{TD}	0.35

Total system uncertainty is calculated as 0.6 from

$$\beta_{TOT} = \sqrt{\beta_{RTR}^2 + \beta_{DR}^2 + \beta_{TD}^2 + \beta_{MDL}^2}\,. \tag{4.4}$$

Previous studies on the construction of fragility functions employ similar values of standard deviation considered here. A study carried out by Luca et. Al. (2007) for the purpose of developing seismic risk maps in the United States, interprets a value of 0.8 as a good approximation for total uncertainty. On the other hand, a value of 0.6 is accepted and used over the country by ASCE 7-16.

4.5.3. Fragility Curves of Each Building

Figure 4.24 shows established lognormal fragility curves of all three buildings. Standard deviation and median values of each curve are indicated on the graph.

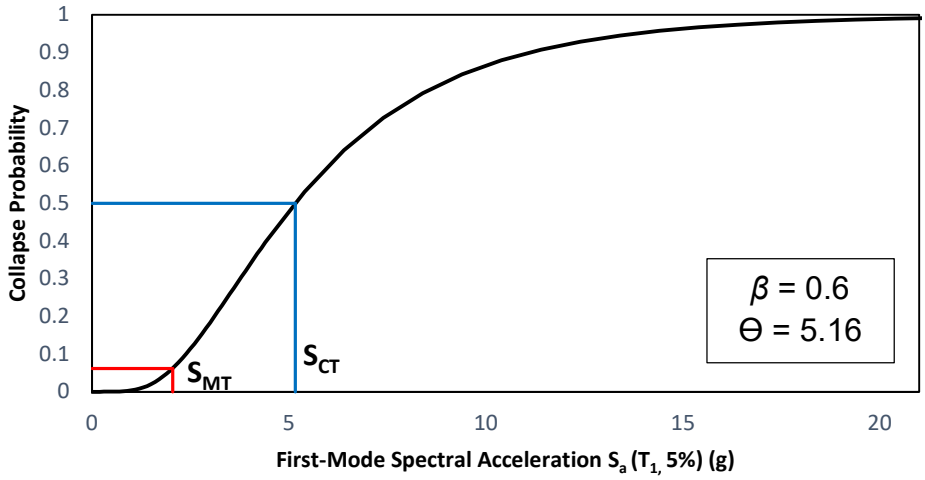

(a)

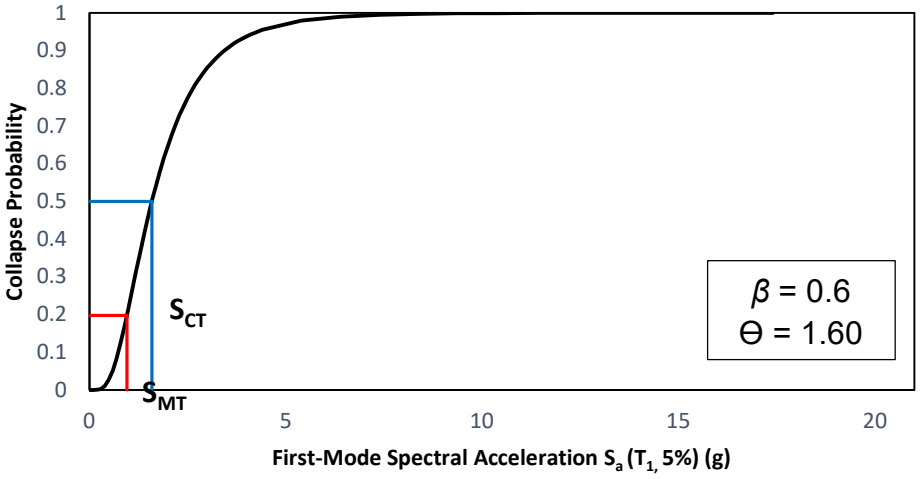

(b)

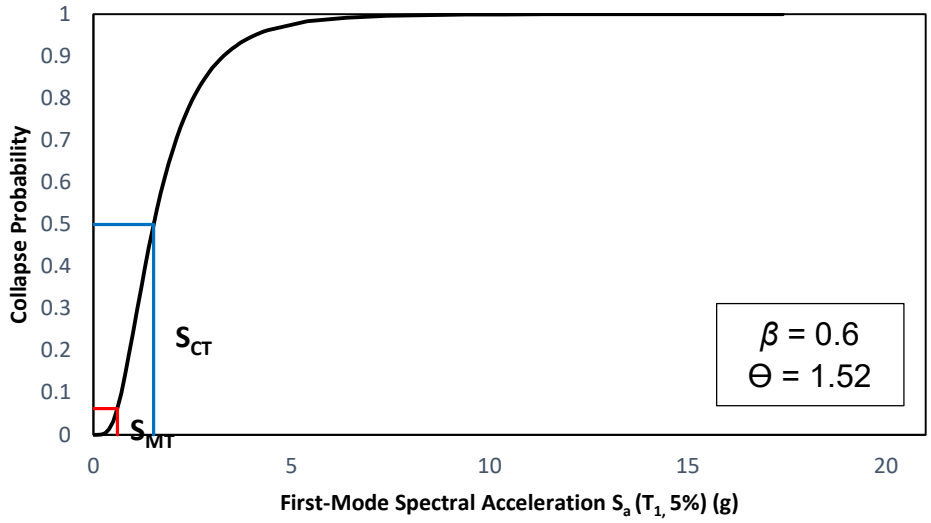

(c)

Figure 4.24. Fragility curves of (a) building-1, (b) building-2, (c) building-3.

As can be seen from the curves, MCE intensity corresponds to a collapse probability of 6%, 20% and 6% for Building-1, Building-2 and Building-3, respectively.

4.5.4. Sensitivity Analysis for Different Values of Standard Deviation

The standard deviation value taken into account has a nonnegligible impact on the fragility curve. Thus, special care should be given to represent variability parameters close to real situations.

Figure 4.25 shows the change in fragility curves according to the different standard deviation values of 0.4, 0.5, and 0.6 for all three buildings. As can be observed from the figures, as the standard deviation value increases, the curve becomes steeper. In other words, a rise in the variability causes higher collapse probabilities for acceleration values smaller than the median value and lower probabilities in values bigger than the median value. If its impact on the risk is argued, a rise in the standard deviation values will bring higher risks obviously, due to the higher exceedance rates in lower acceleration values as will be discussed in the following sections.

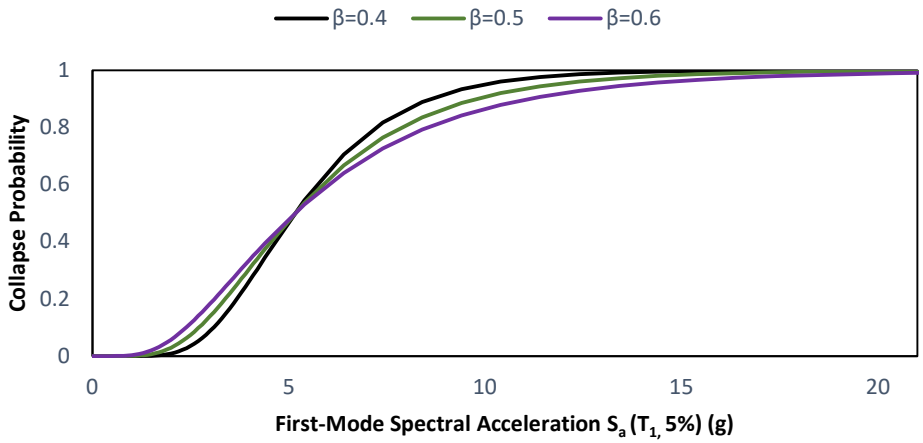

(a)

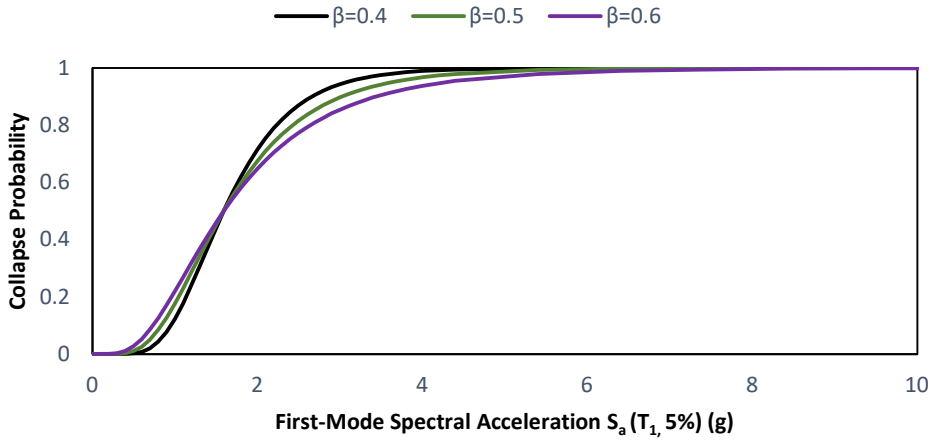

(b)

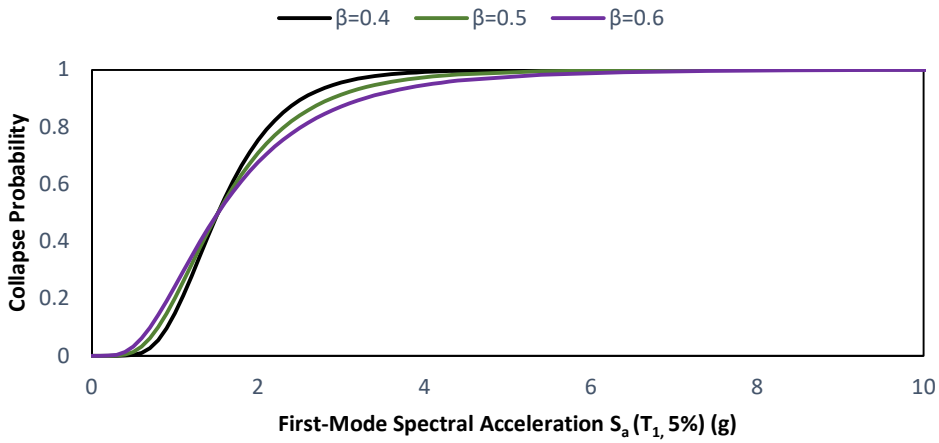

(c)

Figure 4.25. Comparison of different values of variability for (a) building-1, (b) building-2, (c) building-3.

4.5.5. Building Performance Evaluation

According to FEMA P-695, the performance of a building can be considered satisfactory if

$$ACMR \geq ACMR10\%. \tag{4.5}$$

For a system uncertainty of 0.6, the $ACMR10\%$ value is 2.16 from Table 2.5. while the *ACMR* is calculated as 2.52, 1.68 and 2.50 for Building-1,2 and 3, respectively. According to this results, while Building-1 and Building-3 present adequate performance, Building-2 fails in the collapse assessment.

Acceptability of building performance can also be defined by the probability of collapse for MCE intensity, which shall be less than 10% for an acceptable performance level. In Figures 4.26, 4.27, and 4.28 for different values of standard deviation, fragility functions and corresponding probabilities for MCE intensity are given with the collapse capacity of structures for all buildings. Figures demonstrate that as the standard deviation decreases, collapse probability at MCE intensity decreases dramatically. Collapse probabilities at MCE intensity are given in Table 4.7 for different values of standard deviation. It is seen that for all values of standard deviation, Building-1 and Building-2 stay within the acceptable limit, whereas Building-2 fails.

Table 4.7. Collapse probabilities for different values of standard deviation.

BUILDING NO	Probability of Collapse at MCE intensity		
	β=0.6	β=0.5	β=0.4
BUILDING-1	6.2%	3.2%	1.1%
BUILDING-2	19.8%	15.4%	10.2%
BUILDING-3	6.3%	3.3%	1.1%

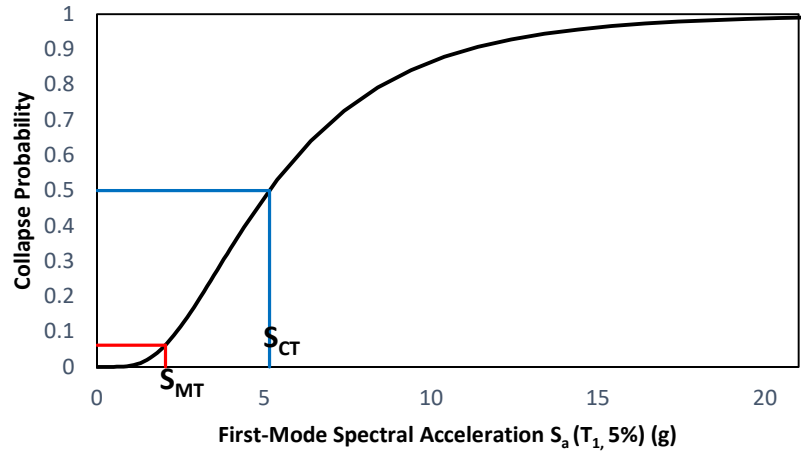

(a)

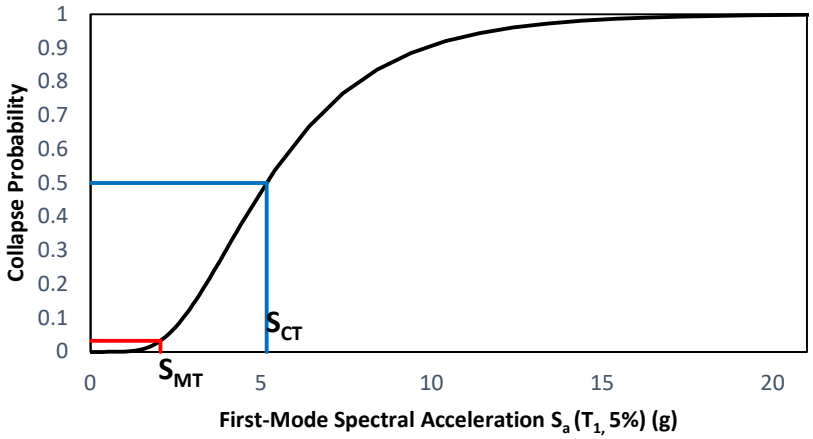

(b)

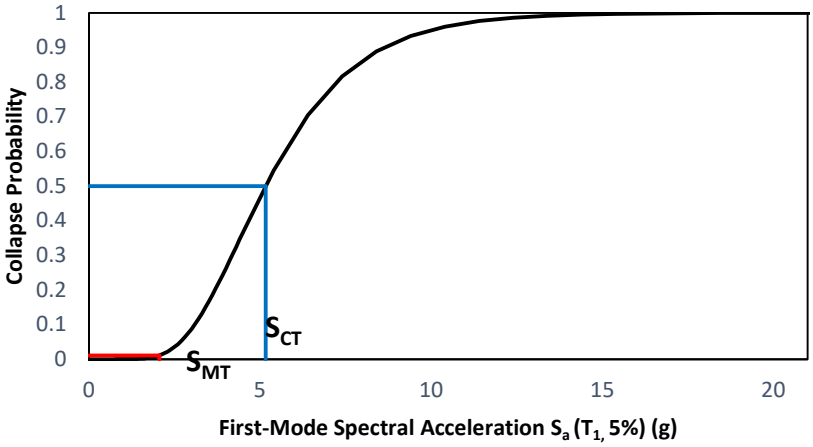

(c)

Figure 4.26. For building-1, probability of collapse at MCE intensity for (a) β=0.6, (b) β=0.5, (c) β=0.4.

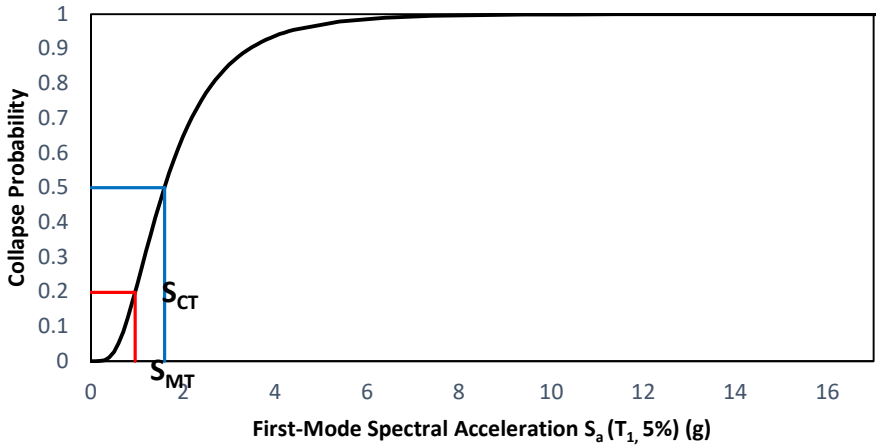

(a)

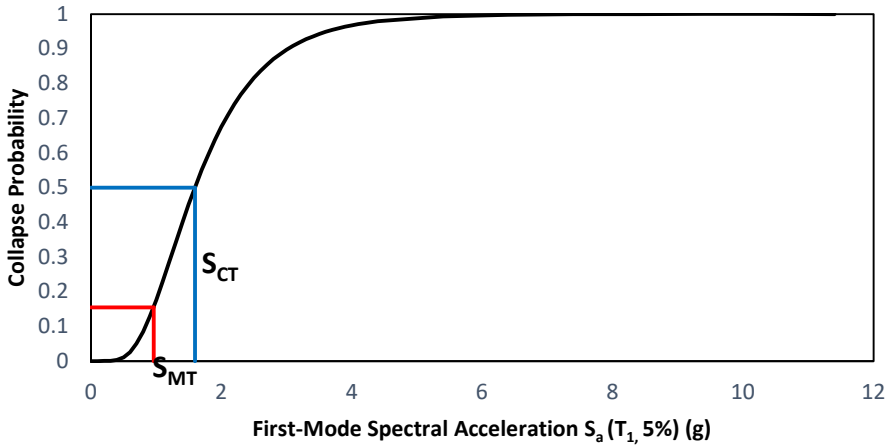

(b)

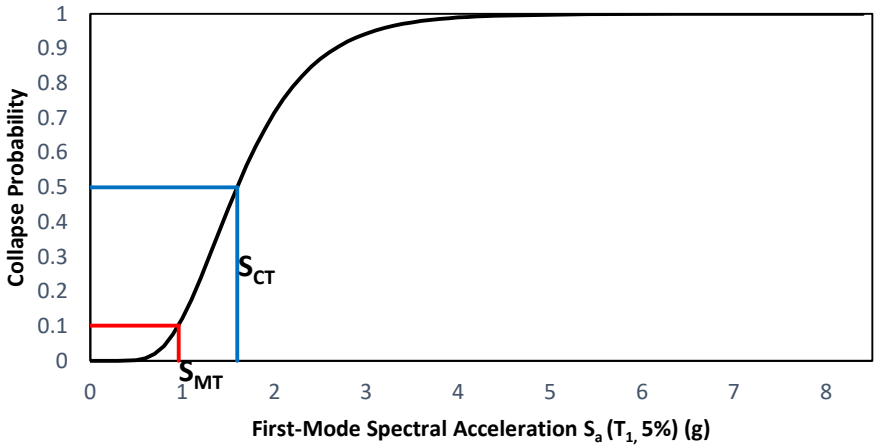

(c)

Figure 4.27. For building-2, probability of collapse at MCE intensity for (a) β=0.6, (b) β=0.5, (c) β=0.4.

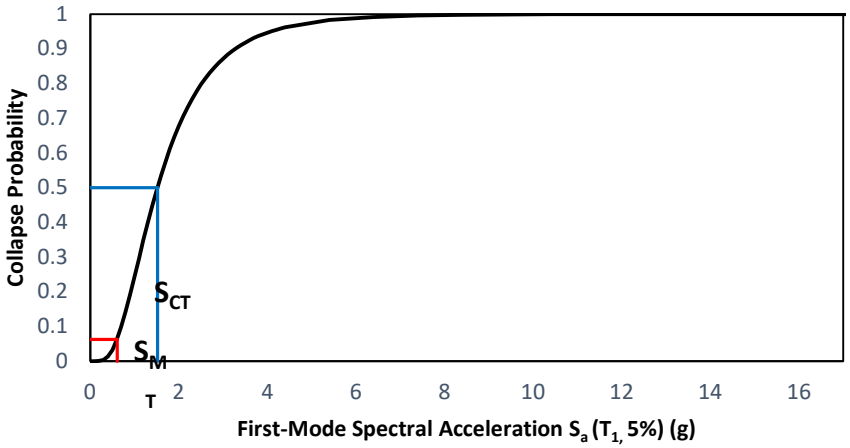

(a)

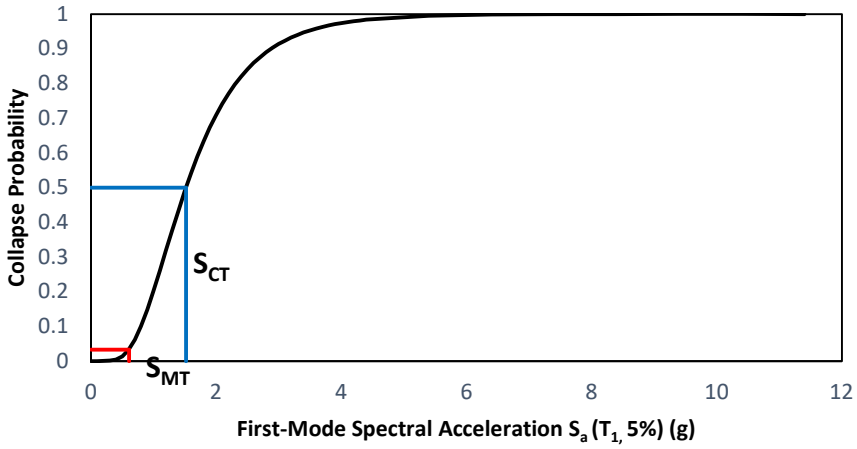

(b)

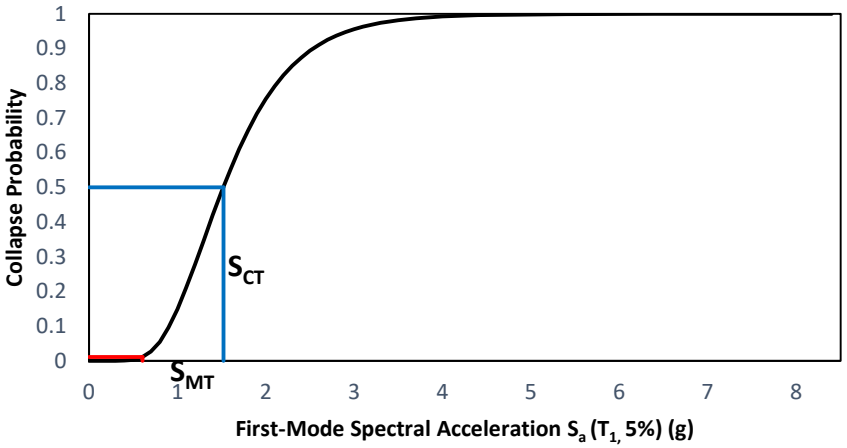

(c)

Figure 4.28. For building-3, probability of collapse at MCE intensity for (a) β=0.6, (b) β=0.5, (c) β=0.4.

4.6. Risk Assessment Result

To achieve the collapse risk of a structure during its lifetime, two functions are required, which are the hazard curve at the location of the building at the fundamental period, and the fragility curve at the fundamental period. Risk is calculated by multiplying these two curves and integrating overall acceleration values. The mean annual frequency of collapse is given as

$$\lambda_C = \int_0^\infty \lambda_x \, f_{Capacity}(x), \tag{4.6}$$

and repeated in this chapter for convenience. For the calculation purposes, this equation can be rewritten as

$$\lambda_C = \int_0^\infty \lambda_x \left| \frac{df_{Capacity}(x)}{dx} \right| dx, \tag{4.7}$$

where $df_{Capacity}(x)/dx$ is the slope of fragility function. Finally, to conduct the collapse probability of structure in 50 years, the equation of

$$P_C(t) = 1 - e^{-\lambda_C x(50)} \tag{4.8}$$

is employed.

In the following figures, calculation steps and the final result of risk are given for all buildings. Figures (a) and (b) showing the hazard curve and fragility function are repeated here for integrity. In figure 4.29, 4.30 and 4.31, (c) representing the derivation of the fragility curve demonstrates that in the acceleration values smaller than the median value, collapse probabilities are higher. In the figures, (d) indicates the deagregation of mean annual collapse probability, which is the product of the hazard curve times derivative of the fragility curve. Since the occurrence and contribution of collapse probability at higher acceleration values are low, small acceleration values contribute to the risk much more. Finally, (e) gives the collapse risk of a building in 50 years. Collapse risk in 50 years is calculated as 0.61%, 1.9%, and 0.62% for Building-1, Building-2, and Building-3, respectively where 1% collapse risk is assumed as an acceptable value by ASCE 7-10.

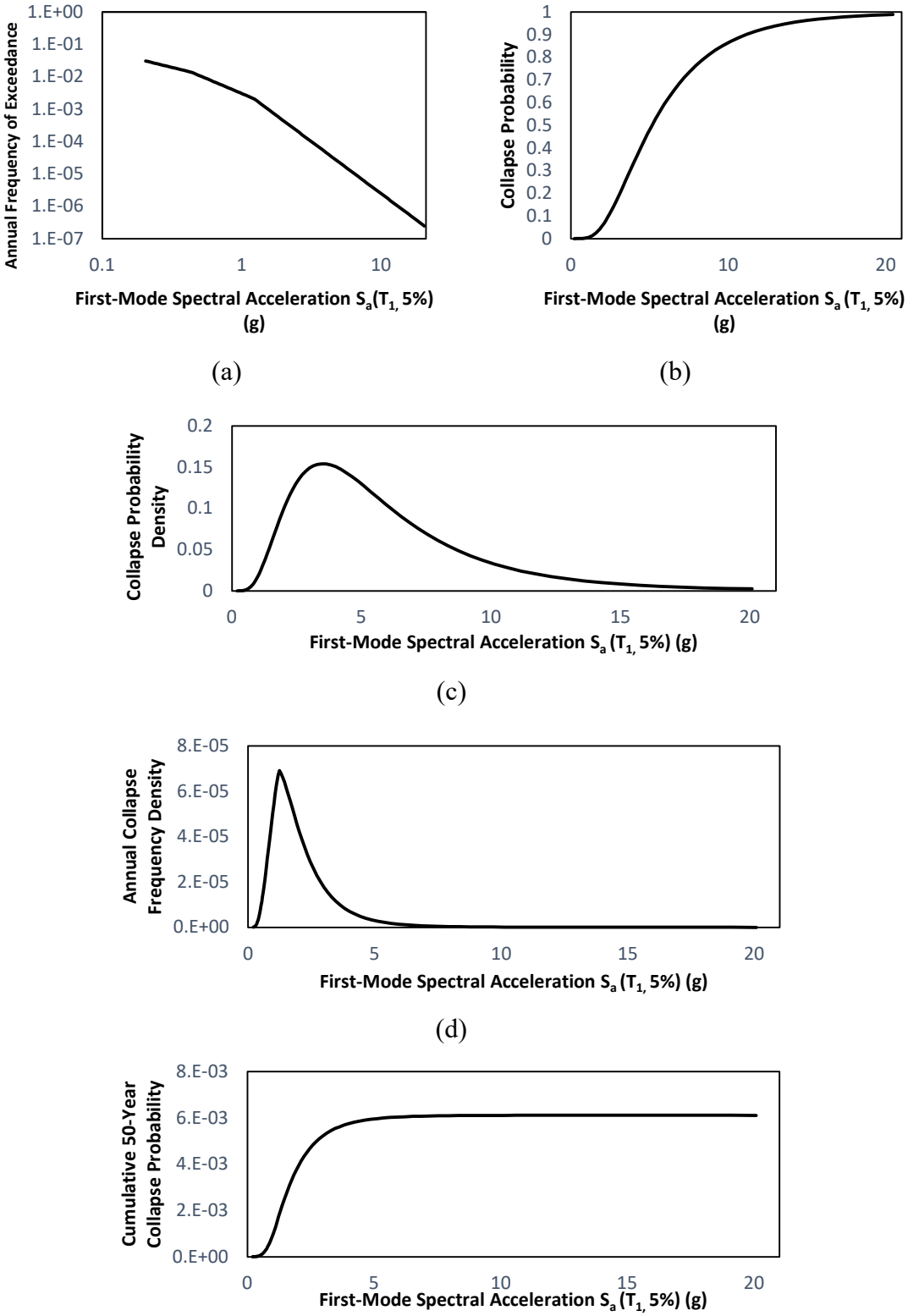

Figure 4.29. For building-1, (a) hazard curve, (b) fragility curve, (c) derivative of fragility curve, (d) hazard curve x derivative of fragility curve, (e) cumulative integral of hazard curve x derivative of fragility curve.

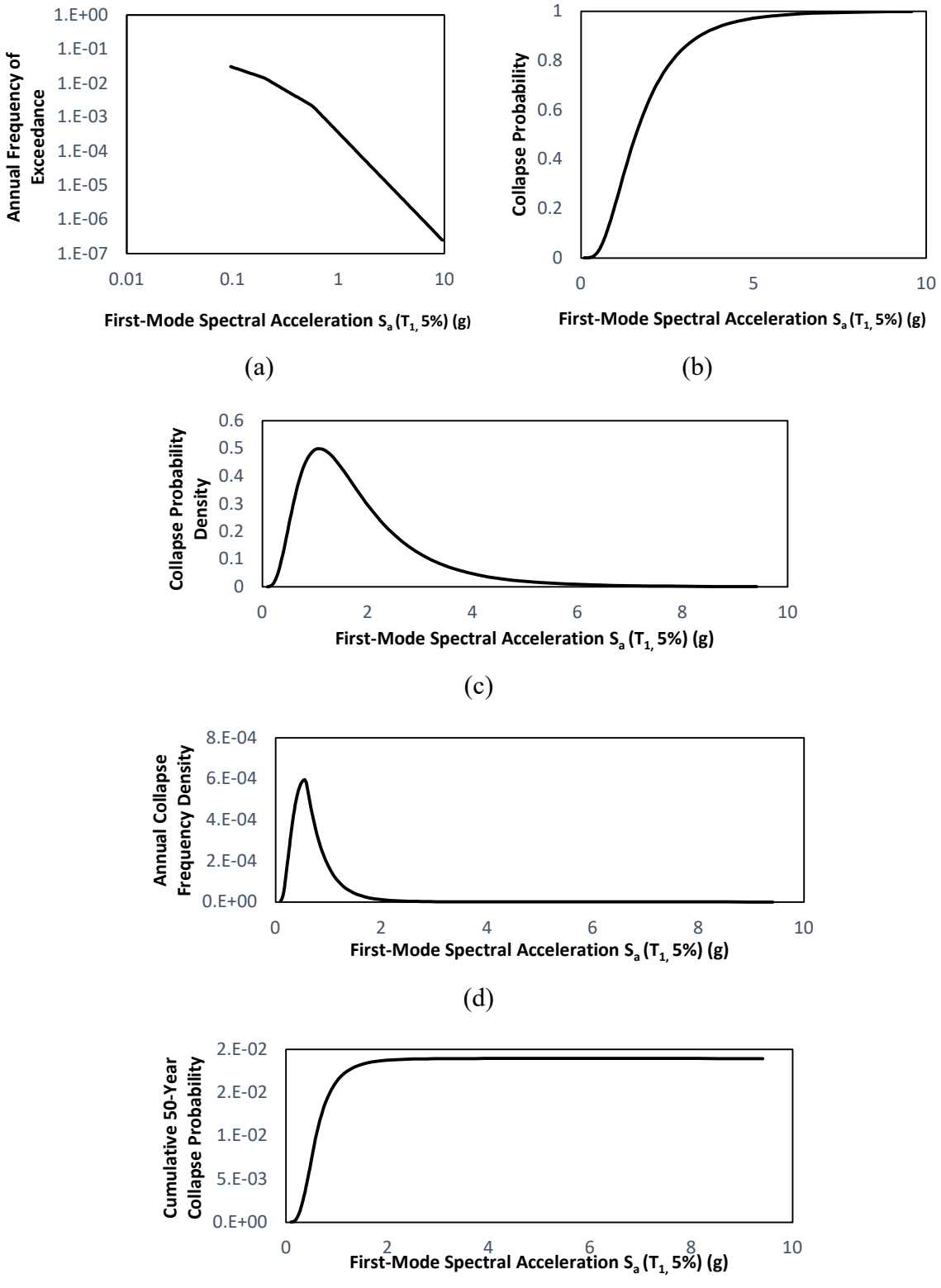

Figure 4.30. For building-2, (a) hazard curve, (b) fragility curve, (c) derivative of fragility curve, (d) hazard curve x derivative of fragility curve, (e) cumulative integral of hazard curve x derivative of fragility curve.

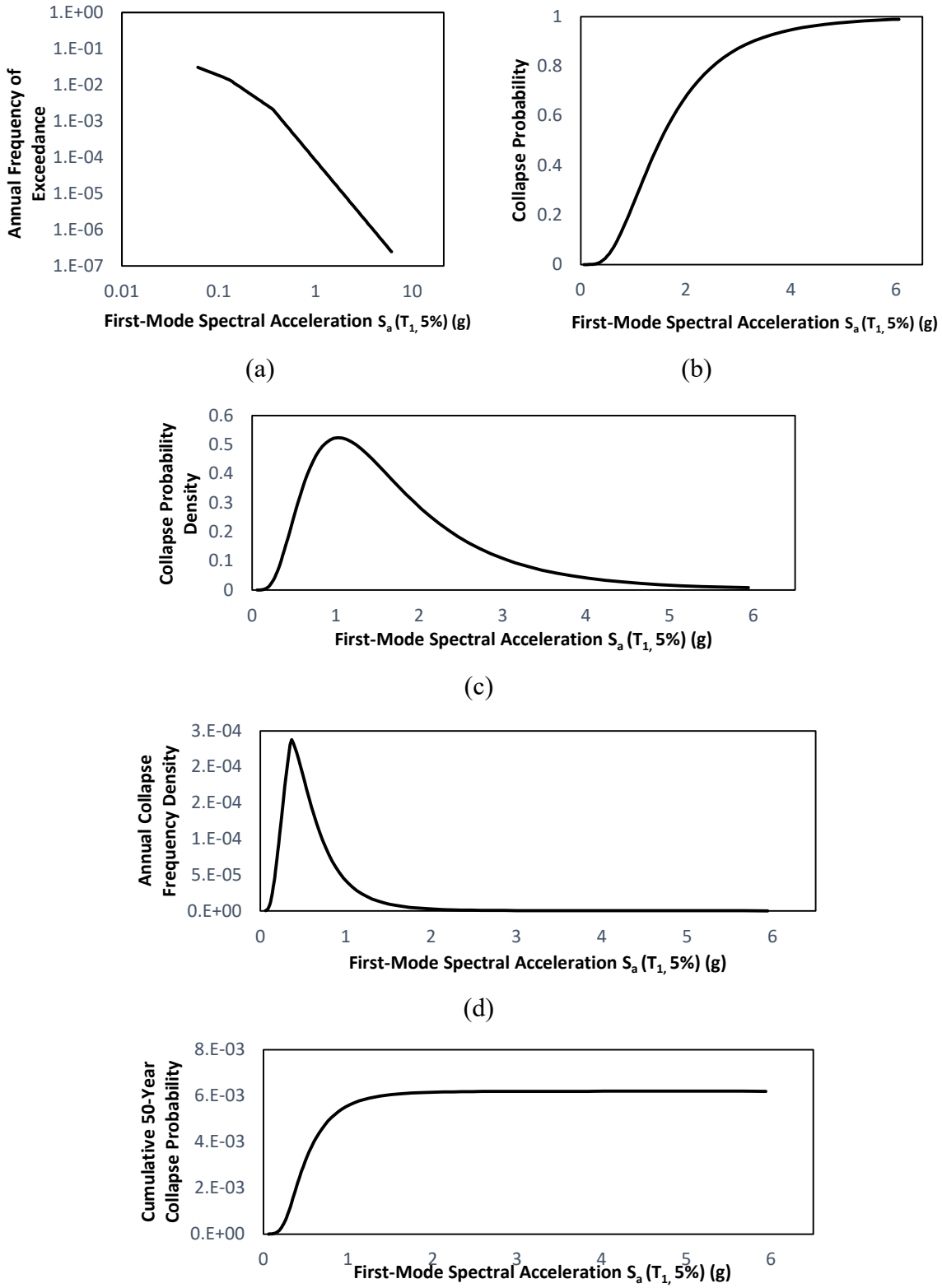

Figure 4.31. For building-3, (a) hazard curve, (b) fragility curve, (c) derivative of fragility curve, (d) hazard curve x derivative of fragility curve, (e) cumulative integral of hazard curve x derivative of fragility curve.

5. SUMMARY AND CONCLUSIONS

5.1. Summary

In this study, three buildings having different fundamental periods with special concentrically braced frames were investigated. The linear design of the buildings is performed according to the Turkish Seismic Code. For the linear structural analysis of the buildings, SAP2000 software is utilized. The capacity design approach is applied to determine the dimensions of the structural members. For the nonlinear analysis, Perform 3D software is employed. Due to the computational time requirements and reliability of analysis results, buildings are analyzed as equivalent well-presented 2D frames in the fundamental period. Nonlinear time history analysis is performed for all buildings with 22 earthquake pairs taken from the PEER website.

FEMA P-695 procedure is followed in the construction of fragility functions of the buildings. Incremental dynamic analysis is conducted to obtain full IDA curves under all the earthquake records with increasing intensities until the collapse occurs. Collapse is defined in terms of maximum inter-story drift ratio and 10% drift is established as a collapse limit. Collapse median capacities of the structures are determined according to the incremental dynamic analysis results. Standard deviation is decided by implying FEMA P-695 procedure and rating variabilities in the structure. The effect of the standard deviation value on the collapse probability is investigated with different values of variability. Evaluation of structural performance is provided according to the FEMA P-695 procedure. Hazard curves are obtained from the TEHM website and the USGS risk-targeted ground motion calculator is used to complete hazard curves. To calculate the collapse risk of the structures in 50 years, risk integrals are utilized. The mean annual collapse probability is calculated by multiplying the hazard curve with the fragility function. Deagragation of risk integrals is presented to demonstrate different contributions of different acceleration values to collapse risk.

5.2. Conclusions

The following conclusions can be drawn based on analysis results and outcomes of risk integrals of each building.

- The collapse risk in 50 years is calculated as 0.61%, 1.89% and 0.62% for Building-1, 2 and 3, respectively. For two of the buildings, the collapse risk achieved remains within the acceptable limit of 1% while for one of them it exceeds it by nearly twofold. This result causes mainly by inadequacy in the collapse capacity of this building rather than the form of the seismic hazard curve. Although the design acceleration value proposed by THEM for this location is above the required, risk exceeds the limit because of the low collapse capacity of the Building-2.

- Based on the calculated *ACMR*s of three buildings, one building fails to provide necessary safety against collapse. The collapse capacity of this building is calculated as lesser than what it is supposed to be for satisfactory performance. The FEMA P-695 procedure adopted for these buildings reveals that the structural behavior factor given in the Turkish Seismic Code for special concentrically braced frames, R=5 may not be suitable for all ranges of buildings.

- According to each individual building's analysis results, although the first building with three stories shows a weak story mechanism, it is less affected by the P-Delta effects. Therefore, the occurrence of the collapse is slower compared to other buildings and negative slope in the capacity curve is smaller. Also, the second building with six stories shows a weak story mechanism under most of the records, plastic hinge forms at the column ends in the first story and the P-Delta effects accelerate the collapse. The third building with nine stories shows a satisfactory result since in the first and second stories plastic hinges form in the beam ends first prior to the column ends and seismic energy can be dissipated by moment frame action in these stories.

- In the design of beams of special concentrically braced frames with rigid beam-to-column connection, acting forces on the beams should be determined by assuming a simple connection at each end since nonlinear analysis reveals that if plastic hinge forms at the column end with a high level of axial stresses, moment transferred from beams to columns decreases dramatically and moments in the middle of the beam increases accordingly. Thus, dimensioning of the beams according to the rigid end connections leads to a plastic hinge in the middle of the beam.

- In a special concentrically braced frame with a rigid beam-to-column connection, after the buckling of a brace, the moment at the beam and column end increases suddenly. If the column already suffers from high axial load levels and the moment capacity of the column is smaller than the beam, the plastic hinge will form under the low level of moment forces at the first story column end. This behavior leads to a high collapse risk in Building-2. On the other hand, a second model of Building-2 considering a pin connection between the frame beam and column demonstrates that plastic hinge forms at the second or third story column end first in most of the records, which delays the collapse.

- Once the plastic hinge at the column end, drifts begin to increase dramatically after the bucking of braces. Thus, to provide a second insurance point to concentrically braced frames after buckling of braces, column sections should be selected such that a plastic hinge occurs at the ends of beams, which is not a requirement in the Turkish Seismic Code.

- The risk is very sensitive to the selected standard deviation value. For example, in Building-2, the selection of β=0.4, β=0.5, and β=0.6 values leads to risk values of 0.92%, 1.33%, and 1.89%, respectively.

- According to the behavior of the three buildings in concern, special concentrically braced frames tend to have a weak story mechanism at the first story and P-Delta effects accelerate the collapse due to this mechanism. Thus, the selection of bigger brace sections for the first stories can significantly reduce the risk.

- Deagragation of the mean annual collapse probability emphasizes that small to medium earthquake intensities contribute to collapse risk the most, and large earthquake intensities have a limited effect on the risk due to the smaller occurrence rates and collapse probabilities.

5.3. Recommendations for Future Studies

For future research in the area of this thesis, the following recommendations can be made:

- Risk assessment can be applied to buildings designed according to the Turkish Seismic Code with different structural systems.

- Risk assessment can be performed for buildings at different locations and changes in the collapse risk can be investigated depending on the location of the buildings and the shape of seismic hazard curves.

- A similar study can be conducted for special concentrically braced frames with simple beam-to-column end connections. The contribution of rigidity of the connection to collapse capacity can be investigated.

- The proper value of standard deviation in the development of fragility functions can be investigated for building types located in Turkey.

- For all structural system types, the structural system behavior factor that results in a 1% of collapse probability in 50 years can be studied.

- For all structural system types, the structural system behavior factor that results in a 1% of collapse probability in 50 years can be studied.

- Sensitivity analysis can be performed for different definitions of collapse point such as different drift ratios, number of failed members, etc.

REFERENCES

1. Turkish Earthquake Code, *Specifications for Structures to be Built in Disaster Areas*, Disaster and Emergency Management Presidency, Ankara, 2018.

2. ASCE/SEI Structural Engineering Institute, *Minimum Design Loads for Buildings and Other Structures*, ASCE/SEI7-10, American Society of Civil Engineers, Reston, VA, 2010.

3. Applied Technology Council, *Quantification of Building Seismic Performance Factors*, FEMA P695, Federal Emergency Management Agency, Washington, D.C., 2008.

4. Disaster and Emergency Management Presidency, "Turkish Earthquake Hazard Map", 2017, https://tdth.afad.gov.tr/, accessed on December 25, 2022.

5. Qammer, S. and S. Dalal, "Development of Performance Based Seismic Design: A Review", paper presented at the *International Conference on Engineering and Technology (ICET)*, Kuala Lumpur, Malaysia, 2016.

6. SEAOC Vision 2000 Committee, "Performance Based Seismic Engineering of Buildings", *Structural Engineers Association of California*, Vol. 2, 2000.

7. ATC-40 Committee, *Seismic Evaluation and Retrofit of Concrete Buildings*, Applied Technology Council, Redwood City, CA, 1996.

8. ATC-33 Committee, *Guidelines for the Seismic Rehabilitation of Buildings*, NEHRP FEMA 273/274, Building Seismic Safety Council, Washington, DC, 1997.

9. Bertero, V., "Strength and Deformation Capacities of Buildings Under Extreme Environments", *Structural Engineering and Structural Mechanics*, Vol. 53, pp. 211– 215, 1977.

10. Vamvatsikos D. and C.A. Cornell, "Incremental Dynamic Analysis", *Earthquake Engineering and Structural Dynamics*, Vol. 31, Issue 3, pp. 491-514, 2002.

11. SAC Joint Venture, *Recommended Seismic Evaluation and Upgrade Criteria for Existing Welded Steel Moment-Frame Buildings*, FEMA-351, the Federal Emergency Management Agency, Washington DC, 2000.

12. Porter K., "A Beginner's Guide to Fragility, Vulnerability, and Risk", 2021, https://www.sparisk.com/pubs/Porter-beginnersguide.pdf, accessed on December 25, 2022.

13. Whitman R.V., T. Anagnos, C.A. Kircher, H.J. Lagorio, R.S. Lawson, P. Schneider, "Development of a National Earthquake Loss Estimation Methodology", *Earthquake Spectra*, Vol. 13, Issue 4, 1997.

14. Ibarra L.F. and H. Krawinkler, *Global Collapse of Frame Structures Under Seismic Excitations*, Report No. 152, John A. Blume Earthquake Engineering Center, Stanford University, Stanford, California, 2005.

15. International Conference of Building Officials, *Uniform Building Code*, 1927 Edition, International Conference of Building Officials, Long Beach, CA, 1928.

16. Mittler E, C. Taylor, W. Petak, *National Earthquake Probabilistic Hazard Mapping Program: Lessons for Knowledge Transfer*, Natural Hazards Research and Applications Information Center, University of Colorado, Boulder, 1996.

17. Anderson A.W., J.A. Blume, H.J. Degenkolb, H.B. Hammil, E.M. Knapik, H.L. Marchand, H.C. Powers, J.E. Rinne, G.A. Sedgwick, H.O. Sjoberg, "Lateral Forces of Earthquake and Wind", *Transactions of American Society of Civil Engineers*, Vol. 117, Issue 1, 1952.

18. Beavers J.E., “A review of seismic hazard descriptions in US design codes and procedures”, *Progress in Structural Engineering and Materials*, Vol. 4, Issue 1, pp.46-63, 2002.

19. Algermissen S.T. and D.M. Perkins, *A Probabilistic Estimate of Maximum Acceleration in Rock in the Contiguous United States*, Open-File Report 76-416, US Geological Survey, 1976.

20. Kramer S.L., *Geotechnical Earthquake Engineering*, Prentice Hall, Upper Saddle River, NJ, 1996.

21. Luco N., B.R. Ellingwood, R.O. Hamburger, J.D. Hooper, J.K. Kimball, C.A. Kircher, “Risk-Targeted Versus Current Seismic Design Maps for the Conterminous United States”, paper presented at the *SEAOC 2007 Convention Proceedings*, Squaw Creek, California, 2007.

22. Dougles J. and A. Gkimorixis, “Using targeted risk in seismic design codes: A summary of the state of the art and outstanding issues”, paper presented at the *6th National Conference on Earthquake Engineering and 2nd National Conference on Earthquake Engineering and Seismology*, Buchrarest, Romania, 2017.

23. Haselton C.B. and J.W. Baker, “Ground Motion Intensity Measures for Collapse Capacity Prediction: Choice of Optimal Spectral Period and Effect of Spectral Shape”, paper presented at the *8th National Conference on Earthquake Engineering*, San Francisco, CA, 2006.

24. Zareian F., *Simplified Performance-Based Earthquake Engineering*, Ph.D. Thesis, Stanford University, 2006.

25. Turkish Standards Institute, *Design Loads for Buildings*, TS498, Turkish Standards Institute, Ankara, 1997.

26. Computers and Structures Inc., Perform 3D Nonlinear Analysis and Performance Assessment for 3D Structures, User Guide, Version 4, Computers and Structures Inc., Berkeley, California, 2006.

27. Hsiao, P-C, D.E. Lehman, and C.W. Roeder, "Improved analytical model for special concentrically braced frames", *Journal of Constructional Steel Research*, Vol. 73, pp. 80-94, 2012.

28. ASCE/SEI Seismic Rehabilitation Committee, *Seismic Evaluation and Retrofit of Existing Buildings*, ASCE/SEI41-17, American Society of Civil Engineers, Reston, VA, 2017.

29. Applied Technology Council, *Example Application Guide for ASCE/SEI 41-13 Seismic Evaluation and Retrofit of Existing Buildings*, FEMA P-2006, Federal Emergency Management Agency, Washington, D.C., 2018.

30. El-Tawil, S. and G. Deierlein, "Nonlinear Analysis of Mixed Steel-Concrete Frames, Parts I and II", *Journal of Structural Engineering*, Vol. 126, No. 6, June 2001.

31. Computers and Structures Inc., Perform 3D Nonlinear Analysis and Performance Assessment for 3D Structures, Components and Elements, Version 4, Computers and Structures Inc., Berkeley, California, 2006.

32. Pasific Earthquake Engineering Research Center, "Next Generation Attenuation-West2", 2013, http://ngawest2.berkeley.edu/, accessed on June 15, 2017.

33. USGS Earthquake Hazards Program, "Risk-Targeted Ground Motion Calculator", https://earthquake.usgs.gov/designmaps/rtgm/, accessed on December 15, 2022.

34. National Institute of Standards and Technology, *Seismic Design of Steel Special Concentrically Braced Frame Systems*, Seismic Design Technical Brief No. 8, National Institute of Standards and Technology, Gaithersburg, MD, 2013.